Energy reliability-constrained method for the multi-objective optimization of a photovoltaic-wind hybrid system with battery storage

Domenico Mazzeo*[,a], Giuseppe Oliveti[a], Cristina Baglivo[b], Paolo M. Congedo[b]

[a]Department of Mechanical, Energy and Management Engineering (DIMEG) - University of Calabria P. Bucci 46/C - 87036 - Rende (CS) - Italy

[b]Department of Engineering for Innovation - University of Salento Via per Arnesano - Lecce - Italy

*Corresponding author: Domenico Mazzeo, email address: domenico.mazzeo@unical.it, tel.: +39 0984 494605, fax: +39 0984 494673

Abstract

A multi-objective optimization for the dimensioning of hybrid photovoltaic-wind-battery systems HPWBS characterized by high-energy reliability is proposed. The energy reliability-constrained (ERC) method permits choosing the most proper indicators combination to be constrained or optimized as a function of the specific application. The ERC method is applicable to grid-connected and stand-alone hybrid systems with and without storage battery, for residential as well as for other users. The indicators defined are the energy missing to meet the load, or the energy produced in excess, or the manufacturability that characterized the system in relation to the available renewable sources and load.

The ERC method was employed for the multi-objective optimization of a grid-connected hybrid system with and without storage battery for the electric energy supply to an urban residential building in a Mediterranean climate. A parametric analysis, for different loads, by varying the photovoltaic and wind power and the battery storage capacity, was developed to evaluate the annual energy reliability in a dimensionless form of 375 system configurations. The results allowed obtaining empiric correlations to be used in the system design. Finally, the ERC method application allowed achieving optimal system configurations with greater reliability compared with those provided by the Pareto-front method.

Keywords: Renewable Energy; Photovoltaic, Wind, Storage; TRNSYS; Simulation; Optimization; Hybrid system

Nomenclature

Abbreviations

ERC	energy reliability-constrained
GEB	generated energy balance (-)
IAM	incidence angle modifier (-)
LB	load balance (-)
NOCT	nominal operating cell temperature (K)
PV	photovoltaic

Symbols

a	modified ideality factor (eV)
C_{bat}	battery capacity (kWh)

1	e_{dtl}	energy fraction sent directly to the load (-)
2	e_{fb}	energy fraction drawn from the battery (-)
3	e_{fg}	energy fraction drawn from the grid (-)
4	e_{g}	energy fraction produced by the generators (-)
5	e_{lb}	energy fraction lost in the battery (-)
6	e_{tb}	energy fraction sent to the battery (-)
7	e_{tg}	energy fraction in excess sent to the grid (-)
8	E_{dtl}	annual energy sent directly to the load (Wh)
9	E_{fb}	annual energy drawn from the battery (Wh)
10	E_{fg}	annual energy drawn from the power grid (Wh)
11	E_{g}	annual energy produced by the generators (Wh)
12	E_{lb}	annual energy lost in the battery (Wh)
13	E_{L}	annual energy required by the load (Wh)
14	E_{pv}	annual energy produced by the photovoltaic generator (Wh)
15	$E_{pv,eff}$	annual effective energy produced by the photovoltaic generator (Wh)
16	E_{tb}	annual energy sent to the battery (Wh)
17	E_{tl}	annual energy produced sent to the load (Wh)
18	E_{tg}	annual energy in excess sent to the grid (Wh)
19	E_{w}	annual energy produced by the wind generator (Wh)
20	$E_{w,eff}$	annual effective energy produced by the wind generator (Wh)
21	$f_{pv,w}$	photovoltaic-wind fraction (-)
22	$\bar{f}_{pv,w}$	constraint on the photovoltaic-wind fraction (-)
23	f_{SOC}	charge fraction (-)
24	f_{u}	utilization factor (-)
25	$\bar{f}_{u}$	constraint on the utilization factor (-)
26	G	hourly solar radiation on the inclined surface (W/m^2)
27	$G_{b,h}$	beam solar radiation on the horizontal surface (W/m^2)
28	$G_{d,h}$	diffuse solar radiation on the horizontal surface (W/m^2)
29	h_{hl}	manufacturability (Wh/W)
30	$\bar{h}_{hl}$	constraint on the manufacturability (Wh/W)
31	k	Boltzmann's constant (1.38066E–23 J/K)
32	I	current (A)
33	I_{o}	diode reverse saturation current (A)
34	I_{L}	light current (A)
35	$I_{mp}(t)$	current at maximum power point (A)
36	ℓ	miscellaneous losses (%)
37	n_{I}	usual ideality factor (-)
38	N_{s}	number of cells in series (-)
39	O	objective function
40	$\bar{O}$	constraint on the objective function
41	p_{b}	storage fraction (-)
42	p_{hbl}	load overall fraction (-)
43	p_{l}	load fraction (-)
44	p_{w}	wind fraction (-)
45	P(t)	power (W)
46	$P_{o}(t)$	wind turbine power at the actual operating height for a reference air density (W)
47	P_{B}	maximum stored energy in one hour by the battery (W)
48	$P_{g}(t)$	overall power generated (W)

1	$P_{fb}(t)$	power drawn from the battery (W)
2	$P_{fg}(t)$	power drawn from the grid (W)
3	$P_{inv,out}(t)$	inverter output power(W)
4	$P_{inv,inp}(t)$	inverter input power(W)
5	$P_L(t)$	power required by the load (W)
6	P_n	overall nominal power of the HPWBS (W)
7	$P_{pv}(t)$	power produced by the photovoltaic generator (W)
8	$P_{pv,eff}(t)$	effective power produced by the photovoltaic generator (W)
9	P_{PV}	nominal power of the photovoltaic generator (W)
10	$P_{tb}(t)$	power sent to the battery (W)
11	$P_{tg}(t)$	power in excess sent to the grid (W)
12	$P_{tl}(t)$	power produced sent to the load (W)
13	$P_w(t)$	power produced by the wind generator (W)
14	$P_{w,eff}(t)$	effective power produced by the wind generator (W)
15	P_W	nominal power of the photovoltaic generator (W)
16	$P_\rho(t)$	wind turbine power as a function of air density (W)
17	$P_{\rho,net}(t)$	power produced by the wind generator (W)
18	q	electron charge (1.60218E–19 C)
19	r	parameters of the objective functions
20	R_b	hourly average geometry factor of the beam radiation (-)
21	R_d	geometry factor of the diffuse radiation (-)
22	R_r	geometry factor of the reflected radiation (-)
23	R_s	series resistance (Ω)
24	R_{sh}	shunt resistance (Ω)
25	SOC(t)	state of charge of the battery (Wh)
26	$SOC_{max}(t)$	maximum allowable SOC (Wh)
27	$SOC_{min}(t)$	minimum allowable SOC (Wh)
28	t	time (s)
29	T_c	cell temperature (°C)
30	$T_{ea}(t)$	external air temperature (K)
31	v(t)	wind speed (m/s)
32	$V_{mp}(t)$	voltage at maximum power point (V)
33	v_{an}	wind speed at the anemometric height (m/s)
34	$v_h(t)$	wind speed at the actual operating height of the wind turbine (m/s)
35	$v_{nom,\rho}$	nominal wind speed as a function of air density (m/s)
36	$v_{nom,\rho o}$	nominal wind speed at the reference air density (m/s)
37	V	voltage (V)
38	z_{an}	anemometric height (m)
39	z_h	actual operating height of the wind turbine (m)
40		
41	*Greek letters*	
42	α(t)	wind shear exponent (-)
43	β	inclination angle of the photovoltaic inclined surface (°)
44	Δt	time interval (s)
45	$\eta_{AC/AC}$	DC/DC converter efficiency (-)
46	$\eta_{AC/DC}$	AC/DC rectifier efficiency (-)
47	η_{bat}	battery efficiency (-)
48	η_{inv}	inverter efficiency (-)
49	η_{reg}	regulator efficiency (-)

$\rho(t)$	air density (kg/ m^3)
ρ_0	power curve air density (kg/m^3)

Subscripts

i	i-th objective function
j	j-th objective function
m	number of constrained objective functions
n	number of objective functions
r	number of parameters of the objective functions
ref	at the reference conditions

1. Introduction

Recent European directives have promoted the improvement of energy performances in the construction sector. The direct effect of these policies is the increase in studies addressed to the development of innovative technological solutions aimed at reducing overall energy consumption, dependence on fossil fuels and greenhouse emissions into the atmosphere. The best solutions to satisfy the provisions of the new directives are hybrid systems. This term indicates the use of multiple technologies like, for example, wind, photovoltaic and geothermal plants integrated in the same system. In the electricity sector, wind and photovoltaic systems have been developing considerably in recent years, thanks to the wider availability in terms of installation costs. However, the significant intermittence and uncertainty of energy sources, also due to climate changes, may make the single use of those systems unreliable in terms of meeting the load. A combination of these two technologies (hybrid photovoltaic-wind system HPWS) allows the uncertainty issue to partially overcome, while the integration of an energy storage system (hybrid photovoltaic-wind-battery system HPWBS) mitigates the intermittence issue. The greater energy reliability of hybrid systems allows their installation even in remote areas, without access to the electricity grid (stand-alone systems), or in areas with access to the electricity grid (grid-connected). When the energy production results more or less than the required load, the difference can be exchanged with the public grid by a net metering service. Moreover, hybrid systems can be used in locations without access to reliable power, thus being an emergency system for significantly long periods in alternative to the traditional uninterruptible power supply (UPS).

In the last decade, in several researches, the reliability criterion has turned out to be the most important in the sizing phase of hybrid systems. A correct sizing requires the use of proper reliability indicators and an optimization analysis. The survey of the literature has highlighted that most of the reliability analysis methods on hybrid systems are related to stand-alone systems [1-13] rather than grid-connected ones [14-16]. As regards the stand-alone systems, different reliability indicators [17-21] were defined by considering only the unsatisfied load in terms of time fraction, energy fraction or probabilistic, such as the loss of power supply probability (LPSP), loss of load probability (LOLP), unmet load (UL), system performance level (SPL), loss of load hours (LOLH), loss of load risk (LOLR), level of autonomy (LA), deficiency in power supply probability (DPSP), expected energy not supplied (EENS), and maxENS. In general, from an energy point of view, further reliability indicators should be employed to make a proper coupling between the renewable energy sources of a locality, the system components and the load. In addition, for the size design of a reliable grid-connected system, other important factors should be considered in order to reduce the energy produced in excess.

Generally, a hybrid system optimization criterion requires the maximization or the minimization of one or more indicators, and the Pareto-front is one of the most applied method [5, 21-23]. It is the authors' belief, in accordance with recent researches [22], in addition to optimizing some indicators, it is necessary to constrain other ones to assign a weight to each indicator and guarantee an appropriate reliability. Moreover, the indicators to be constrained and those to be optimized should be chosen in relation to the importance associated with each of the objectives to be achieved and the specific application.

The present research proposes the use of the energy reliability-constrained (ERC) method. The method allows differently constraining the reliability indicators and can be applied in the design or in the performance verification phase of a specific HPWS or HPWBS, whether grid-connected or stand-alone, for residential users as well as for other users. In the design phase, when the location is defined, the ERC method allows the identification of the proper technical characteristic and the overall nominal power of the system components, or the identification of a suitable location for specific system components. Such flexibility makes the ERC method of a general nature from a methodological point of view.

Other critical aspects, emerged from the previous studies, regard: a scarcity of applications for grid-connected hybrid systems; the infrequency of a direct comparison between HPWS and HPWBS; specific cases studies, relating to certain power sizes of the system or fixed load levels; the prevalent use of estimated weather data rather than experimentally measured instantaneous actual data sets. In addition, as mentioned previously and highlighted in [18], several size optimization applications have been conducted worldwide and mostly the locations are characterized by high winds, such as remotely located hilly areas where the transmission extension may not be feasible or coastal areas [6-14, 22-26] The studies in the urban context with low wind regime are very limited [4, 15, 25-27]. Instead, a great number of researches were conducted in the Mediterranean area [1-3, 9-13, 15, 26-28], where the elevated availability of solar radiation makes the use of these system very promising.

For all these reasons, the ERC method was applied to a grid-connected hybrid system with or without electric battery storage for an urban residential use. A width range of variation of the component sizes, for different hourly average daily load values, was considered. The climatic data used in this study were measured at the Solar Engineering Laboratory located on the roof of a building of the University of Calabria Campus, in Southern Italy. This study is the first in this area of Italy, and the results obtained are useful for similar climate regions of the Mediterranean area.

2. Methodology

The procedure consists in the energy reliability evaluation of the hybrid system in accordance with the following phases: (i) mathematical modelling to describe the non-linear characteristics of the system components; (ii) hourly dynamic simulation to obtain the powers in input and in output from each component; (ii) evaluation of the annual energies associated with these powers; (iii) dimensionless representation of the results by means of the fractions referring to the energy required by the load and referring to energy generated; (iv) definition and calculation of proper indicators that identify the system energy reliability; (v) parametric analysis to evaluate the effects of the components size variation on the system energy reliability; (vi) multi-objective optimization analysis development by means of ERC method used to identify, for a certain load, the optimal system configurations that simultaneously ensure maximization of some indicators and, for the other ones, higher values than predetermined constraints.

2.1. Mathematical modelling

Figure 1 shows the scheme of the grid-connected HPWBS for residential use.

Figure 1 - Scheme of the grid-connected HPWBS for a residential use.

The plant consists of a wind micro-generator and an AC/DC rectifier, a photovoltaic (PV) generator and an AC/AC converter, an electric battery storage system, a regulator and a DC/AC inverter.

2.1.1. Photovoltaic generator

The hourly solar radiation G incident on the inclined plane of the PV generator is the sum of direct, diffuse and reflected radiation [29]:

$$G = G_{b,h}R_b + G_{d,h}R_d + \left(G_{b,h} + G_{d,h}\right)R_r \quad (1)$$

where $G_{b,h}$ and $G_{d,h}$ are the direct and diffuse components on the horizontal plane, R_b is the hourly average geometry factor of the direct radiation, R_d and R_r are the geometry factors of diffuse and reflected radiation.

The PV generator performances are determined by solving the equivalent electric circuit consisting of a direct/ideal-current generator, a diode and two resistances [30].

The current-voltage characteristic of the circuit is represented by the following equation:

$$I = I_L - I_0\left[e^{\frac{V+IR_s}{a}} - 1\right] - \frac{V + IR_s}{R_{sh}} \quad (2)$$

with

$$a = \frac{N_s n_I k T_C}{q} \quad (3)$$

Where,

q is the electron charge, k is Boltzmann's constant, n_I is the usual ideality factor (dimensionless diode curve-fitting factor, with a minimum possible), N_s is the number of cells in series and Tc is the cell temperature.

The model parameters that characterize the electric circuit, as a function of absorbed solar radiation and cell temperature, are: the light current (I_L), the diode reverse saturation current (I_0), the series resistance (R_s), the shunt resistance (R_{sh}) and the modified ideality factor (a).

In the reference conditions, $I_{L,ref}$, $I_{0,ref}$, $R_{s,ref}$, $R_{sh,ref}$ and a_{ref} are obtained using the simplified hypothesis introduced by Fry [31], which determines the shunt resistance directly from the slope in the short-circuit point of the I-V curve. In this way, the unknown quantities are reduced to four parameters and are obtained by imposing the conditions at open-circuit point, short-circuit point and maximum power point into Eq. (2), and using the analytic expression of the voltage derivative compared to the temperature in open-circuit conditions, namely temperature coefficient of open-circuit voltage. The system, consisting of the four equations, is solved by an iterative search routine, which provides the values of $I_{L,ref}$, $I_{0,ref}$, $R_{s,ref}$ and a_{ref}. The parameter values under operating conditions are obtained by updating the I_L and I_0 values, as a function of solar radiation absorbed and the cell temperature respectively. The latter is calculated using the nominal operating cell

temperature (NOCT). In this way, the characteristic curve is updated at each time instant as a function of the cell temperature and the solar radiation absorbed [32]. In addition, absorbed solar power is evaluated considering the incidence angle modifier IAM [33]. The electric PV power produced is calculated at the maximum power point of the characteristic curve by Eq. (4):

$$P_{pv}(t) = I_{mp}(t)V_{mp}(t) \tag{4}$$

2.1.2. Wind generator

The wind electric power as a function of the wind speed is evaluated through the reference experimental power curve. This curve is determined to a specific value of the air density using the wind speed values measured at the turbine hub height. Under operating conditions, the power delivered is determined using a calculation algorithm, which employs at each instant the following steps [34]:

(i) calculation of the air density at the actual operating height z_h of the wind turbine, as a function of air temperature and pressure;

(ii) calculation of the wind speed $v_h(t)$ at the actual operating height z_h of the wind turbine, starting from the wind speed $v_{an}(t)$ at the anemometric height z_{an}, by Eq. (5), known the shear exponent α;

(iii) evaluation of the turbine power $P_0(t)$ at the actual operating height through the use of the experimental power curve traced for a reference air density ρ_0;

(iv) determination of the correct power $P_\rho(t)$ and the correct nominal speed $v_{nom,\rho}$, respectively by means of Eq. (6) and Eq. (7), in order to consider the updated air density value, in relation to the method of power control mode;

(v) calculation of net power $P_{\rho,net}$ considering the miscellaneous losses ℓ (Eq. 8).

$$\frac{v_h(t)}{v_{an}(t)} = \left(\frac{z_h}{z_{an}}\right)^{\alpha(t)} \tag{5}$$

$$\frac{P_\rho(t)}{P_0(t)} = \frac{\rho(t)}{\rho_0} \tag{6}$$

$$\frac{v_{nom,\rho}(t)}{v_{nom,\rho_0}} = \left(\frac{\rho_0}{\rho(t)}\right)^{1/3} \tag{7}$$

$$P_w(t) = P_{\rho,net}(t) = P_\rho(t)\left(1 - \frac{\ell}{100}\right) \tag{8}$$

2.1.3. Electric storage battery

Battery performances are evaluated through a model, which uses the instantaneous balance equation of the state of charge (SOC). In the charging phase, the charge rate is obtained from:

$$\frac{dSOC}{dt} = P(t)\,\eta_{bat} = P_{tb}(t) \tag{9}$$

In the discharge phase, the discharge rate is obtained from:

$$\frac{dSOC}{dt} = P(t) = -P_{fb}(t) \tag{10}$$

where η_{bat} is the battery efficiency, $P(t)$ is the power sent to the battery or the power from the battery.

SOC at the time instant *t* is determined discretizing Eq. (9) and Eq. (10):

$$\begin{cases} SOC(t+1) = SOC(t) + P_{tb}(t)\eta_{bat}\Delta t & P(t) > 0 \\ SOC(t+1) = SOC(t) - P_{fb}(t)\,\Delta t & P(t) < 0 \end{cases} \tag{11}$$

At any time, the SOC is subject to the constraints $SOC_{min}(t) < SOC(t) < SOC_{max}$, with SOC_{max} and $SOC_{min}(t)$ the maximum and minimum allowable SOC. Once the SOC is known, the charge fraction is calculated as a function of the battery capacity C_{bat} by Eq. (12):

$$f_{SOC}(t+1) = \frac{SOC(t+1)}{C_{bat}} \tag{12}$$

2.1.4. Static converters

The output electric power from each of the static converters shown in Figure 1 is calculated, starting from the input values, through an electric conversion efficiency:

- DC/DC converter

$$P_{pv,eff}(t) = P_{pv}(t)\,\eta_{DC/DC} \tag{13}$$

  where $P_{pv,eff}(t)$ is the output power and $P_{pv}(t)$ input power coming from the PV generator.

- AC/DC rectifier

$$P_{w,eff}(t) = P_{w}(t)\,\eta_{AC/DC} \tag{14}$$

  where $P_{w,eff}(t)$ is the output power and $P_{w}(t)$ input power coming from the wind generator.

- DC/AC inverter

$$P_{inv,out} = P_{inv,in}\,\eta_{inv} \tag{15}$$

  where $P_{inv,out}$ is the output power and $P_{inv,inp}$ input power coming from the two generators and battery.

In the Eqs. (13)-(15), $\eta_{AC/AC}$, $\eta_{AC/DC}$ and η_{inv} are the efficiencies of the correspondent static converters.

2.1.5. Regulator

The regulator, characterized by an efficiency η_{reg}, at each instant compares the power generated $P_g(t)$, sum of the power produced by the PV system $P_{pv,eff}(t)$ and wind system $P_{w,eff}(t)$, with the instantaneous load $P_L(t)$. The result of the comparison between $P_g(t)$ and $P_L(t)$ at any time instant determines the operating mode of the system and the power provided by HPWBS to the load $P_{tl}(t)$.

2.2. Dynamic simulation and instantaneous balance

The system was simulated on an hourly basis for a whole year using a computational model built in TRNSYS 17 (Transient System Simulation) environment [35], see Figure 2.

Figure 2 - Assembled model of the HPWBS in TRNSYS environment.

The system components are simulated under dynamic conditions, using mathematical models, described in the previous Section 2.1, implemented in specific Types. In particular: Type 94 simulates the PV generator, Type 90 the wind generator, Type 48 the storage battery, Type 47 the regulator and inverter, equation blocks the static converters and Type 14 the load trend; Type 9 allows to import the experimental climate data; Type 16 reports on the inclined plane the incident solar radiation on the horizontal plane; Type 25 allows results to be printed. Through the parameters setting of each Type, it is possible to determine the power produced by the PV $P_{pv}(t)$ and wind generator $P_w(t)$, the output power from the AC/DC rectifier $P_{w,eff}(t)$, from the DC/DC static converter $P_{pv,eff}(t)$ and from the DC/AC inverter $P_{inv,out}$, the input $P_{tb}(t)$ or output $P_{fb}(t)$ power from the battery, the power delivered to the load $P_{tl}(t)$, the excess power $P_{tg}(t)$ and the power drawn from the grid $P_{fg}(t)$ at any time instant.

Three different operating modes of the system can be identified:

Mode 1): $\eta_{reg}\eta_{inv}P_g(t) > P_L(t)$

When the overall net power generated $\eta_{reg}\eta_{inv}P_g(t)$ is greater than the power required by the load $P_L(t)$, the excess power is used to charge the battery $P_{tb}(t)$ and, in the totally charged conditions, is sent to the grid $P_{tg}(t)$. In this operation mode, the power drawn from the battery $P_{fb}(t)$ and from the grid $P_{fg}(t)$ are null.

Referring to Figure 1, the balance equation of the generated power is:

$$P_g(t) = \left[P_{pv,eff}(t) + P_{w,eff}(t)\right] = \frac{P_{tl}(t)}{\eta_{reg}\eta_{inv}} + \frac{P_{tb}(t)}{\eta_{reg}} + \frac{P_{tg}(t)}{\eta_{reg}\eta_{inv}} \quad (16)$$

Mode 2): $\eta_{inv}\eta_{reg}P_g(t) < P_L(t)$

When the overall net power generated $\eta_{reg}\eta_{inv}P_g(t)$ is less than that required by the load $P_L(t)$, the missing power is drawn from the battery $P_{fb}(t)$ and, if necessary, from the grid $P_{fg}(t)$. Under such conditions, the power sent to the battery $P_{tb}(t)$ and the excess power $P_{tg}(t)$ are null.

Referring to Figure 1, the balance equation of the power sent to the load is:

$$P_{tl}(t) = P_g(t)\eta_{reg}\eta_{inv} + P_{fb}(t)\eta_{inv} = \left[P_{pv,eff}(t) + P_{w,eff}(t)\right]\eta_{reg}\eta_{inv} + P_{fb}(t)\eta_{inv} \quad (17)$$

Mode 3): $\eta_{inv}\eta_{reg}P_g(t) = P_L(t)$

When the net overall power generated $\eta_{reg}\eta_{inv}P_g(t)$ is equal to the load $P_L(t)$, the power sent and drawn from the battery, $P_{tb}(t)$ and $P_{fb}(t)$, and that sent and drawn from the grid, $P_{tg}(t)$ and $P_{fg}(t)$, are null.

Referring to Figure 1, the balance equation of the generated power is:

$$P_g(t) = \left[P_{pv,eff}(t) + P_{w,eff}(t)\right] = \frac{P_{tl}(t)}{\eta_{reg}\eta_{inv}} \tag{18}$$

Referring to the instantaneous load:

- Both in Mode 1) and Mode 3), the power required by the load is supplied entirely from the system:

$$P_L(t) = P_{tl}(t) \tag{19}$$

- In Mode 2), the power required by the load is partly provided by HPWBS and partially withdrawn from the grid:

$$P_L(t) = P_{tl}(t) + P_{fg}(t) \tag{20}$$

2.3. Annual energy balance

The overall annual energy required by load E_L is partly provided by the HPWBS E_{tl} and partly by the grid E_{fg}:

$$E_L = E_{tl} + E_{fg} \tag{21}$$

The overall annual energy produced by the PV and wind generator is:

$$E_g = E_{pv}\,\eta_{DC/DC} + E_w\,\eta_{AC/DC} \tag{22}$$

E_g is partly sent directly to the load, E_{dtl}, partly stored in the battery, E_{tb}, and partly sent to the grid, E_{tg}:

$$E_g = \frac{E_{dtl}}{\eta_{reg}\eta_{inv}} + \frac{E_{tb}}{\eta_{reg}} + \frac{E_{tg}}{\eta_{reg}\eta_{inv}} \tag{23}$$

Where, the energy sent directly to the load E_{dtl} can be obtained from the Eq. (24).

$$E_{tl} = E_{dtl} + E_{fb}\eta_{inv} \tag{24}$$

In Eq. (24) the overall energy produced by the HPWBS sent to the load E_{tl} is the sum of the energy sent directly to the load E_{dtl} and that received from the battery $E_{fb}\eta_{inv}$.

The balance Eq. (23) can be made dimensionless by dividing each term to the energy required by load E_L. In addition, multiplying both members of Eq. (23) for the regulator and inverter efficiencies $\eta_{reg}\eta_{inv}$, Eq. (25) is obtained.

$$\frac{E_g}{E_L}\eta_{reg}\eta_{inv} = \frac{E_{dtl}}{E_L} + \frac{E_{tb}}{E_L}\eta_{inv} + \frac{E_{tg}}{E_L} \tag{25}$$

Eq. (25) can be written in the corresponding form:

$$e_g = e_{dtl} + e_{tb} + e_{tg} \tag{26}$$

Considering Eq. (27) of the annual energy balance of the battery:

$$E_{fb} = \eta_{bat}E_{tb} \tag{27}$$

and extracting E_{tl} from Eqs. (23) and (24) and replacing it in Eq. (21), the balance equation of the energy required by the load is obtained:

$$E_L = E_g\eta_{reg}\eta_{inv} - [E_{tb}(1-\eta_{bat})\eta_{inv}] - E_{tg} + E_{fg} \tag{28}$$

The annual energy required by the load is the sum of two contributions: (i) the overall net energy produced by the generators, $E_g\eta_{reg}\eta_{inv}$, reduced by the energy lost in the battery $E_{tb}(1-\eta_{bat})\eta_{inv}$ and by the excess energy sent to the grid E_{tg}; (ii) the energy drawn from the grid E_{fg}. The balance Eq. (28) can be made dimensionless by dividing each term to the energy required by the load E_L:

$$1 = \frac{E_g}{E_L}\eta_{reg}\eta_{inv} - \left[\frac{E_{tb}}{E_L}(1-\eta_{bat})\eta_{inv}\right] - \frac{E_{tg}}{E_L} + \frac{E_{fg}}{E_L} \tag{29}$$

Eq. (29) can be written in the corresponding form:

$$1 = e_g - e_{lb} - e_{tg} + e_{fg} \tag{30}$$

Replacing Eq. (26) in Eq. (30), and taking into account that $e_{tb} - e_{lb} = e_{fb}$, a new relation of the energy balance equation of the energy required by the load (load balance LB) is obtained:

$$1 = e_{dtl} + e_{fb} + e_{fg} \tag{31}$$

The addends of the second member in Eq. (31) are the fractions, referred to the energy required by the load, of the energy sent directly to the load (e_{dtl}), energy extracted from the battery (e_{fb}) and from the grid (e_{fg}).

The balance equation of the energy generated (generated energy balance GEB), per unit of energy required by the load, e_g, expressed by Eq. (26), can be written as follows:

$$1 = \frac{e_{dtl}}{e_g} + \frac{e_{tb}}{e_g} + \frac{e_{tg}}{e_g} \quad (32)$$

The addends of the second member in Eq. (32) are the fractions, referred to the energy generated, of energy sent directly to the load$\left(e_{dtl}/e_g \right)$, energy sent directly to the battery (e_{tb}/e_g), and excess energy sent to the network $\left(e_{tg}/e_g\right)$.

Eqs. (31)-(32) are used in Sections 4.1.1 and 4.1.2 to evaluate the energy reliability of the system as a function of the following dimensionless parameters:

$$p_w = \frac{P_W}{P_W + P_{PV}} \quad (33)$$

$$p_b = \frac{P_B}{P_n} = \frac{P_B}{P_W + P_{PV} + P_B} \quad (34)$$

$$p_l = \frac{P_L}{P_W + P_{PV}} \quad (35)$$

$$p_{hbl} = \frac{P_L}{P_n} = \frac{P_L}{P_W + P_{PV} + P_B} \quad (36)$$

Where,

- p_w represents the *wind fraction*, the ratio of the wind nominal power P_W to the overall nominal PV-wind power. The p_w parameter runs between zero and one: when $p_w = 0$ the system is without the wind generator, for $p_w = 1$ the system is devoid of the PV generator.
- p_b is the *storage fraction*, the ratio of the nominal battery power P_B (maximum stored energy in one hour) to the overall nominal power P_n of the HPWBS, sum of the nominal PV, wind and battery power. The p_b parameter ranges between 0 and 1: when $p_b = 0$ the system is without battery, for $p_b = 1$ the system is constituted only by the storage battery, since $P_W + P_{PV} = 0$.
- p_l is the *load fraction*, the ratio of the hourly average daily load P_L to the nominal PV-wind power. Parameter p_l can be less or greater than 1; in this latter case, the hourly average daily power required by the load is higher than the sum of the PV and wind nominal power.
- p_{hbl} is the *load overall fraction*, the ratio of the hourly average daily load P_L to the overall nominal power P_n of the HPWBS.

2.4. Energy reliability indicators

This section defines the dimensionless indicators to be used in the energy reliability analysis to identify the optimal system configurations. The indicators are:

a) the **photovoltaic-wind fraction $f_{pv,w}$** (-) defined as the ratio of the energy supplied by the HPWBS to the load E_{tl} to the energy required by load E_L. Considering Eq. (31), this indicator can be expressed as sum of the energy fractions e_{dtl} and e_{fb}:

$$f_{pv,w} = \frac{E_{tl}}{E_L} = e_{dtl} + e_{fb} \quad (37)$$

$f_{pv,w}$ measures the fraction of energy required by the load satisfied by the system (the complement to one 1 is the energy fraction missing to meet the load), and it varies between 0 and 1; for $f_{pv,w} = 1$, all the energy required by the load is provided by the system, and the energy supplied by the grid is zero.

b) the **utilization factor** of the generated energy $\mathbf{f_u}$ (-) defined as the ratio of the energy supplied by the HPWBS to the load E_{tl} to the generated energy E_g. Considering Eq. (32), this indicator is expressed as the sum of the energy fractions e_{dtl}/e_g and e_{tb}/e_g:

$$f_u = \frac{E_{tl}}{E_g} = \frac{e_{dtl}}{e_g} + \frac{e_{tb}}{e_g} \tag{38}$$

f_u quantifies the fraction of produced energy employed to satisfy the load (the complement to one 1 is the excess energy fraction), and it varies between 0 and 1; for $f_u = 1$, all the energy generated is supplied to the load, and the excess energy is zero.

c) the **system manufacturability $\mathbf{h_{hl}}$** (kWh/kWh) defined as the ratio of the energy supplied by the HPWBS to the load E_{tl} to the overall nominal power of the HPWBS P_n. Considering Eqs. (36)-(37), this indicator is expressed as the product of the load overall fraction p_{hbl} and the PV-wind fraction:

$$h_{hl} = \frac{E_{tl}}{P_n} = 8760\ p_{hbl}\ f_{pv,w} \tag{39}$$

Where, 8760 are the hours of one year.

This indicator provides the energy sent to the load per each kW installed, namely the number of operating equivalent hours of the system in a year in which all the system components operate simultaneously in the nominal conditions.

2.5. Multi-objective optimization

This section presents the multi-objective optimization methods used, such as the Pareto-front method and the energy reliability-constrained (ERC) method proposed by the authors.

In general, in multi-objective optimization there is no one unique solution satisfying all objectives simultaneously, and then it is necessary to find a trade-off between a set of *n* conflicting objective functions O_i:

$$\{O_1(r), O_2(r), \dots, O_n(r)\} \tag{40}$$

each of which depends on the *r* parameters $r = (r_1, r_2, \dots, r_r)$.

In the application at hand, these objective functions are the maximization of the energy reliability indicators described in Section 2.4, namely the PV-wind fraction $f_{pv,w}$, the utilization factor of the generated energy f_u, the system manufacturability h_{hl} or a combination of these latter. A multi-objective optimization based on the Pareto-front method [36], described in subsection 2.5.1, is requested since the three indicators have different trends by varying the dimensions of the system components. For example, an increase of the overall nominal power of the system determines a higher energy produced sent to the load with a greater $f_{pv,w}$, and simultaneously, a higher energy in

excess with a lower f_u. Instead, the variation of h_{hl} is not determinable beforehand. Alternatively, to the Pareto-front, the ERC method, described in subsection 2.5.2, can be applied to guarantee that some reliability indicators were higher than a predetermined constraint.

2.5.1. Pareto-front method

In a multi-objective maximization, the Pareto optimal solutions are based on the following definition of dominance, where a feasible solution r^* is said to Pareto dominate another solution r' if:

$$O_i(r^*) \geq O_i(r') \ \forall i \in \{1,2,\dots n\} \quad \text{and} \quad O_j(r^*) > O_j(r') \ \text{for at least one } j \in \{1,2,\dots n\} \quad (41)$$

that is, r^* is as good as r' in all objectives and is strictly better than r' in at least one. A r^* not dominated by any other is called Pareto optimal solution. The set of all Pareto optimal solutions constitutes the Pareto-front.

The application of this method to an HPWBS allows the identification of the trade-off system configurations. These configurations might not assure a high energy reliability since among these are also included those configurations with high values of an objective and a low values of the other. Hybrid systems with high reliability are those that ensure values of indicators exceeding prefixed constraints. For these reason the objectives functions must be constrained.

2.5.2. Energy reliability-constrained (ERC) method

In the method proposed some solutions are excluded subjecting *m* objective functions to prefixed constraints:

$$\{O_1(p) < \overline{O}_1, O_2(p) < \overline{O}_2, \dots, O_m(p) < \overline{O}_m\} \quad (42)$$

In this way, several Pareto optimal solutions are excluded and others not belonging to the Pareto-front are considered. Among the solutions not excluded, the optimal solutions are those that optimize the other *n-m* objective functions:

$$max \ or \ min \{O_{n-m}(p), O_{n-m+1}(p), \dots, O_n(p)\} \quad (43)$$

Therefore, the ERC method is a general procedure that in the case of absence of objective functions to be constrained (m=0) becomes the Pareto-front method.

In the case of an HPWBS, some indicators are subjected to the prefixed constraints: $f_{pv,w} > \overline{f}_{pv,w}$, or $f_u > \overline{f}_u$, or $h_{hl} > \overline{h}_{hl}$, or a combination of these latter, with $\overline{f}_{pv,w}$, $\overline{f}_u$, and $\overline{h}_{hl}$ constraint values. Then, the optimal system configurations are identified by maximizing the remaining indicators.

The choice of the indicators to be constrained or to be maximized depends on the presence or absence of a grid connection:

- in an energy reliable grid-connected HPWBS, the energy drawn from the grid and the energy produced in excess must be limited ($f_{pv,w} > \overline{f}_{pv,w}$ and $f_u > \overline{f}_u$);

- in an energy reliable stand-alone HPWBS, only the missing energy to meet the load must be limited ($f_{pv,w} > \bar{f}_{pv,w}$), while and the energy produced in excess must be minimized (max f_u);

In both cases, the indicator h_{hl} must be maximized. Consequently, in the grid-connected HPWBS m=2 and n=1, while in the stand-alone HPWBS m=1 and n=2.

3. Case study

In this section are presented: the experimental climatic data of the location (Section 3.1); the technical data relative to all the system components (Section 3.2); the hourly trend of the daily electric load (Section 3.3); the different configurations of the HPWBS considered in the parametric analysis (Section 3.4).

3.1. Climatic data

The experimental meteorological data regards the values collected during the entire 2015 year in an urban context, namely in the Solar Engineering laboratory located at the Department of Mechanical, Energetics and Management Engineering (DIMEG) at the University of Calabria, Cosenza (Italy). The Mediterranean climate of Cosenza, identified as Csa in the Köppen climate classification [37], has moderate temperatures with changeable and rainy weather in winter, while summers are hot and dry.

In Figure 3 the hourly values, on the left, and the monthly average daily, on the right, of the solar radiation on the horizontal plane, external air temperature, and wind speed are shown. The measurements were carried out on the roof of a university building at a height of 10 meters from the ground. As regards solar radiation, the values on the PV generator inclined plane, exposed to the South and inclined at a $\beta = 33\ °$ angle, were obtained with Type 16a which employs Eq. (1). Instead, Type 90 reports the wind speed data from the anemometric measure height to the hub height of the wind turbine by Eq. (5).

Figure 3 – Hourly and monthly average daily solar radiation on the horizontal plane, of the external air temperature and of wind speed in Cosenza (Italy).

3.2. System components

The PV generator consists of Sharp modules [38] with polycrystalline silicon cells, each of which has a dimension of $(15.65\ \text{cm} \times 15.65\ \text{cm})$. The wind micro-generator employed is the Proven Energy of Angel Wind Energy [39]. The wind turbine was placed 5 meters higher from the roof, i.e. 15 meters in height from the ground. The electric storage is a set of Type BAT-2.0-A-SE-10 batteries, at lithium ions of LG Chem [40]. The main electric and thermal characteristics of the system components taken from the manufacturer's data sheet and the parameters used in the TRNSYS software are shown in Table 1. In addition, Table 1 shows the type and efficiency of the DC/DC converter [41], AC/DC rectifier [42], DC/AC inverter [43] and regulator [44].

Table 1. Characteristics at reference conditions of the components and parameters set in TRNSYS.

3.3. Electric loads

The electric load considered is typical of a residential use with a daily trend variable hourly. Figure 4 shows the values of electric loads obtained by varying the daily average hourly value and keeping

the trend unchanged. Globally, five hourly average daily loads P_L ranges between 0.5 kW and 10 kW were considered. The corresponding annual energy required by the load E_L vary between 4.38 MWh and 87.6 MWh.

Figure 4 - Hourly trends of the daily load for different hourly average daily values.

3.4. Parametric analysis

Referring to Table 2, the calculation scheme developed in TRNSYS was used to perform an annual energy parametric analysis of different hybrid system configurations in the presence and in the absence of storage battery, for each considered load.

Table 2 – Parametric analysis: nominal powers of the PV and wind generator, and storage capacity of electric battery

Overall, 375 system configurations were considered in the parametric analysis, obtained varying: (i) the nominal power of the PV generator by varying the number of PV module; (ii) the nominal power of the wind generator by varying the number of wind turbine; (iii) the storage capacity by varying the number of storage battery. For each case, the calculation scheme of TRNSYS was used to calculate the hourly values of the output powers from each component defined in Sections 2.1 and 2.2. These powers were used for the calculation of the relative hourly and annual energy defined in Section 2.3, used to evaluate the dimensionless fractions, Eqs. (31)-(32) and Eqs. (37)-(39), defined in Section 2.4.

4. Results and discussion

In Section 4.1, the system energy reliability was studied by varying the wind fraction p_w, the storage fraction p_b and the load fraction p_l, evaluating the influence on the energy fractions of the LB, Eq. (31), and comparing them with the energy fractions of GEB, Eq. (32). These energy fractions and the reliability indicators, Eqs. (37)-(39), were also studied as a function of the load overall fraction p_{hbl}, by providing some analytical correlations. In Section 4.2, an energy reliability multi-objective optimization was developed to identify the optimal system configurations based on ERC method. These optimal configurations are compared with those obtained by using the Pareto-front method.

4.1. Parametric analysis

4.1.1. Balance of the energy required by the load LB

Figures 5-7 show, as a function of the wind fraction p_w, the trends of the energy fraction sent directly to the load e_{dtl}, energy fraction taken from the battery e_{fb}, and energy fraction extracted from the grid e_{fg}. The figures regard three different load values P_L, 0.5 kW, 2.5 kW and 10 kW. In each figure, four images obtained by assigning to the storage capacity C_B the values 0 kWh, 2 kWh, 6 kWh and 10 kWh are reported. Each image shows the trend of e_{dtl}, e_{fb} and e_{fg} as a function of p_w for three different values of the nominal power of the PV generator P_{PV}, 2.5 kW, 5 kW and 10 kW, considering P_L and C_B constants.

Figure 5 - Energy fraction sent directly to the load, energy fraction drawn from the battery and energy fraction drawn from the grid as a function of the wind fraction. $P_L = 0.5\ kW$.

Figure 6 - Energy fraction sent directly to the load, energy fraction drawn from the battery and energy fraction drawn from the grid as a function of the wind fraction. $P_L = 2.5\ kW$.

Figure 7 - Energy fraction sent directly to the load, energy fraction drawn from the battery and energy fraction drawn from the grid as a function of the wind fraction. $P_L = 10\ kW$.

In Figures 8-10 are reported, as a function of the storage fraction p_b, the trends of the energy fraction sent directly to the load e_{dtl}, energy fraction drawn from the battery e_{fb}, and energy fraction extracted from the grid e_{fg}. The figures are obtained by considering three different load values P_L, 0.5 kW, 2.5 kW and 10 kW. In each figure, three images obtained by assigning to the nominal power of the PV generator P_{PV} the values 2.5 kW, 5 kW and 10 kW are reported. Each image shows the trend of e_{dtl}, e_{fb} and e_{fg} by varying p_b for five different values of the nominal power of the wind generator P_W, 2.5 kW, 5 kW, 7.5 kW, 10 kW and 15 kW, with P_L and C_B constants.

Figure 8 - Energy fraction sent directly to the load, energy fraction drawn from the battery and energy fraction taken from the grid as a function of the storage fraction. $P_L = 0.5\ kW$.

Figure 9 - Energy fraction sent directly to the load, energy fraction drawn from the battery and energy fraction taken from the grid as a function of the storage fraction. $P_L = 2.5\ kW$.

Figure 10 - Energy fraction sent directly to the load, energy fraction drawn from the battery and energy fraction taken from the grid as a function of the storage fraction. $P_L = 10\ kW$.

Figures 11-13 show, by varying the load fraction p_l, the trends of the energy fraction sent directly to the load e_{dtl}, energy fraction drawn from the battery e_{fb} and energy fraction extracted from the grid e_{fg} are reported. The figures are obtained considering three different values of the nominal power of the PV generator P_{PV}, 2.5 kW, 5 kW and 10 kW. In each figure, three images obtained by assigning to the nominal power of the wind generator P_W the values 2.5 kW, 7.5 kW and 15 kW are reported. Each image shows the trend of e_{dtl}, e_{fb} and e_{fg} by varying the load fraction p_l, for six different values of storage capacity C_B, 0 kWh, 2 kWh, 4 kWh, 6 kWh, 8 kWh, and 10 kWh, with P_W and P_{PV} costants.

Figure 11 - Energy fraction sent directly to the load, energy fraction drawn from the battery and energy fraction taken from the grid as a function of the storage fraction. $P_{PV} = 2.5\ kW$.

Figure 12 - Energy fraction sent directly to the load, energy fraction drawn from the battery and energy fraction taken from the grid as a function of the storage fraction. $P_{PV} = 5\ kW$

Figure 13 - Energy fraction sent directly to the load, energy fraction drawn from the battery and energy fraction taken from the grid as a function of the storage fraction. $P_{PV} = 10\ kW$.

4.1.2. Comparison of the LB and GEB

Figures 14-16 show a comparison, through unitary histograms obtained as the sum of different color bars, of the LB (on the right), and the GEB (on the left). The histograms were obtained for different values of load P_L, storage capacity C_B, and nominal power of the PV generator P_{PV} and wind generator P_W. Setting the previous values:

- the GEB is expressed by the sum of the energy fraction sent directly to the load e_{dtl}/e_g (green), of the energy fraction sent to the battery e_{tb}/e_g (blue), and the energy fraction in excess sent to the grid e_{tg}/e_g (yellow);
- the LB is expressed by the sum of the energy fraction sent directly to the load e_{dtl} (light blue), of the energy fraction taken from the battery e_{fb} (cyan) and of the energy fraction taken from the grid e_{fg} (red).

Figure 14 – (a) and (b) GEB and LB for different load values without the storage battery; (c) and (d) GEB and LB in the presence of storage battery for $P_L = 0.5\ kW$.

Figure 15 – GEB and LB in the presence of the storage battery. $P_L = 1\ kW$; $P_L = 2.5\ kW$.

Figure 16 – GEB and LB in the presence of the storage battery. $P_L = 5\ kW$; $P_L = 10\ kW$.

Images 14a and 14b concerns the system configurations in the absence of storage battery, $C_B = 0$, and the histograms are related to different values of P_L and P_{PV}. Fixed P_L and P_{PV}, the five bars, from left toward right, represent the increasing values of P_W. Images 14c and 14d and each image of Figures 15 and 16, relative to a given value of P_L, is obtained by varying C_B and P_{PV}. Fixed C_B and P_{PV}, the five bars, from left toward right represent increasing values of P_W. The comparison of the HPWBS with HPWS shows that the presence of the battery, highlighted by the ratios e_{tb}/e_g and e_{fb}: in GEB, does not modify e_{dtl}/e_g and leads to a reduction of di e_{tg}/e_g; in the LB, determines a reduction of e_{fg} with e_{dtl} constant. In addition, Figures 14-16 permit indirect determination of the utilization factor f_u and the PV-wind fraction $f_{pv,w}$. The f_u value is obtained from the histograms of the GEB by summing e_{dtl}/e_g and e_{tb}/e_g (green and blue bar), while the $f_{pv,w}$ value is obtained from the histograms of the LB adding up e_{dtl} and e_{fb} (light blue and cyan bar). Consequently, to identify the PV-wind fraction and utilization factor, it is necessary read the corresponding value in the ordinate axes to the cumulative histogram of the first two bars.

4.1.3. General considerations on the LB and GEB

From the previous parametric analysis, both in the absence and presence of the storage battery, the following considerations can be deduced:

- an increase in nominal power of the wind and PV generators results in a reduction of the energy fraction extracted from the grid, with an increase of the energy fraction produced in excess; by increasing the wind fraction, the variation of the fractions of the LB and GEB is determined by the load value and storage capacity. This is due to the time shift between the availability of wind power and solar power and the load.
- A rise in load determines an increase of the energy fraction from the grid and a reduction of the energy fraction in excess.
- The energy fraction sent directly to the load, which appears in the LB, increases as the nominal powers of the wind and PV generator grow, and it decreases as the load value increases. In addition, it is not determined by the storage capacity; this is due to the operation mode of the system, which gives priority in the distribution of the energy produced to the satisfaction of the load and, in the case of excess energy, to the charge of the battery.

- The energy fraction sent directly to the load, that appears in the GEB, regardless of the storage capacity, with the increase of the wind and PV nominal powers, for low loads is reduced while for high loads increases; this is due to the variation of the energy fraction in excess when the nominal powers increases. The energy fraction in excess for low loads increases significantly whereas for high loads the increase is less remarkable.

The presence of the storage battery causes a reduction in the energy fraction drawn from the grid and energy fraction produced in excess; these reductions are more evident by raising the storage capacity, since the energy fraction in excess recovered is higher. As regards, the energy fraction drawn from the battery:

- for small nominal power of the generators and storage capacity, it is reduced when the load increases, since the energy produced is mainly sent to the load;
- for high values of the nominal power of the generators and storage capacity, there is a load value where the stored energy fraction is maximum and, independently of the nominal power of the generators, a subsequent load value above which the energy fraction drawn from the battery is null, since there is no recoverable energy fraction in excess;
- an increase of the nominal power of the generators determines a reduction in the produced energy fraction stored by the battery for reduced load values, and an increase for higher load values; this is due to the sharp increase in the energy fraction sent directly to the load for reduced loads, while for high loads this increase is limited.

In addition, the results obtained can be employed valuably also to evaluate the energy reliability of the same HPWB but stand-alone in the locality considered. In this case, as previously highlighted in Section 2.5.2, the main indicator is the PV-wind fraction, which identifies the energy missing to meet the load. Instead, the utilization factor, which is complementary to that of the energy produced in excess, becomes energy to be dissipated.

4.1.4. Analytic correlations

Figure 17 shows, as a function of the load overall fraction p_{hbl}, the values of the energy fractions which appear in the LB and GEB, and the values of the reliability indicators f_u and $f_{pv,w}$. In particular, image 17a shows the energy fractions e_{dtl}/e_g and e_{tb}/e_g; image 17b e_{tg}/e_g and f_u; image 17c e_{dtl} and e_{fb}; image 17d e_{fg} and $f_{pv,w}$.

Figure 17 – a) and b) Energy fractions of the LB and PV-wind fraction; c) and d) energy fractions of the GEB and utilization factor.

The figures show the energy fractions that appear in the LB and GEB are dependent on p_{hbl}; this parameter influences the two energy balances to a more remarkable extent than the p_w, p_b and p_l parameters. In particular, the fractions e_{dtl} and e_{fg} have a high correlation with a low dispersion for $p_{hbl} \leq 0.15$ and a growing dispersion for higher values of p_{hbl}. Instead, the e_{fb} fraction presents a reduced dispersion throughout the variation range of p_{hbl}.

Even fractions e_{tg}/e_g and e_{dtl}/e_g are dependent on p_{hbl} with a higher dispersion than the fractions of the LB, while for e_{tb}/e_g the dispersions are more pronounced.

Empiric equations obtained by the nonlinear regression technique, for the energy fractions of the LB are:

$$e_{dtl} = 0.4958\exp(-8.492\ p_{hbl}) + 0.3202\exp(-1.693\ p_{hbl}) \qquad R^2 = 0.9563 \qquad (42)$$

$$e_{fb} = -0.2659\exp(-10\ p_{hbl}) + 0.6071\exp(-11.4\ p_{hbl}) \qquad R^2 = 0.8743 \qquad (43)$$

$$e_{fg} = 0.8028\exp(0.1502\ p_{hbl}) - 0.9477\exp(-8.959\ p_{hbl}) \qquad R^2 = 0.9711 \qquad (44)$$

For the energy fractions of the GEB, the empiric equations are:

$$e_{tg}/e_g = \exp(-18.31\ p_{hbl}) \qquad R^2 = 0.8599 \qquad (45)$$

$$e_{dtl}/e_g = 1 - \exp(-12.12\ p_{hbl}) \qquad R^2 = 0.9308 \qquad (46)$$

The e_{tb}/e_g empiric equation can be obtained through the Eq. (32).

As regards the empiric equations of the indicators f_u and $f_{pv,w}$, as they have complementary trends to e_{tg}/e_g and e_{fg}, they can be obtained by Eqs. (37)-(38). These correlations can be used to evaluate the p_{hbl} value, which permits obtaining a predefined value of energy fractions that appear in the LB and the GEB, the utilization factor and the PV-wind fraction. After determining the value of p_{hbl} and, once known the hourly average daily power required by the load P_L, it is possible to determine the overall nominal power of the system P_n required.

Images 17c and 17d permit identification of the variation range of p_{hbl} within which f_u and $f_{pv,w}$ show the highest values. In addition, they show that with an p_{hbl} increase is associated a reduction of f_u and a rise of $f_{pv,w}$. For this reason, for the identification of the most energy reliable system configurations, a trade-off multi-objective optimization is required.

4.2. Multi-objective optimization

The parametric analysis results were employed to develop an energy reliability multi-objective optimization based on the Pareto-front method and on the ERC method described, respectively, in Sections 2.5.1 and 2.5.2. The multi-objective optimization consists in the identification of the system configurations that simultaneously ensure high values of the utilization factor of the generated energy f_u and PV-wind fraction $f_{pv,w}$ used to meet the load.

In Figures 18-22, for each value of the considered load P_L, there is a comparison of the values of f_u and $f_{pv,w}$ at the variation of the storage capacity C_B, and for the different values of nominal power of the PV generator P_{PV} and wind generator P_W. For the determination of the points that identify the optimal configurations, each image reports a graphical representation of the Pareto-front and constraint and objective function values employed in the ERC method.

Figure 18 – Results of the multi-objective optimization analysis. $P_L = 0.5\ kW$.

Figure 19 – Results of the multi-objective optimization analysis. $P_L = 1\ kW$.

Figure 20 – Results of the multi-objective optimization analysis. $P_L = 2.5\ kW$.

Figure 21 – Results of the multi-objective optimization analysis. $P_L = 5\ kW$.

Figure 22 – Results of the multi-objective optimization analysis. $P_L = 10\ kW$.

4.2.1. Pareto front method

Figures 18-22 show that, for all load values, almost all system configurations on the Pareto-front have a storage capacity of the battery equal to the maximum (10 kWh). For fixed values of the PV and wind power, as battery capacity decreases, the points move away from the Pareto-front determining a reduction of both of f_u and $f_{pv,w}$. Furthermore, as the load increases, the Pareto-front moves towards higher values of utilization factors and lower values of the PV-wind fraction.

Table 3 reports the PV, wind and battery nominal powers, and the corresponding indicators values associated with the Pareto-front points for each load value.

Table 3 – Pareto-front optimal HPWBS configurations

The table highlights the trade-off behavior of the optimization problem as, for each load value, with an increase of an indicator is associated a reduction of the other one. In particular, an increase in the nominal power of the PV or wind generator results in a rise of $f_{pv,w}$ and a reduction of f_u. Since high values of f_u and $f_{pv,w}$ are simultaneously requested to an energy reliability grid-connected HPWBS, then some Pareto-front optimal system configurations have a low energy reliability. In addition, the table shows that different values of the overall nominal power installed P_n correspond to these optimal configurations.

4.2.2. Energy reliability-constrained (ERC) method

The identification of the most energy reliable system configurations requires the ERC method application. Moreover, this method allows to take into account power P_n by means of the use of the manufacturability indicator h_{hl}, which normalize the energy delivered to the load compared to the nominal power installed. Since for the grid-connected hybrid system considered the number of indicators to be constrained and to be optimized are equal to, respectively, m=2 and n=1, then this goal has been achieved: (i) tracing the quadrant (light red in Figures 18-22) which identifies the system configurations that satisfies the constraints described in Section 2.5.2, in this case $\bar{f}_{pv,w} = 0.60$ and $\bar{f}_u = 0.60$; (ii) identifying the system configurations within this quadrant resulting in the higher values of manufacturability h_{hl}.

For a load of 5 kW and 10 kW, no system configuration falls within the selected quadrant. For loads of 0.5 kW, 1 kW and 2.5 kW, in the selected quadrant, are shown only the optimal system configurations with the maximum values of h_{hl} in hours/year. For these system configurations, Table 4 reports, for load values P_L of 0.5 kW, 1 kW and 2.5 kW, the nominal powers of the PV generator P_{PV} and wind generator P_W, maximum storable energy in one hour from the battery P_B, overall power of the system P_n, wind fraction p_w, storage fraction p_b, load fraction p_l, and load overall fraction p_{hbl}. Furthermore, the energy fractions that appear in the GEB and LB, Eqs. (26), (30)-(32), values of the utilization factor f_u, PV-wind fraction $f_{pv,w}$ and manufacturability h_{hl} are reported.

Table 4 – ERC optimal HPWBS configurations

The table shows that the optimal HPWBS configurations obtained with the ERC method, unlike the Pareto-front optimal configurations, are not necessarily those with the maximum battery capacity. The optimal configurations are characterized by a load overall fraction p_{hbl} between 0.05 and 0.11,

storage fraction p_b from 0.17 to 0.55, and wind fraction p_w between 0.33 and 0.75. These system configurations ensure e_{dtl} values between 0.48 and 0.64, e_{fb} values between 0.08 and 0.30, e_{fg} values between 0.12 and 0.40, e_{dtl}/e_g values between 0.46 and 0.74, e_{tb}/e_g values between 0.09 and 0.28, and e_{tg}/e_g values between 0.07 and 0.39. In these conditions, the reliability indicators are included in the following ranges: f_u between 0.61 and 0.93, $f_{pv,w}$ between 0.60 and 0.88, and h_{hl} between 335 hours and 556 hours.

5. Conclusions

The ERC method proposed, for the multi-objective optimization of hybrid systems, employs several indicators to identify the most energy reliable system configurations. It can be applied easily to a grid-connected and stand-alone PV-wind hybrid system with and without storage battery, in any climate context and load conditions, and allows optimizing the system in accordance with the specific application and the objectives. In addition, it can be applied in both the design phase and performance verification phase of a specific HPWBS.

The ERC method was applied to a grid-connected HPWBS and HPWS used to supply a variable load on an hourly basis in an urban residential context with Mediterranean climate, and it was compared with the Pareto-front multi-objective optimization classic method.

The results of the energy reliability parametric analysis, obtained considering 375 different system configurations, have showed that:

- the energy reliability is determined by the wind fraction, on the storage fraction and on the load fraction;
- the energy fractions that appear in the LB and GEB, turned out to be correlated strongly to load overall fraction, which takes into account the size of all components. The obtained empiric correlations are to be used for the system sizing;
- the presence of the storage battery gives rise to an increase in the utilization factor and the PV-wind fraction, which present complementary trends, respectively to that of the energy fraction in excess and to that of the energy fraction drawn from the grid.
- high values the PV-wind fraction, variable between 1 and 0.80, can be obtained with a load overall fraction ranging from 0 to 0.05, while high values of the utilization factor can be obtained throughout the variation range of load overall fraction.

In addition, the analysis parametric results can also be employed in the locality considered to evaluate the energy reliability of the same hybrid system but stand-alone, with the PV-wind fraction that assumes the meaning of energy missing to meet the load.

The comparison between the ERC and Pareto-front multi-objective optimization methods has highlighted that:

- the Pareto-front optimal configurations are those with the highest values of the battery storage capacity, and among these configurations, just some assure a high energy reliability;
- the ERC method identifies the most energy reliable system configurations, which ensure simultaneously high values of the PV-wind fraction and utilization factor. These optimal configurations are not necessarily those with the maximum battery capacity; in addition, among these system configurations, the ERC method allows the selection of those with the greatest values of energy sent to the load per kW installed, by means the use of the further indicator manufacturability.

The optimal HPWBS, found by means of the ERC method, needs an overall nominal power of 10-20 times the daily average hourly load, a storage capacity of the battery between 17 % and 55 % of the overall nominal power, and a wind fraction between 33% and 75%. These system configurations ensure utilization factor values between 0.61 and 0.93, PV-wind fractions between 0.60 and 0.88, and a manufacturability between 335 hours and 556 hours/year.

References

1. A. Abbassi, M. A. Dami, M. Jemli, A statistical approach for hybrid energy storage system sizing based on capacity distributions in an autonomous PV/Wind power generation system. Renew Energy, Volume 103, 2017, Pages 81-93, ISSN 0960-1481, https://doi.org/10.1016/j.renene.2016.11.024.
2. A. Kaabeche, M. Belhamel, R. Ibtiouen, Sizing optimization of grid-independent hybrid photovoltaic/wind power generation system, Energy, Volume 36, Issue 2, 2011,Pages 1214-1222, ISSN 0360-5442, https://doi.org/10.1016/j.energy.2010.11.024.
3. R. Maouedj, A. Mammeri, M.D. Draou, B. Benyoucef, Techno-economic Analysis of a Standalone Hybrid Photovoltaic-wind System. Application in Electrification of a House in Adrar Region, Energy Procedia, Volume 74, 2015, Pages 1192-1204, ISSN 1876-6102, https://doi.org/10.1016/j.egypro.2015.07.762.
4. B. Getachew, P. Björn, Feasibility study for a standalone solar–wind-based hybrid energy system for application in Ethiopia, Applied Energy Volume 87, Issue 2, 2010, Pages 487-495, ISSN 0306-2619, https://doi.org/10.1016/j.apenergy.2009.06.006.
5. N. Ghorbani, A. Kasaeian, A. Toopshekan, L. Bahrami, A. Maghami, Optimizing a Hybrid Wind-PV-Battery System Using GA-PSO and MOPSO for Reducing Cost and Increasing Reliability, Energy, 2017, ISSN 0360-5442, https://doi.org/10.1016/j.energy.2017.12.057
6. H.C. Chen, Optimum capacity determination of stand-alone hybrid generation system considering cost and reliability, Applied Energy, Volume 103, 2013, Pages 155-164, ISSN 0306-2619, https://doi.org/10.1016/j.apenergy.2012.09.022.
7. T. Ma, H. Yang, L. Lu, A feasibility study of a stand-alone hybrid solar–wind– battery system for a remote island, Applied Energy, Volume 121, 2014, Pages 149-158, ISSN 0306-2619, https://doi.org/10.1016/j.apenergy.2014.01.090..
8. B. Ould Bilal, V. Sambou, P.A. Ndiaye, C.M.F. Kébé, M. Ndongo, Optimal design of a hybrid solar–wind-battery system using the minimization of the annualized cost system and the minimization of the loss of power supply probability (LPSP), Renewable Energy, Volume 35, Issue 10, 2010, Pages 2388-2390, ISSN 0960-1481, https://doi.org/10.1016/j.renene.2010.03.004.
9. P.S. Georgilakis, Y.A. Katsigiannis, Reliability and economic evaluation of small autonomous power systems containing only renewable energy sources, Renewable Energy, Volume 34, Issue 1, 2009, Pages 65-70, ISSN 0960-1481, https://doi.org/10.1016/j.renene.2008.03.004.
10. A. Kaabeche, S. Diaf, R. Ibtiouen, Firefly-inspired algorithm for optimal sizing of renewable hybrid system considering reliability criteria, Solar Energy, Volume 155, 2017, Pages 727-738, ISSN 0038-092X, https://doi.org/10.1016/j.solener.2017.06.070.
11. S. Diaf, D. Diaf, M. Belhamel, M. Haddadi, A. Louche, A methodology for optimal sizing of autonomous hybrid PV/wind system, Energy Policy, Volume 35, Issue 11,2007, Pages 5708-5718, ISSN 0301-4215, https://doi.org/10.1016/j.enpol.2007.06.020.
12. S. Diaf, M. Belhamel, M. Haddadi, A. Louche, A. Technical and economic assessment of hybrid photovoltaic/wind system with battery storage in Corsica Island, Energy Policy, Volume 36, Issue 2, 2008, Pages 743-754, ISSN 0301-4215, https://doi.org/10.1016/j.enpol.2007.10.028.
13. S. Diaf, G. Notton, M. Belhamel, M. Haddadi, A. Louche, Design and techno-economical optimization for hybrid PV/wind system under various meteorological conditions, Applied

Energy, Volume 85, Issue 10, 2008, Pages 968-987, ISSN 0306-2619, https://doi.org/10.1016/j.apenergy.2008.02.012.
14. F. Caballero, E. Sauma, F. Yanine, Business optimal design of a grid-connected hybrid PV (photovoltaic)-wind energy system without energy storage for an Easter Island's block, Energy, Volume 61, 2013, Pages 248-261, ISSN 0360-5442, https://doi.org/10.1016/j.energy.2013.08.030.
15. A. González, J.R. Riba, A. Rius, R. Puig, Optimal sizing of a hybrid grid-connected photovoltaic and wind power system, Applied Energy, Volume 154, 2015, Pages 752-762, ISSN 0306-2619, https://doi.org/10.1016/j.apenergy.2015.04.105.
16. M.Z. Daud, A. Mohamed, M.A. Hannan, An improved control method of battery energy storage system for hourly dispatch of photovoltaic power sources, Energy Conversion and Management, Volume 73, 2013, Pages 256-270, ISSN 0196-8904, https://doi.org/10.1016/j.enconman.2013.04.013.
17. S. Sinha, S.S. Chandel, Review of recent trends in optimization techniques for solar photovoltaic–wind based hybrid energy systems, Renewable and Sustainable Energy Reviews, Volume 50,
2015, Pages 755-769, ISSN 1364-0321, https://doi.org/10.1016/j.rser.2015.05.040.
18. A. Mahesh, K.S. Sandhu, Hybrid wind/photovoltaic energy system developments: Critical review and findings, Renewable and Sustainable Energy Reviews, Volume 52, 2015, Pages 1135-1147,
ISSN 1364-0321, https://doi.org/10.1016/j.rser.2015.08.008.
19. V. Khare, S. Nema, P. Baredar, Solar – wind hybrid renewable energy system: A review, Renewable and Sustainable Energy Reviews, Volume 58, 2016, Pages 23-33, ISSN 1364-0321, https://doi.org/10.1016/j.rser.2015.12.223.
20. R. Luna-Rubio, M. Trejo-Perea, D. Vargas-Vázquez, G.J. Ríos-Moreno, Optimal sizing of renewable hybrids energy systems: A review of methodologies, Solar Energy, Volume 86, Issue 4, 2012, Pages 1077-1088, ISSN 0038-092X, https://doi.org/10.1016/j.solener.2011.10.016.
21. H.R. Baghaee, M. Mirsalim, G.B. Gharehpetian, H.A. Talebi, Reliability/cost-based multi-objective Pareto optimal design of stand-alone wind/PV/FC generation microgrid system, Energy, Volume 115, Part 1, 2016, Pages 1022-1041, ISSN 0360-5442, https://doi.org/10.1016/j.energy.2016.09.007.
22. L.G. Acuña, R.V. Padilla, A.S. Mercado, Measuring reliability of hybrid photovoltaic-wind energy systems: A new indicator, Renewable Energy, Volume 106, 2017, Pages 68-77, ISSN 0960-1481, https://doi.org/10.1016/j.renene.2016.12.089.
23. M.A.M. Ramli, H.R.E.H. Bouchekara, A.S. Alghamdi, Optimal Sizing of PV/wind/diesel hybrid microgrid system using multi-objective self-adaptive differential evolution algorithm, Renewable Energy 2018, ISSN 0960-1481, https://doi.org/10.1016/j.renene.2018.01.058.
24. M.A. Ramli, A. Hiendro, Y.A. Al-Turki, Techno-economic energy analysis of wind/solar hybrid system: Case study for western coastal area of Saudi Arabia, Renewable Energy, Volume 91, 2016, Pages 374-385, ISSN 0960-1481, https://doi.org/10.1016/j.renene.2016.01.071.
25. S. Sinha, S.S. Chandel, Improving the reliability of photovoltaic-based hybrid power system with battery storage in low wind locations, Sustainable Energy Technologies and Assessments, Volume 19, 2017, Pages 146-159, ISSN 2213-1388, https://doi.org/10.1016/j.seta.2017.01.008.
26. S. Aissou, D. Rekioua, N. Mezzai, T. Rekioua, S. Bacha, Modeling and control of hybrid photovoltaic wind power system with battery storage, Energy Conversion and Management, Volume 89, 2015, Pages 615-625, ISSN 0196-8904, https://doi.org/10.1016/j.enconman.2014.10.034.
27. M. Boussetta, R. El Bachtiri, M. Khanfara, K. El Hammoumi Assessing the potential of hybrid PV–Wind systems to cover public facilities loads under different Moroccan climate conditions, Sustainable Energy Technologies and Assessments, Volume 22, 2017, Pages 74-82, ISSN 2213-1388, https://doi.org/10.1016/j.seta.2017.07.005.

28. O. Ekren, B.Y. Ekren, Size optimization of a PV/wind hybrid energy conversion system with battery storage using simulated annealing, Applied Energy, Volume 87, Issue 2, 2010, Pages 592-598, ISSN 0306-2619, https://doi.org/10.1016/j.apenergy.2009.05.022.
29. D.G. Erbs, S.A. Klein, J.A. Duffie, Estimation of the diffuse radiation fraction for hourly, daily and monthly-average global radiation, Solar Energy, Volume 28, Issue 4, 1982, Pages 293-302, ISSN 0038-092X, http://dx.doi.org/10.1016/0038-092X(82)90302-4.
30. J.A. Duffie, W.A. Beckman, Solar Engineering of Thermal Processes 4th Edition, Solar Energy Laboratory University of Wisconsin-Madison, John Wiley & Sons, 2013.
31. Fry, A. Bryan, Simulation of Grid-Tied Building Integrated Photovoltaic Systems. M. S. Thesis –Solar Energy Laboratory, University of Wisconsin, Madison: 1999.
32. R. Chenni, M. Makhlouf, T. Kerbache, A. Bouzid, A detailed modeling method for photovoltaic cells, Energy, Volume 32, Issue 9, 2007, Pages 1724-1730, ISSN 0360-5442, https://doi.org/10.1016/j.energy.2006.12.006.
33. D. L. King, J.A. Kratochvil, W.E. Boyson, Measuring the Solar Spectral and Angle-of-Incidence Effects on Photovoltaic Modules and Irradiance Sensors, Proceedings of the 1994 IEEE Photovoltaics Specialists Conference. Sept 30-Oct 3, 1997. pp. 1113-1116.
34. P. J. A. Quinlan, Time series modeling of hybrid wind photovoltaic diesel power systems. M. S. Thesis –Solar Energy Laboratory, University of Wisconsin, Madison: 1996.
35. TRNSYS; Version 17. (2012) Solar Energy Laboratory University of Wisconsin-Madison: Madison, WI, USA.
36. A.M. Kanakkithodi, G. Pilania, R. Ramprasad, T. Lookman, J.E. Gubernatis, Multi-objective optimization techniques to design the Pareto front of organic dielectric polymers, Computational Materials Science, Volume 125, 2016, Pages 92-99, ISSN 0927-0256, https://doi.org/10.1016/j.commatsci.2016.08.018.
37. M. Kottek, J. Grieser, C. Beck, B. Rudolf, F. Rubel, World Map of the Köppen-Geiger climate classification updated, Meteorologische Zeitschrift 15.3 (2006): 259-263. DOI: 10.1127/0941-2948/2006/0130.
38. Sharp Energy Solutions, Hamburg (Germany). Website: www.sharp.eu/cps/rde/xchg/eu/, last access: 23/02/2018.
39. Angel Wind Energy Inc., Onarga, IL (United States). Website: www.angelwindenergy.com/ , last access: 23/02/2018.
40. LG Chem Michigan Inc., Seoul (Korea). Website: www.lgchem.com/, last access: 23/02/2018.
41. EPsolar Technology CO., Ltd., Beijing (China). Website: www.epsolarpv.com, last access: 23/02/2018.
42. Ditta 3T s.r.l., Perugia (Italy). Website: www.ditta3t.com, last access: 23/02/2018.
43. ABB Ltd., Zürich(Switzerland). Website: www.abb.com/, last access: 23/02/2018.
44. Steca Elektronik GmbH, Memmingen (Germany). Website: www.steca.com, last access: 23/02/2018.

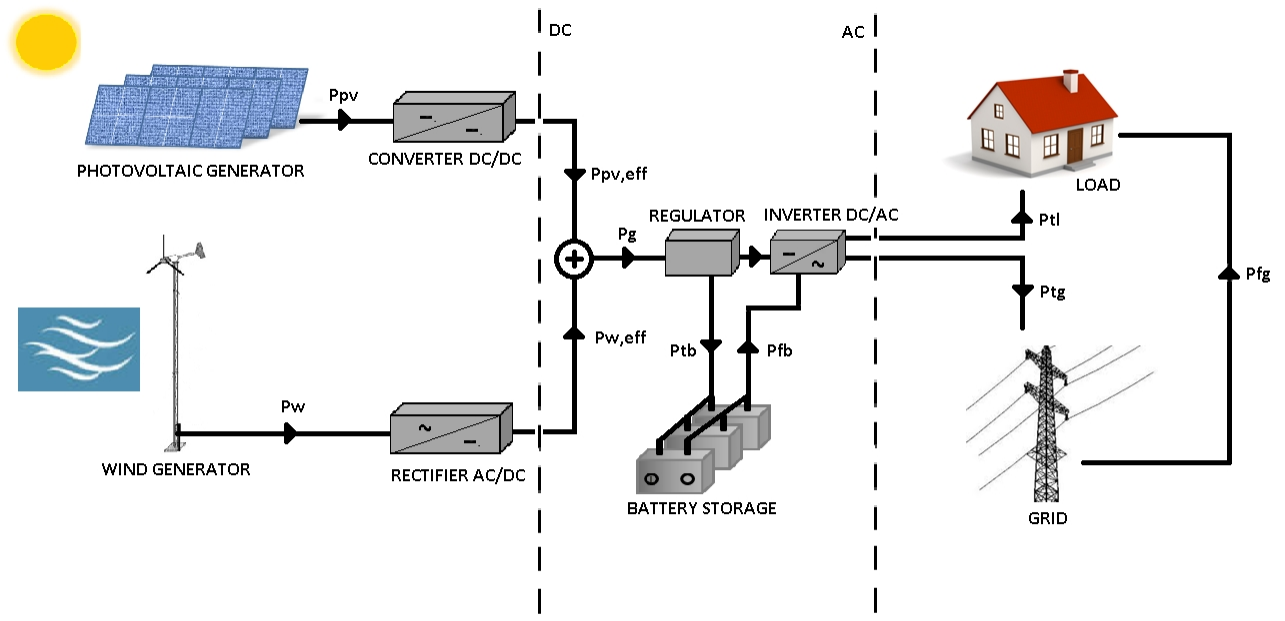
DC
AC
Ppv
PHOTOVOLTAIC GENERATOR
CONVERTER DC/DC
Ppv,eff
REGULATOR
INVERTER DC/AC
Pg
LOAD
Ptl
Ptg
Pfg
Pw,eff
Ptb
Pfb
Pw
WIND GENERATOR
RECTIFIER AC/DC
BATTERY STORAGE
GRID

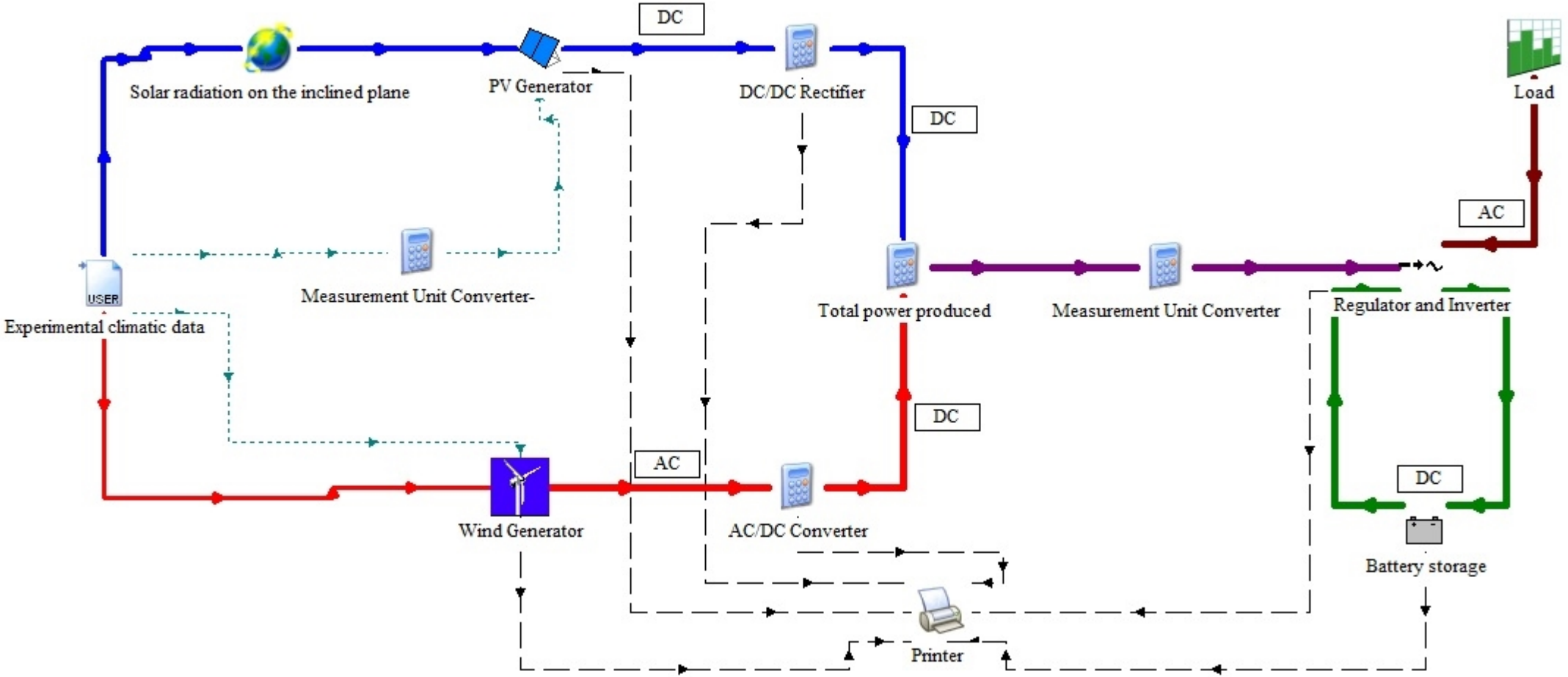
DC
Solar radiation on the inclined plane
PV Generator
DC/DC Rectifier
DC
Load
AC
USER
Experimental climatic data
Measurement Unit Converter-
Total power produced
Measurement Unit Converter
Regulator and Inverter
DC
AC
Wind Generator
AC/DC Converter
DC
Battery storage
Printer

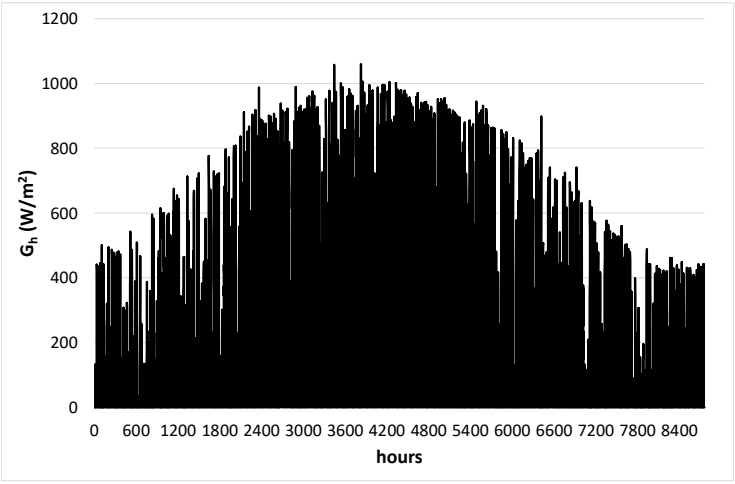
1200
1000
800
600
400
200
0
G_h (W/m²)
0 600 1200 1800 2400 3000 3600 4200 4800 5400 6000 6600 7200 7800 8400
hours

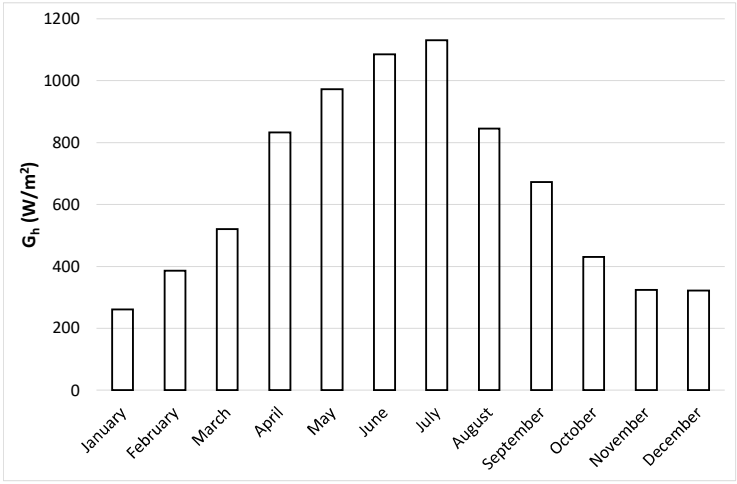
1200
1000
800
600
400
200
0
G_h (W/m²)
January
February
March
April
May
June
July
August
September
October
November
December

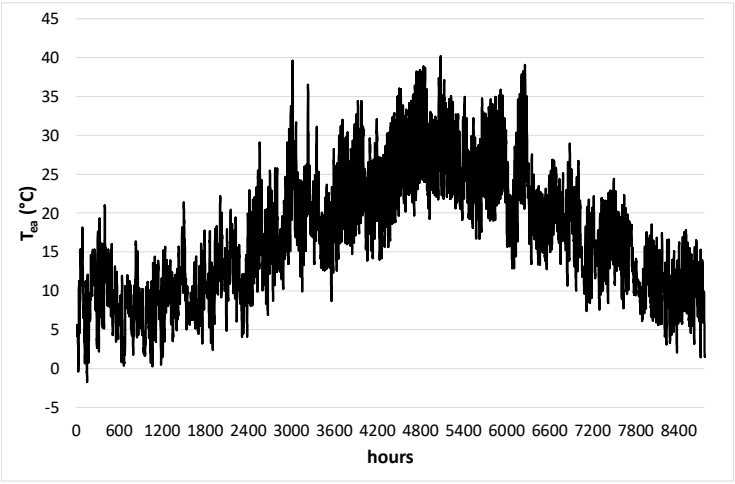
45
40
35
30
25
20
15
10
5
0
-5
T_{ea} (°C)
0 600 1200 1800 2400 3000 3600 4200 4800 5400 6000 6600 7200 7800 8400
hours

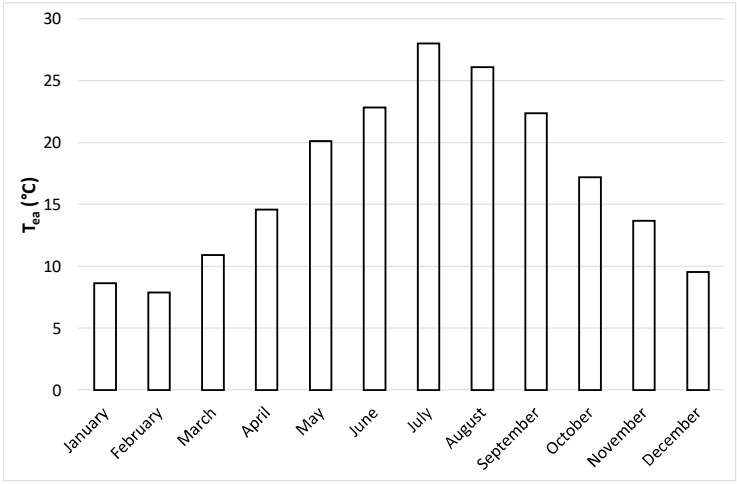
30
25
20
15
10
5
0
T_{ea} (°C)
January
February
March
April
May
June
July
August
September
October
November
December

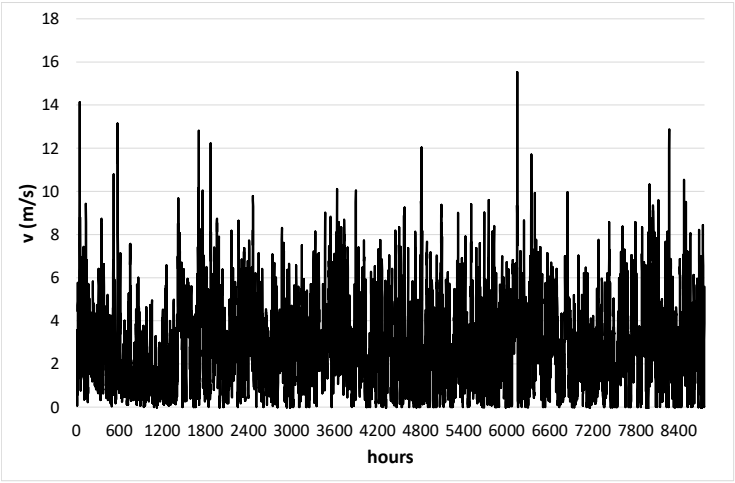
18
16
14
12
10
8
6
4
2
0
v (m/s)
0 600 1200 1800 2400 3000 3600 4200 4800 5400 6000 6600 7200 7800 8400
hours

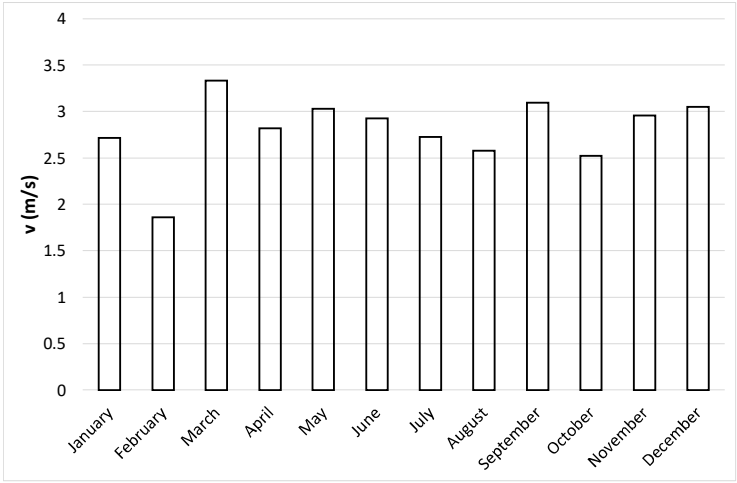
4
3.5
3
2.5
2
1.5
1
0.5
0
v (m/s)
January
February
March
April
May
June
July
August
September
October
November
December

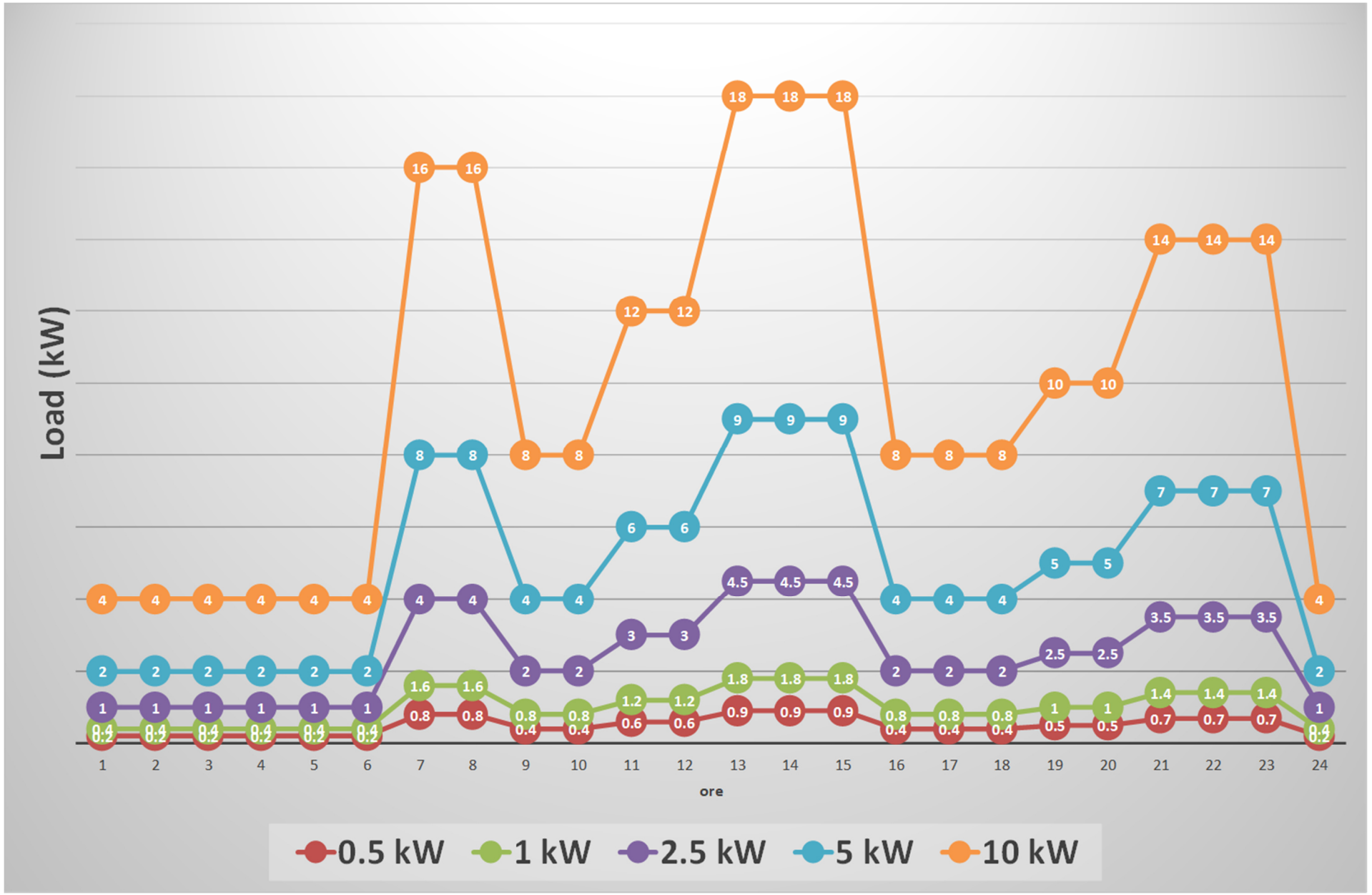
Load (kW)
ore
1 2 3 4 5 6 7 8 9 10 11 12 13 14 15 16 17 18 19 20 21 22 23 24
0.5 kW
1 kW
2.5 kW
5 kW
10 kW

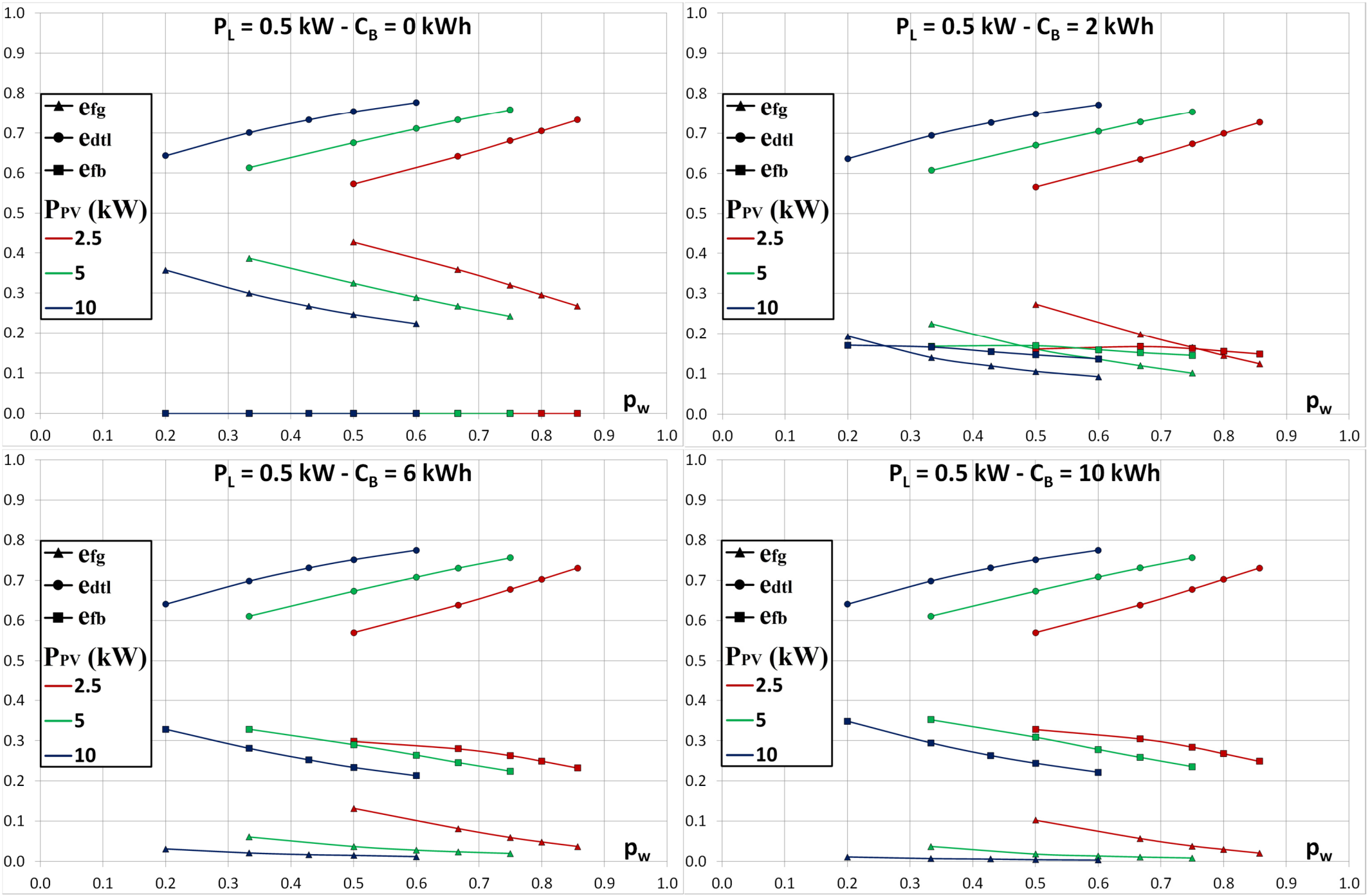
P_L = 0.5 kW - C_B = 0 kWh
P_L = 0.5 kW - C_B = 2 kWh
P_L = 0.5 kW - C_B = 6 kWh
P_L = 0.5 kW - C_B = 10 kWh
efg
edtl
efb
PPV (kW)
2.5
5
10
pw
0.0
0.1
0.2
0.3
0.4
0.5
0.6
0.7
0.8
0.9
1.0

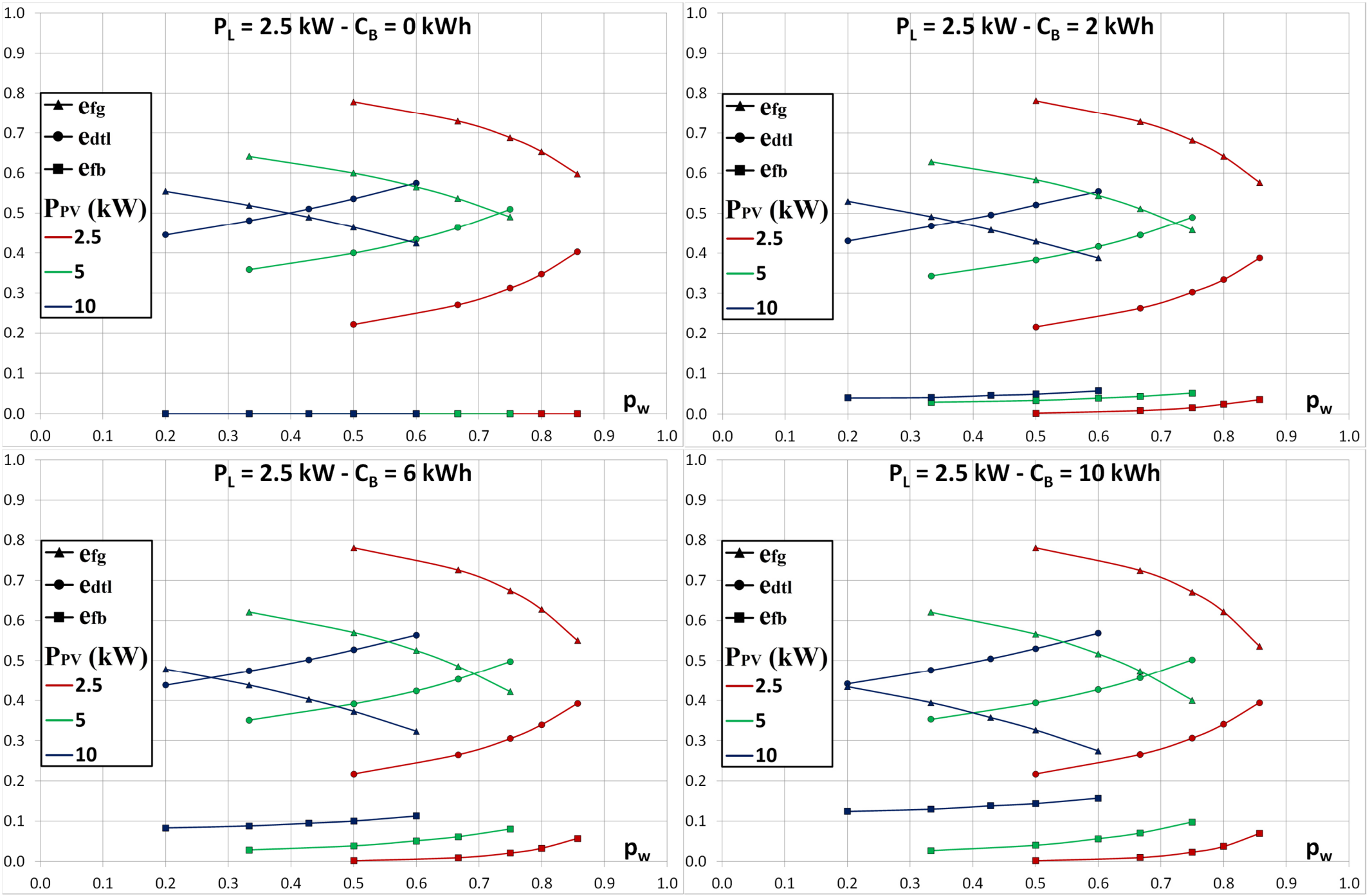
P_L = 2.5 kW - C_B = 0 kWh
P_L = 2.5 kW - C_B = 2 kWh
P_L = 2.5 kW - C_B = 6 kWh
P_L = 2.5 kW - C_B = 10 kWh
efg
edtl
efb
PPV (kW)
2.5
5
10
pw

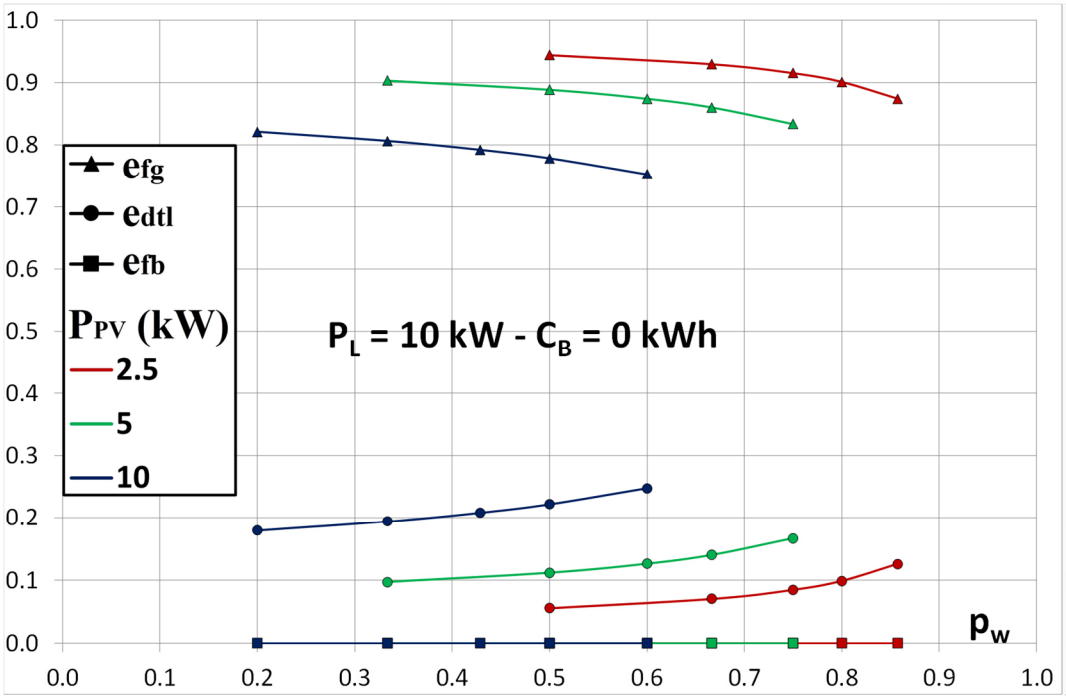
efg
edtl
efb
PPV (kW)
2.5
5
10
PL = 10 kW - CB = 0 kWh
pw

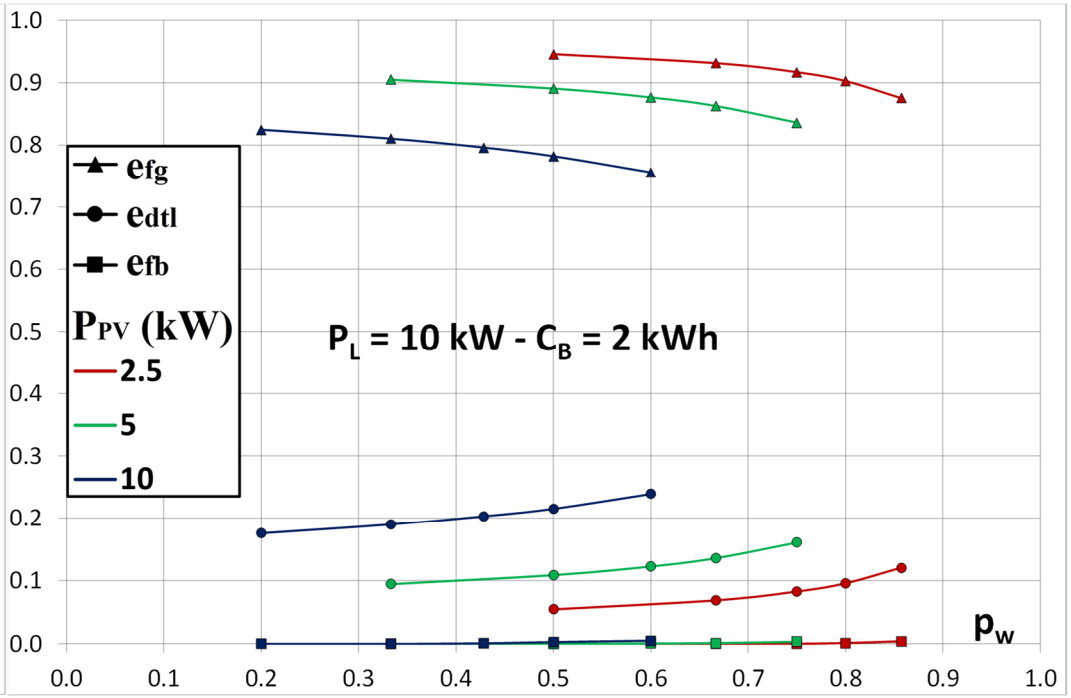
efg
edtl
efb
PPV (kW)
2.5
5
10
PL = 10 kW - CB = 2 kWh
pw

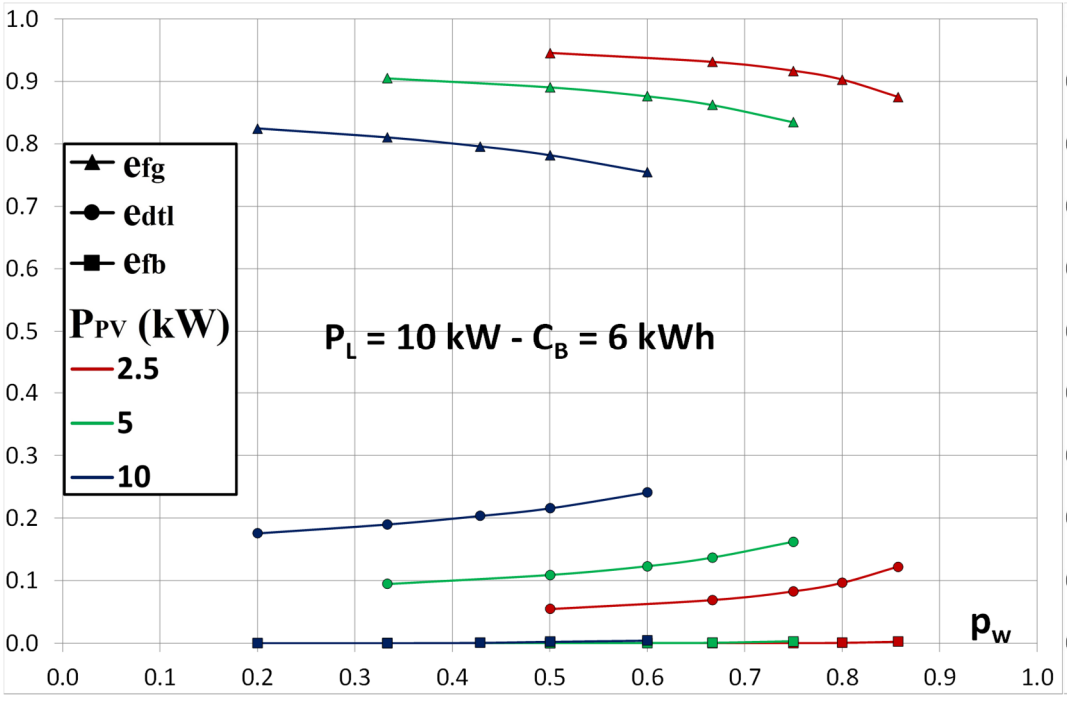
efg
edtl
efb
PPV (kW)
2.5
5
10
PL = 10 kW - CB = 6 kWh
pw

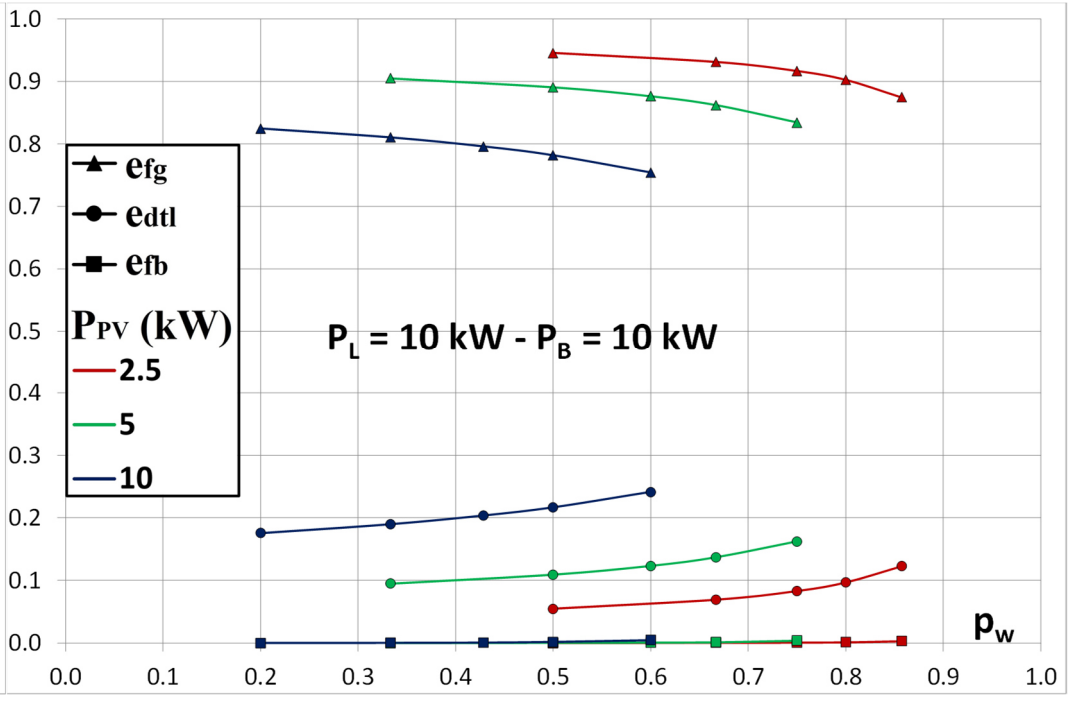
efg
edtl
efb
PPV (kW)
2.5
5
10
PL = 10 kW - PB = 10 kW
pw

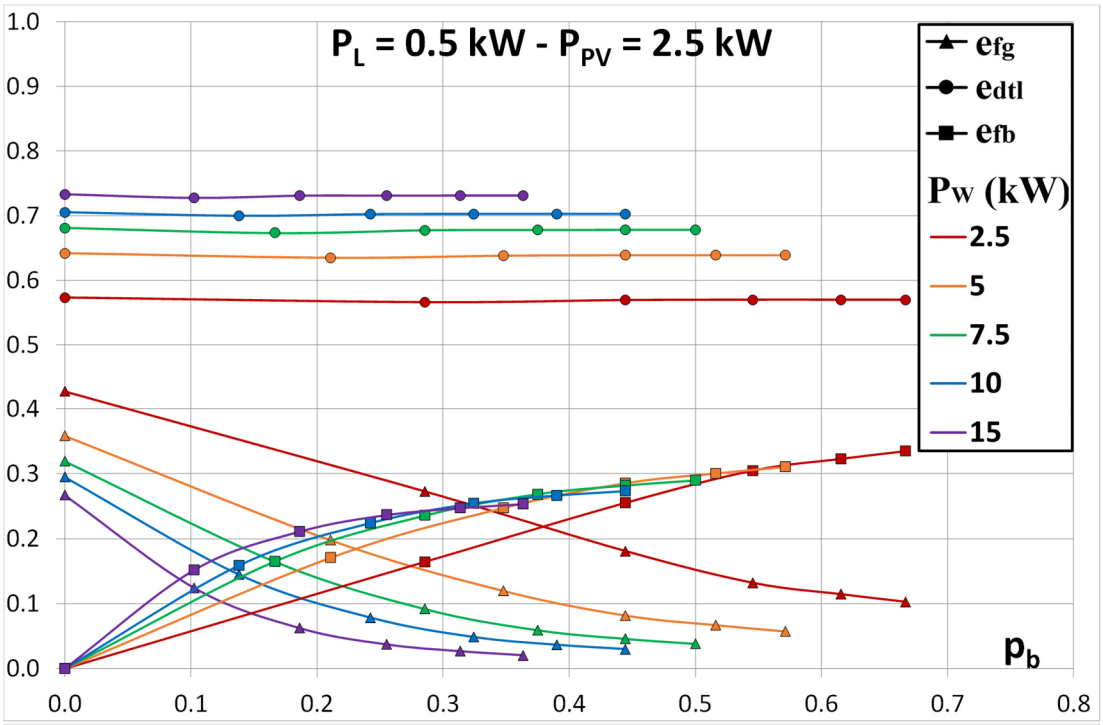
P_L = 0.5 kW - P_{PV} = 2.5 kW
efg
edtl
efb
Pw (kW)
2.5
5
7.5
10
15
pb

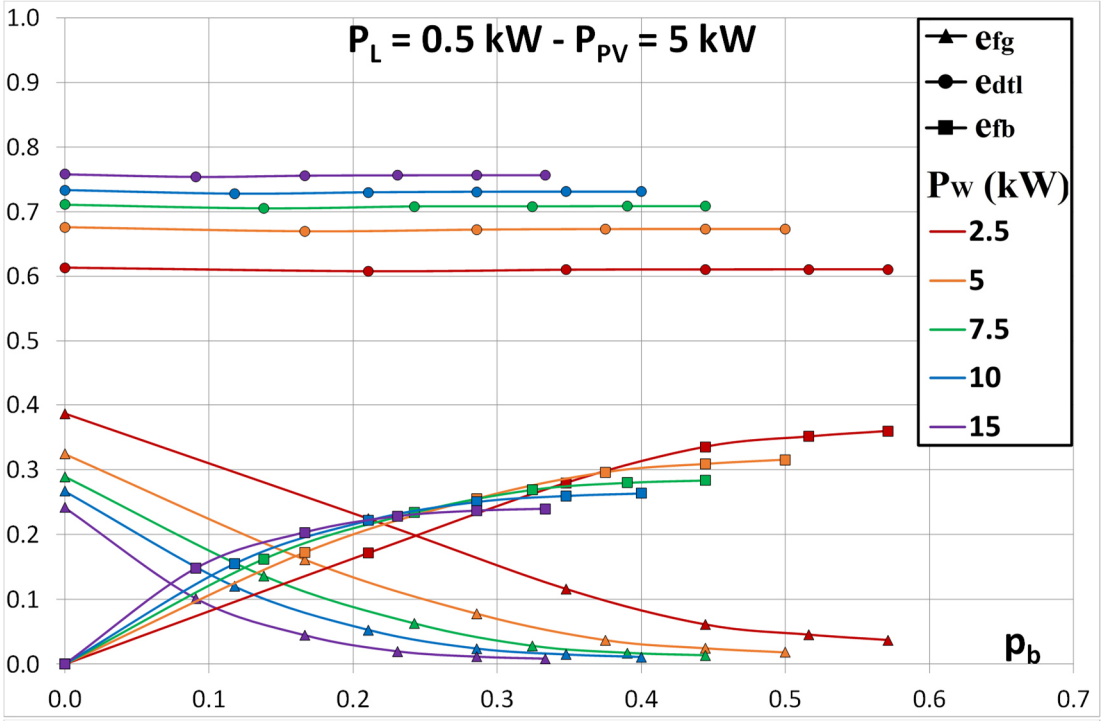
P_L = 0.5 kW - P_{PV} = 5 kW
efg
edtl
efb
Pw (kW)
2.5
5
7.5
10
15
pb

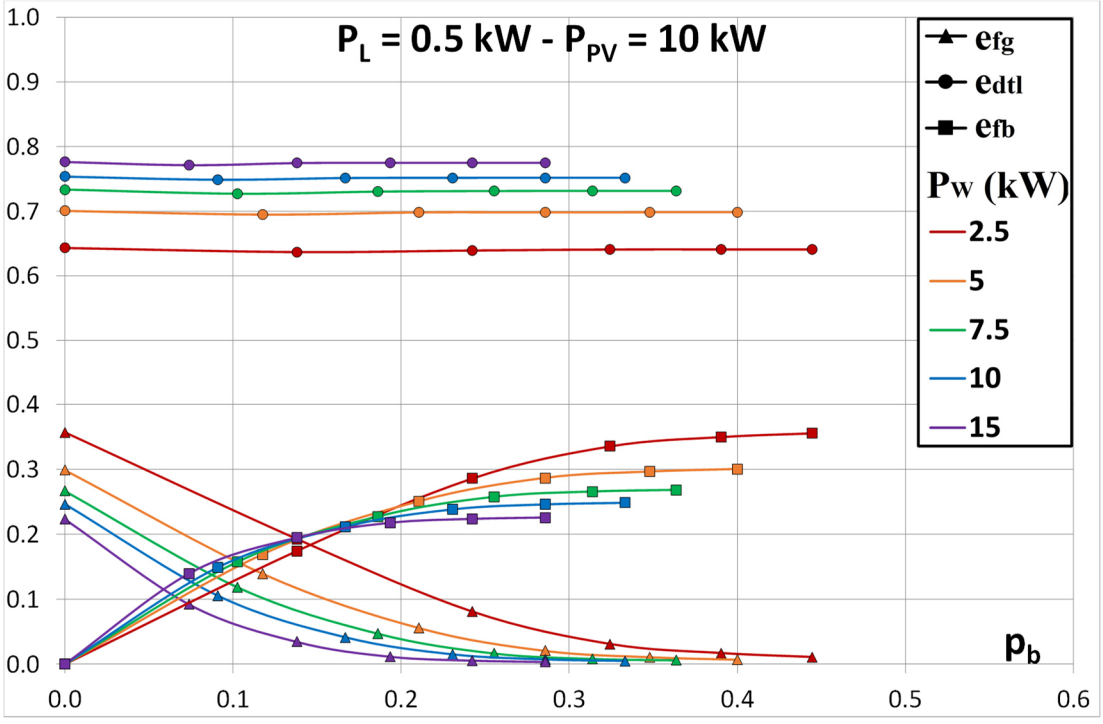
P_L = 0.5 kW - P_{PV} = 10 kW
efg
edtl
efb
Pw (kW)
2.5
5
7.5
10
15
pb

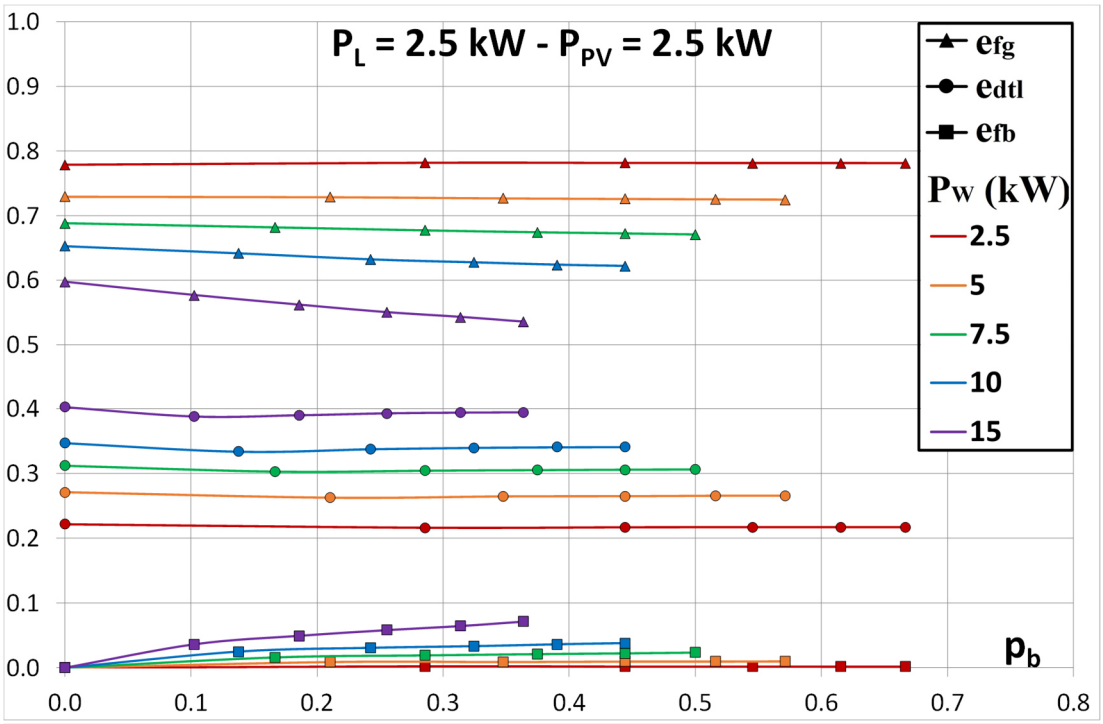
P_L = 2.5 kW - P_{PV} = 2.5 kW
efg
edtl
efb
Pw (kW)
2.5
5
7.5
10
15
pb

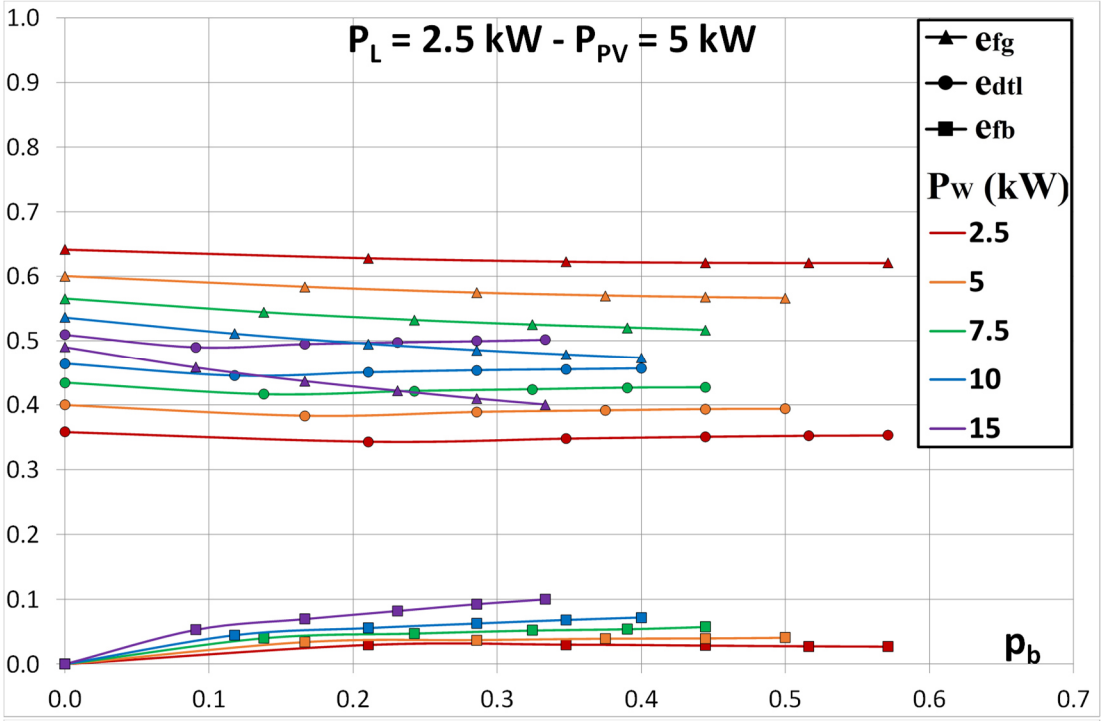
P_L = 2.5 kW - P_{PV} = 5 kW
efg
edtl
efb
Pw (kW)
2.5
5
7.5
10
15
pb

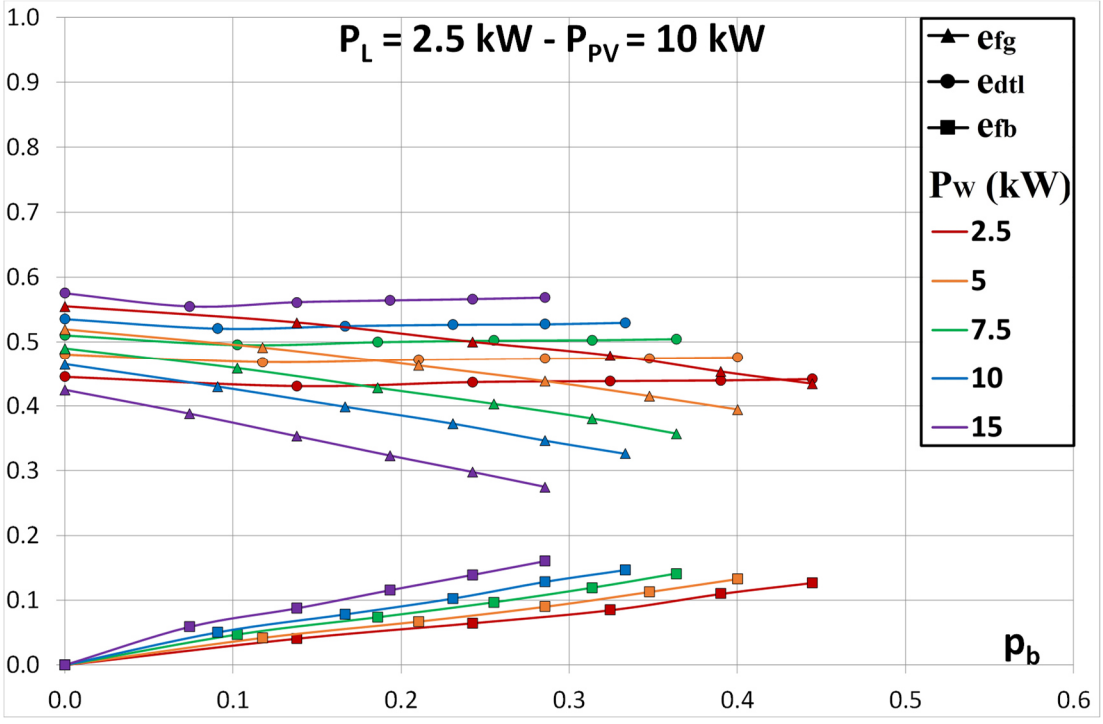
P_L = 2.5 kW - P_{PV} = 10 kW
efg
edtl
efb
Pw (kW)
2.5
5
7.5
10
15
pb

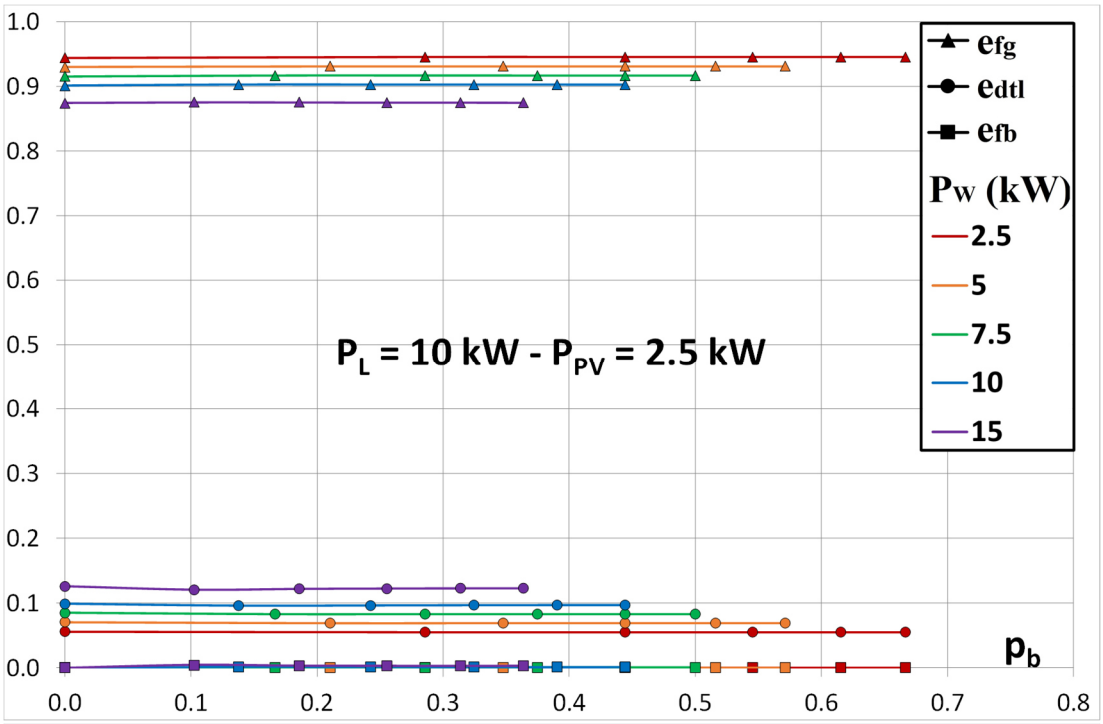
efg
edtl
efb
Pw (kW)
2.5
5
7.5
10
15
PL = 10 kW - PPV = 2.5 kW
pb

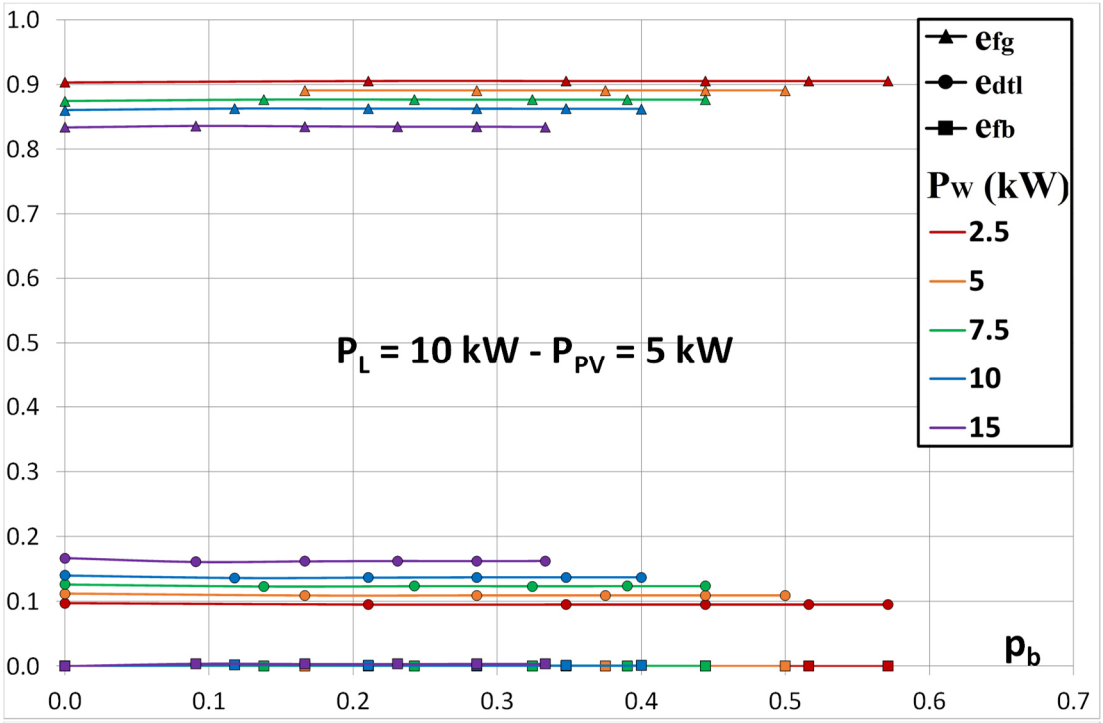
efg
edtl
efb
Pw (kW)
2.5
5
7.5
10
15
PL = 10 kW - PPV = 5 kW
pb

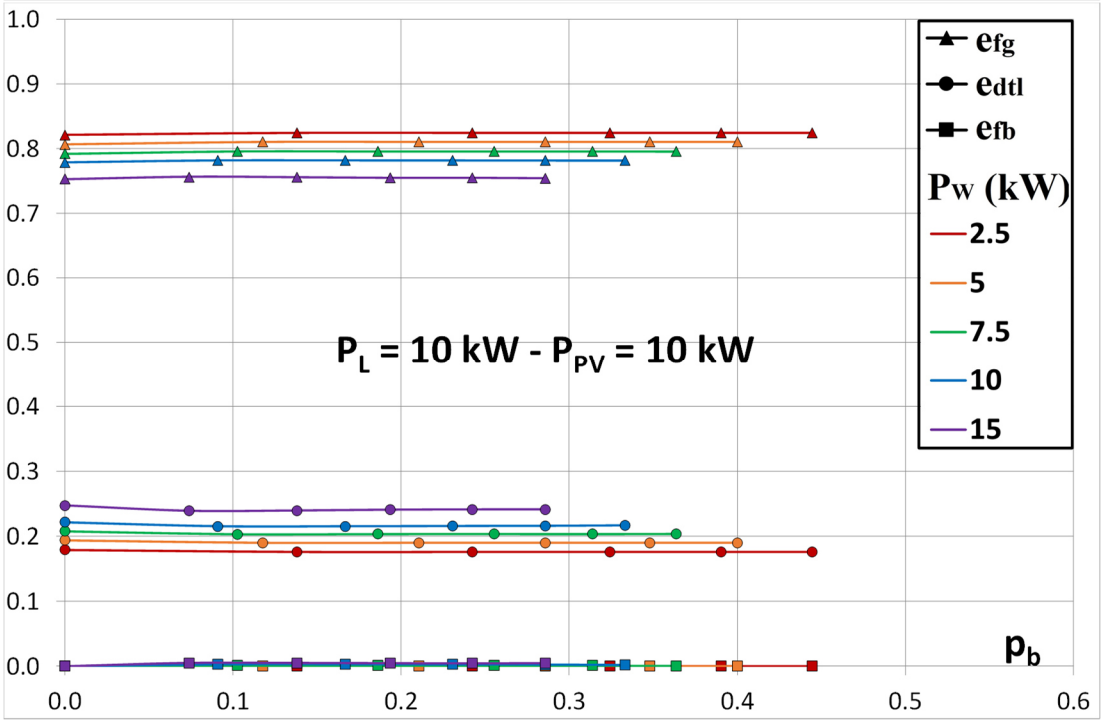
efg
edtl
efb
Pw (kW)
2.5
5
7.5
10
15
PL = 10 kW - PPV = 10 kW
pb

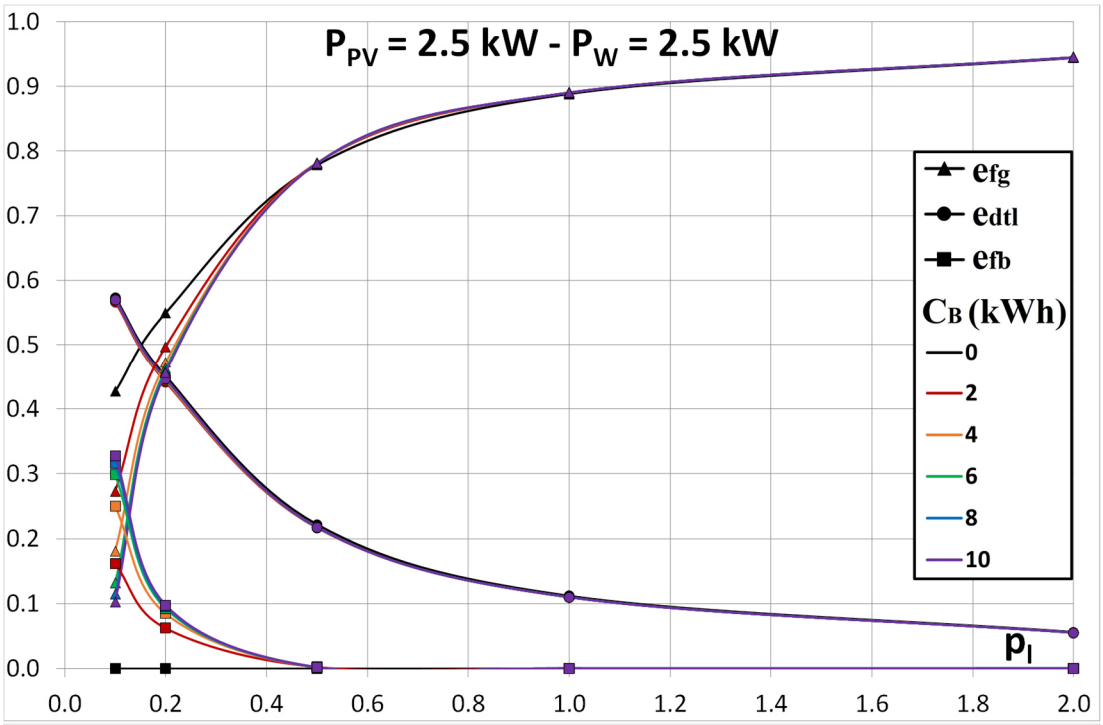
P_{PV} = 2.5 kW - P_W = 2.5 kW
e_{fg}
e_{dtl}
e_{fb}
C_B (kWh)
0
2
4
6
8
10
p_l

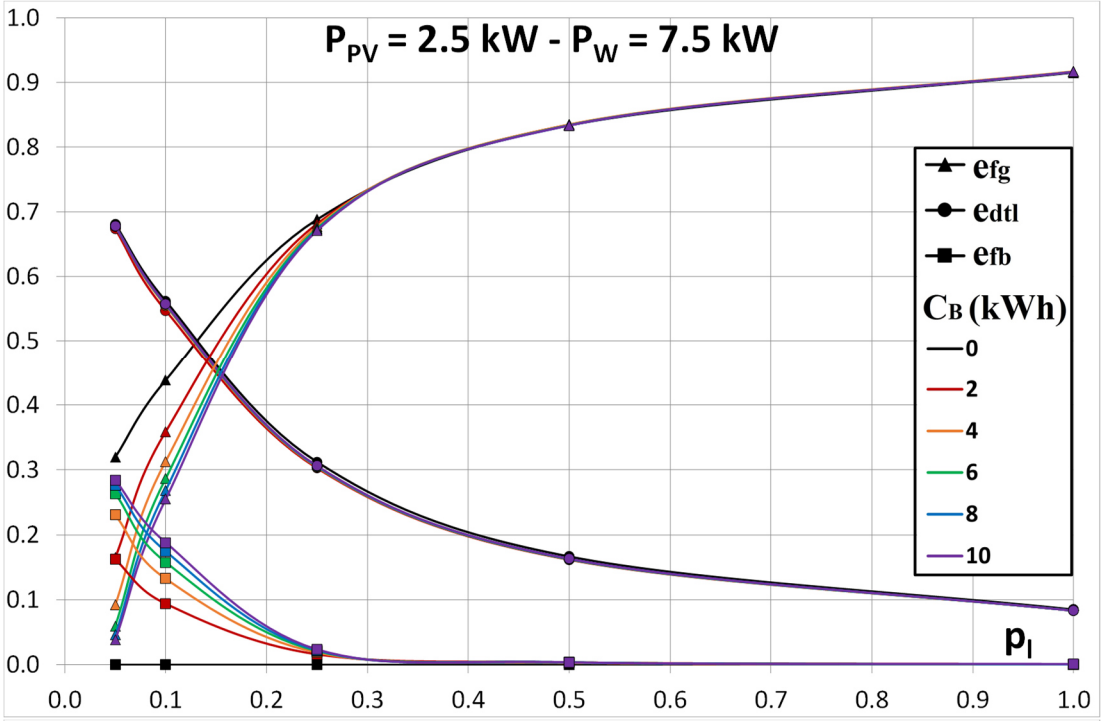
P_{PV} = 2.5 kW - P_W = 7.5 kW
e_{fg}
e_{dtl}
e_{fb}
C_B (kWh)
0
2
4
6
8
10
p_l

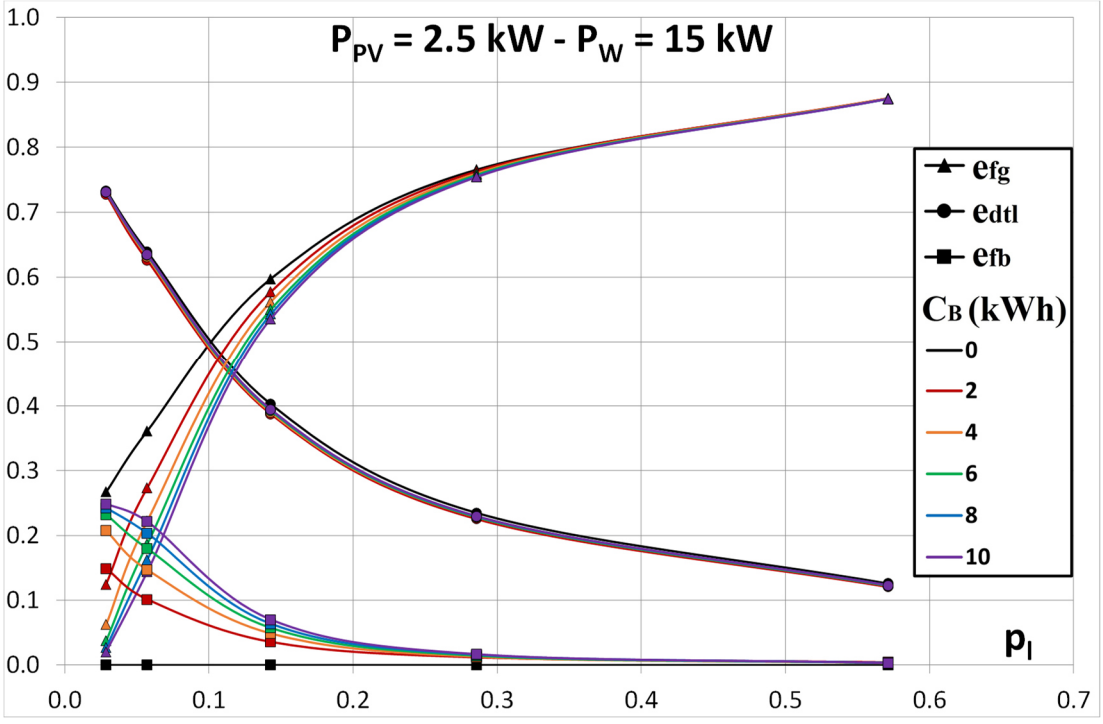
P_{PV} = 2.5 kW - P_W = 15 kW
e_{fg}
e_{dtl}
e_{fb}
C_B (kWh)
0
2
4
6
8
10
p_l

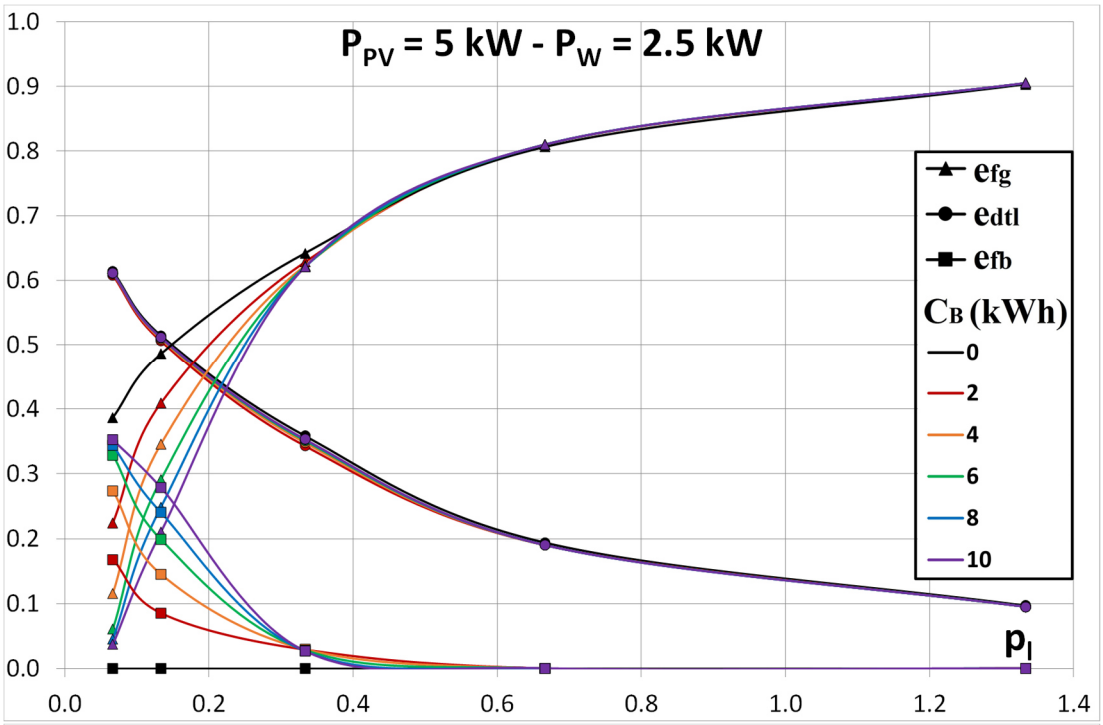
P_{PV} = 5 kW - P_W = 2.5 kW
efg
edtl
efb
CB (kWh)
0
2
4
6
8
10
pl

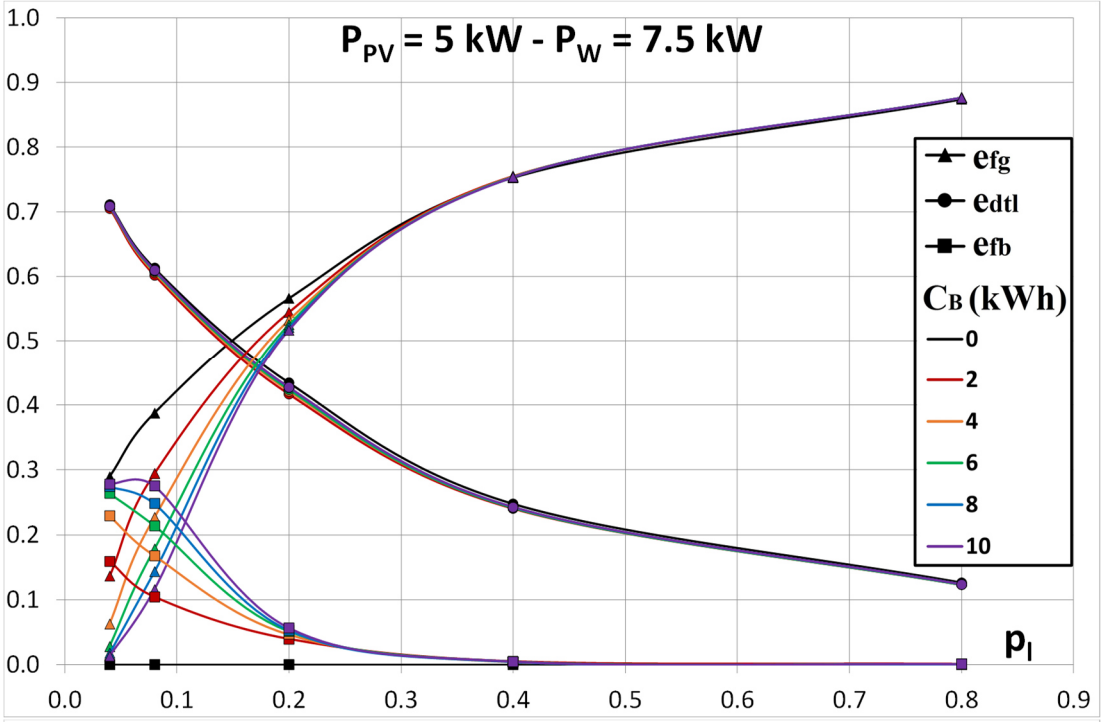
P_{PV} = 5 kW - P_W = 7.5 kW
efg
edtl
efb
CB (kWh)
0
2
4
6
8
10
pl

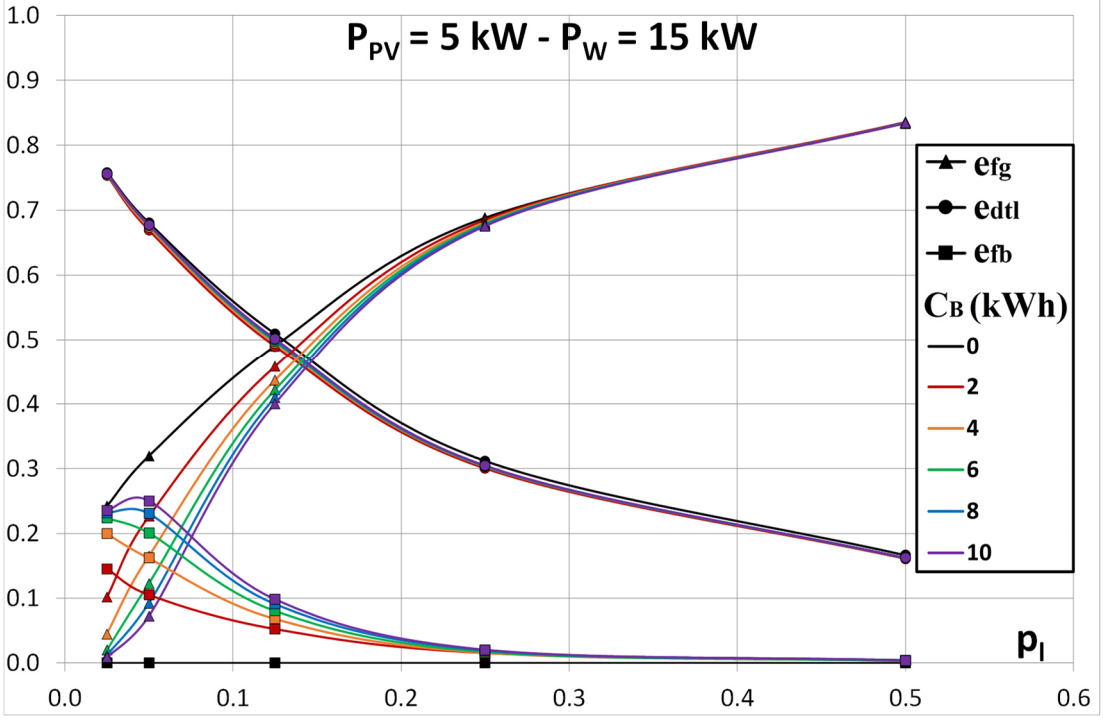
P_{PV} = 5 kW - P_W = 15 kW
efg
edtl
efb
CB (kWh)
0
2
4
6
8
10
pl

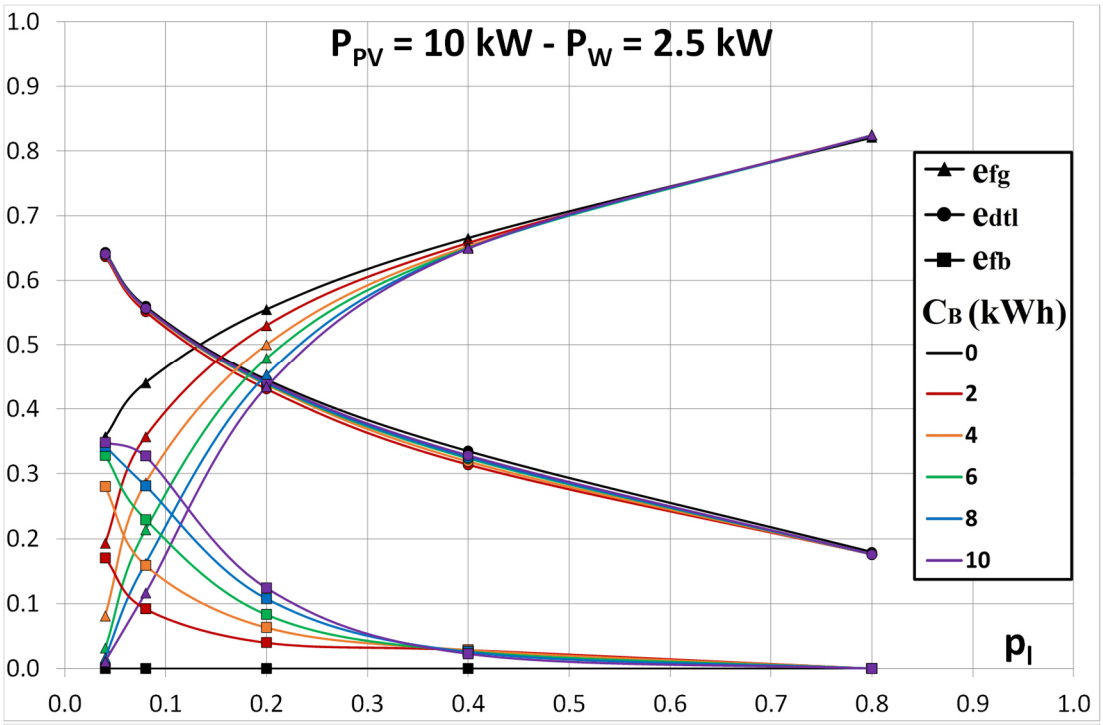
P_{PV} = 10 kW - P_W = 2.5 kW
e_{fg}
e_{dtl}
e_{fb}
C_B (kWh)
0
2
4
6
8
10
p_l

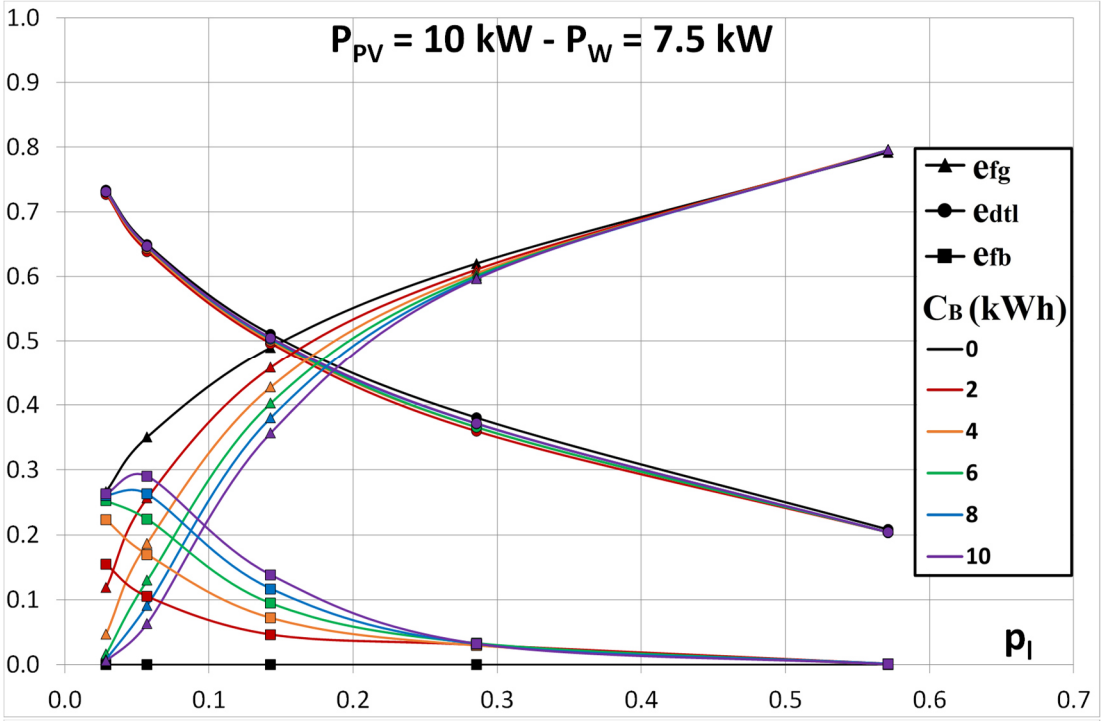
P_{PV} = 10 kW - P_W = 7.5 kW
e_{fg}
e_{dtl}
e_{fb}
C_B (kWh)
0
2
4
6
8
10
p_l

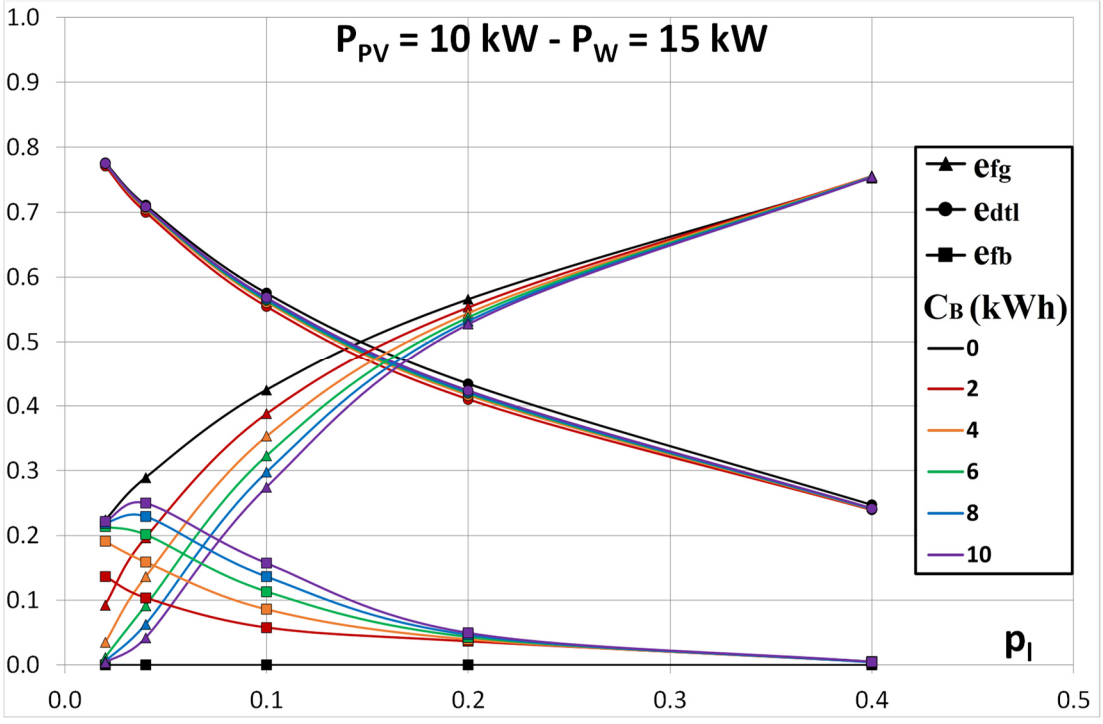
P_{PV} = 10 kW - P_W = 15 kW
e_{fg}
e_{dtl}
e_{fb}
C_B (kWh)
0
2
4
6
8
10
p_l

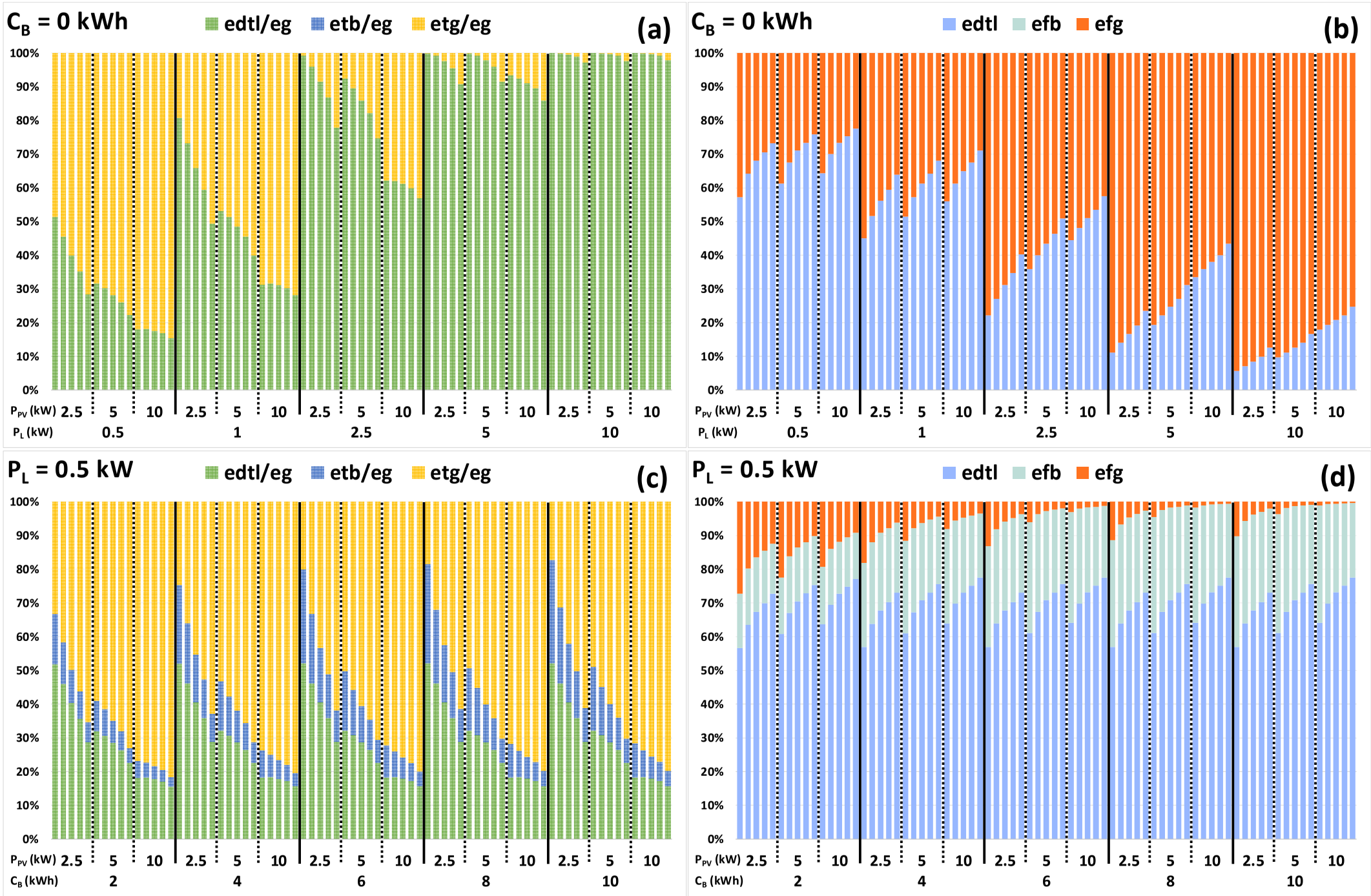
C_B = 0 kWh
edtl/eg
etb/eg
etg/eg
(a)
100%
90%
80%
70%
60%
50%
40%
30%
20%
10%
0%
P_{PV} (kW) 2.5 5 10 2.5 5 10 2.5 5 10 2.5 5 10 2.5 5 10
P_L (kW) 0.5 1 2.5 5 10
C_B = 0 kWh
edtl
efb
efg
(b)
P_{PV} (kW) 2.5 5 10 2.5 5 10 2.5 5 10 2.5 5 10 2.5 5 10
P_L (kW) 0.5 1 2.5 5 10
P_L = 0.5 kW
edtl/eg
etb/eg
etg/eg
(c)
P_{PV} (kW) 2.5 5 10 2.5 5 10 2.5 5 10 2.5 5 10 2.5 5 10
C_B (kWh) 2 4 6 8 10
P_L = 0.5 kW
edtl
efb
efg
(d)
P_{PV} (kW) 2.5 5 10 2.5 5 10 2.5 5 10 2.5 5 10 2.5 5 10
C_B (kWh) 2 4 6 8 10

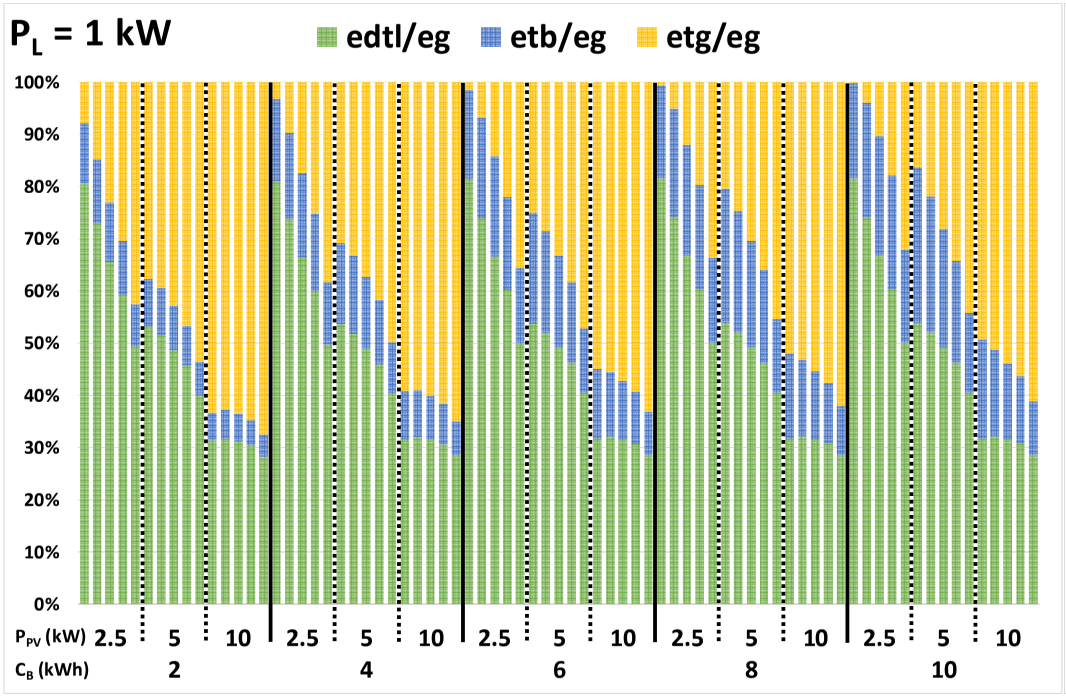
P_L = 1 kW
edtl/eg
etb/eg
etg/eg
100%
90%
80%
70%
60%
50%
40%
30%
20%
10%
0%
P_{PV} (kW) 2.5 5 10 2.5 5 10 2.5 5 10 2.5 5 10 2.5 5 10
C_B (kWh) 2 4 6 8 10

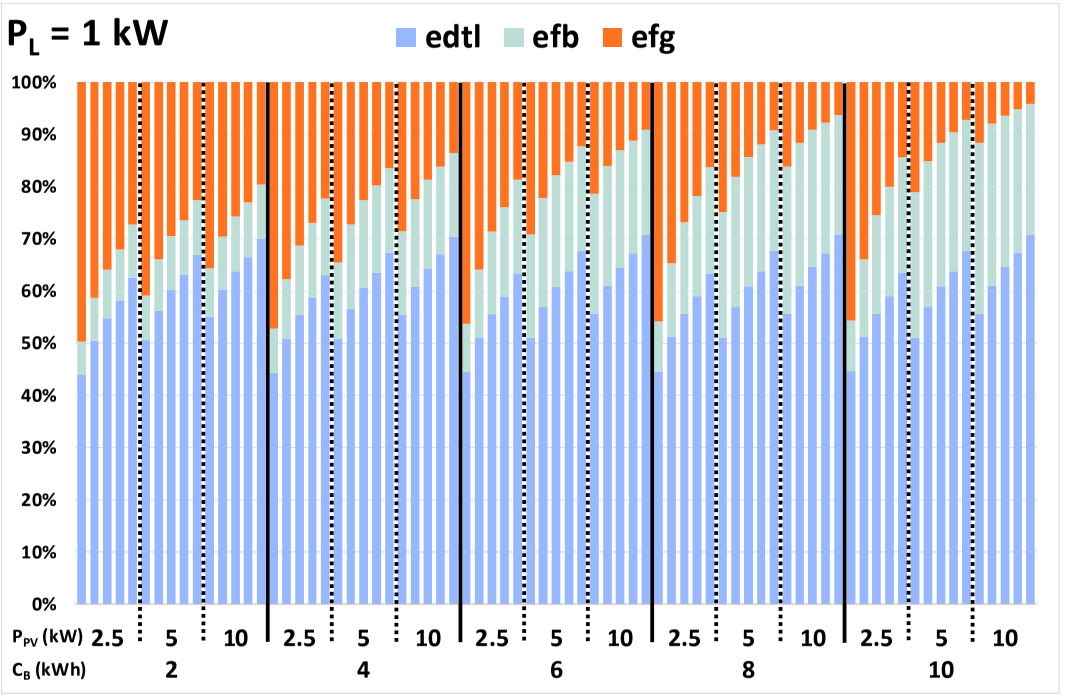
P_L = 1 kW
edtl
efb
efg
100%
90%
80%
70%
60%
50%
40%
30%
20%
10%
0%
P_{PV} (kW) 2.5 5 10 2.5 5 10 2.5 5 10 2.5 5 10 2.5 5 10
C_B (kWh) 2 4 6 8 10

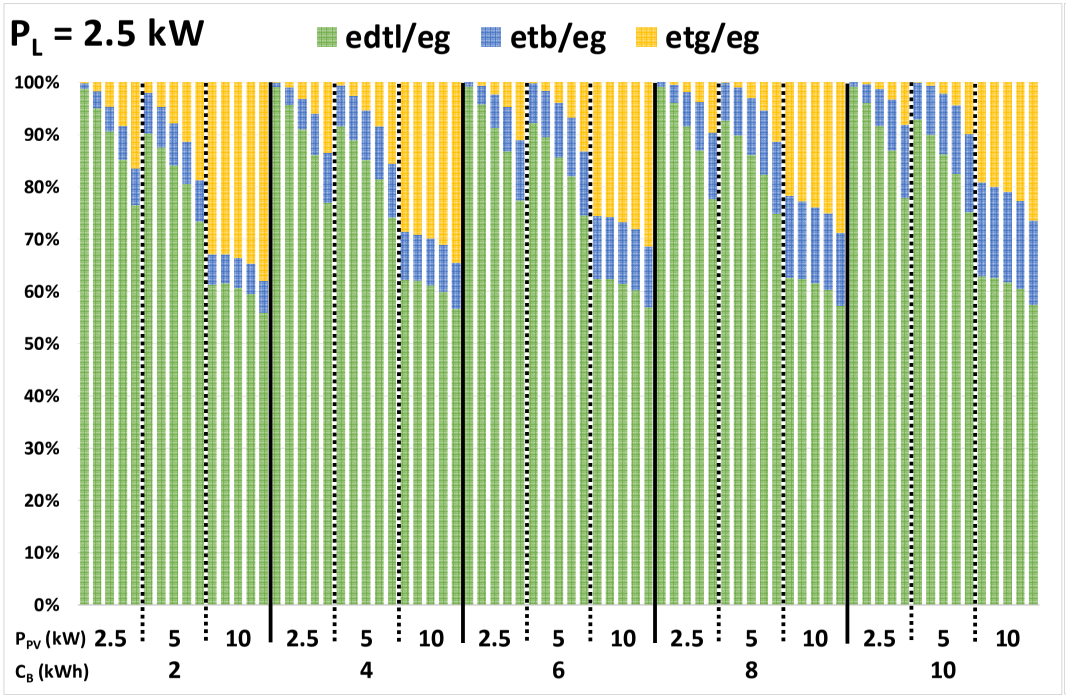
P_L = 2.5 kW
edtl/eg
etb/eg
etg/eg
100%
90%
80%
70%
60%
50%
40%
30%
20%
10%
0%
P_{PV} (kW) 2.5 5 10 2.5 5 10 2.5 5 10 2.5 5 10 2.5 5 10
C_B (kWh) 2 4 6 8 10

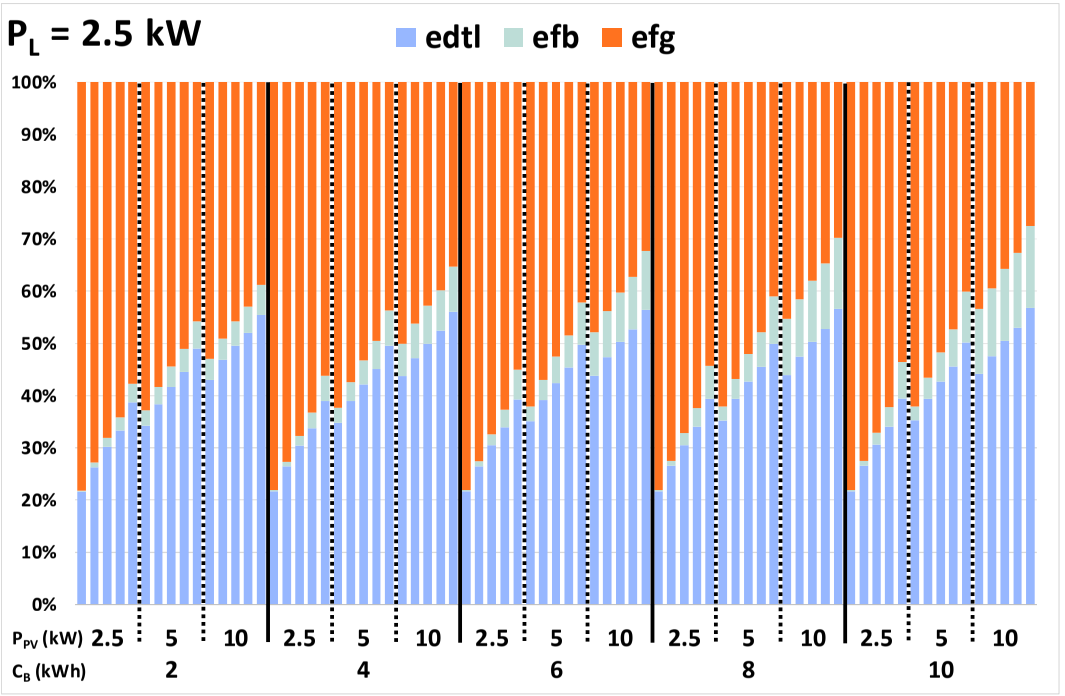
P_L = 2.5 kW
edtl
efb
efg
100%
90%
80%
70%
60%
50%
40%
30%
20%
10%
0%
P_{PV} (kW) 2.5 5 10 2.5 5 10 2.5 5 10 2.5 5 10 2.5 5 10
C_B (kWh) 2 4 6 8 10

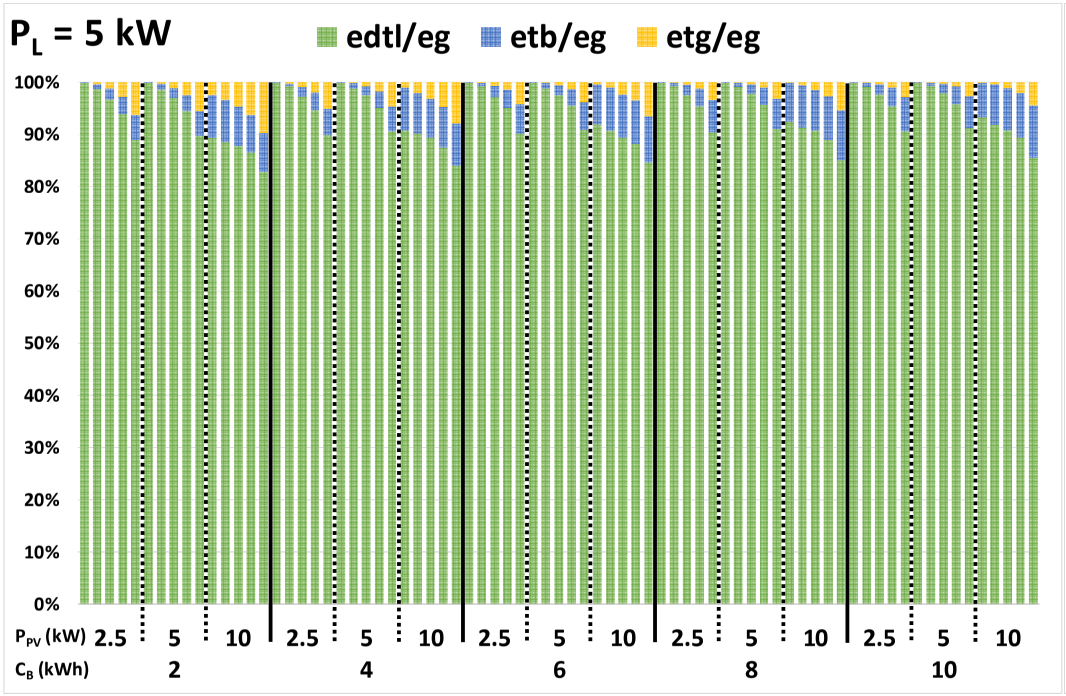
P_L = 5 kW
edtl/eg
etb/eg
etg/eg
100%
90%
80%
70%
60%
50%
40%
30%
20%
10%
0%
P_PV (kW) 2.5 5 10 2.5 5 10 2.5 5 10 2.5 5 10 2.5 5 10
C_B (kWh) 2 4 6 8 10

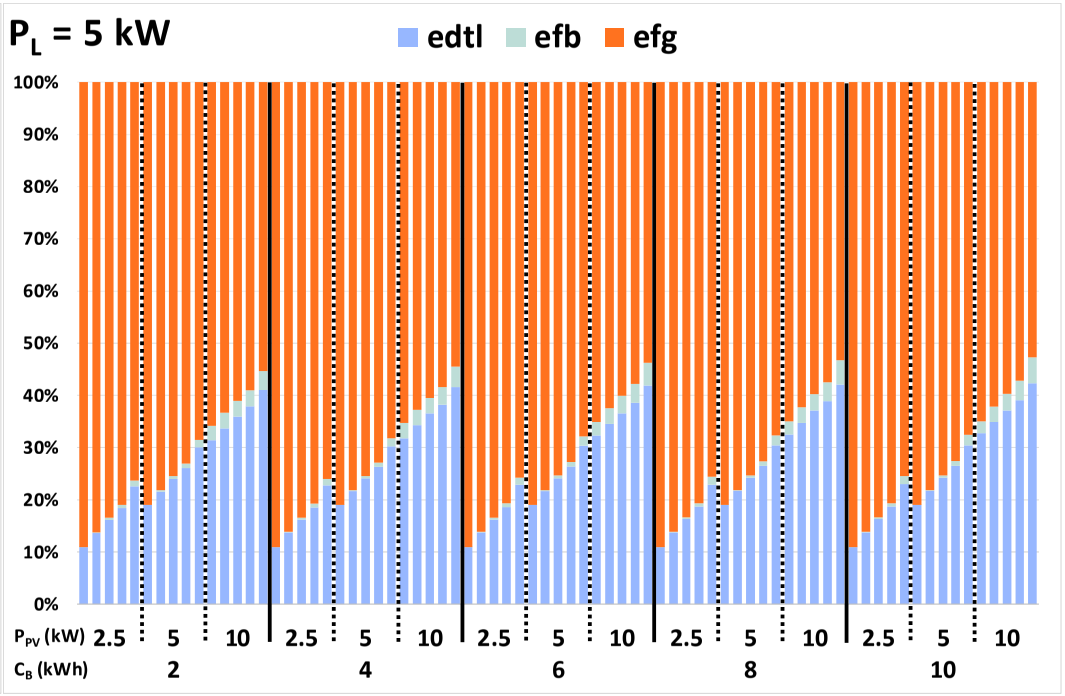
P_L = 5 kW
edtl
efb
efg
100%
90%
80%
70%
60%
50%
40%
30%
20%
10%
0%
P_PV (kW) 2.5 5 10 2.5 5 10 2.5 5 10 2.5 5 10 2.5 5 10
C_B (kWh) 2 4 6 8 10

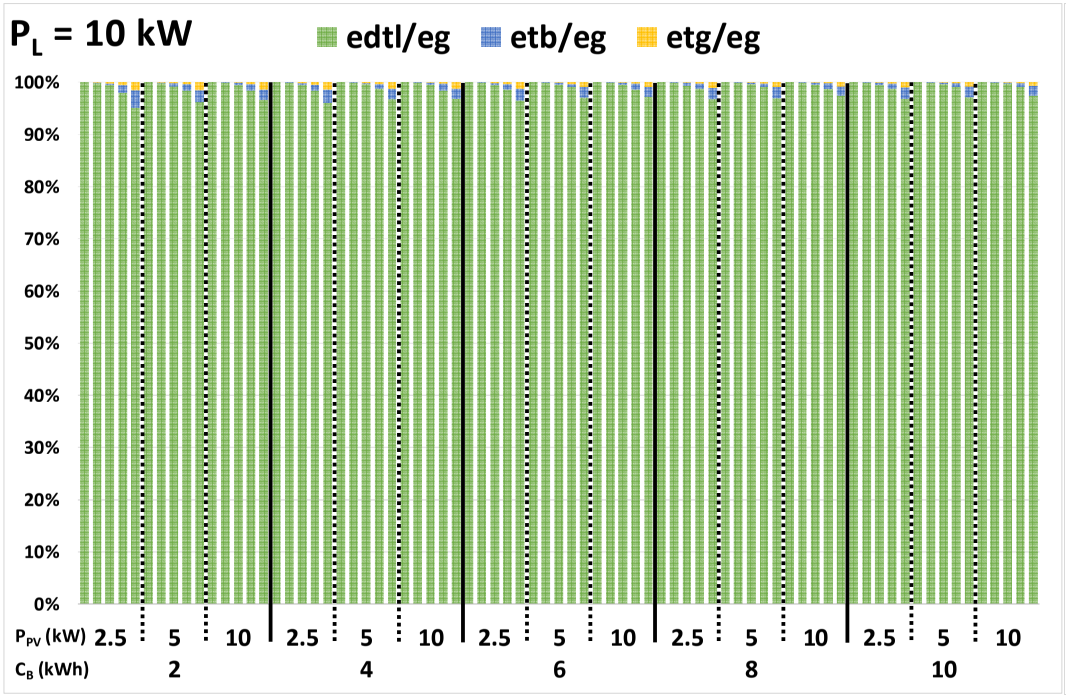
P_L = 10 kW
edtl/eg
etb/eg
etg/eg
100%
90%
80%
70%
60%
50%
40%
30%
20%
10%
0%
P_PV (kW) 2.5 5 10 2.5 5 10 2.5 5 10 2.5 5 10 2.5 5 10
C_B (kWh) 2 4 6 8 10

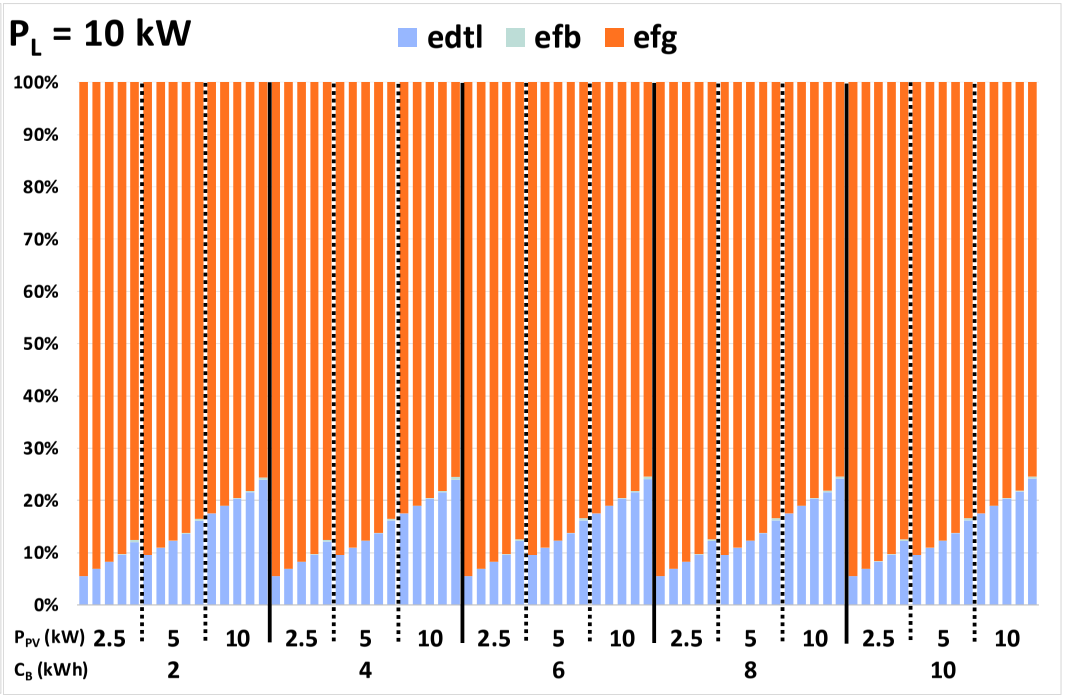
P_L = 10 kW
edtl
efb
efg
100%
90%
80%
70%
60%
50%
40%
30%
20%
10%
0%
P_PV (kW) 2.5 5 10 2.5 5 10 2.5 5 10 2.5 5 10 2.5 5 10
C_B (kWh) 2 4 6 8 10

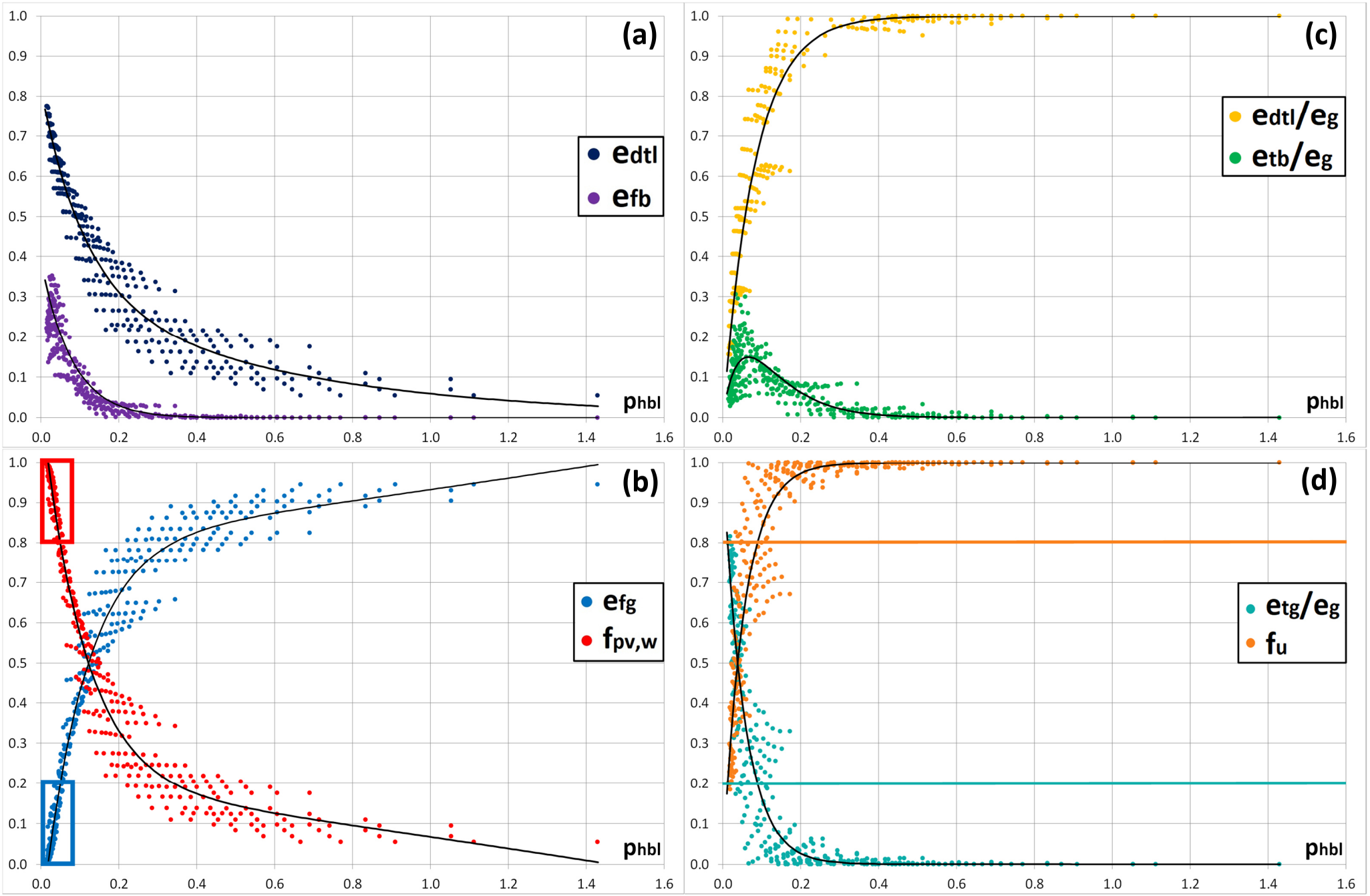
(a)
edtl
efb
phbl
(c)
edtl/eg
etb/eg
phbl
(b)
efg
fpv,w
phbl
(d)
etg/eg
fu
phbl

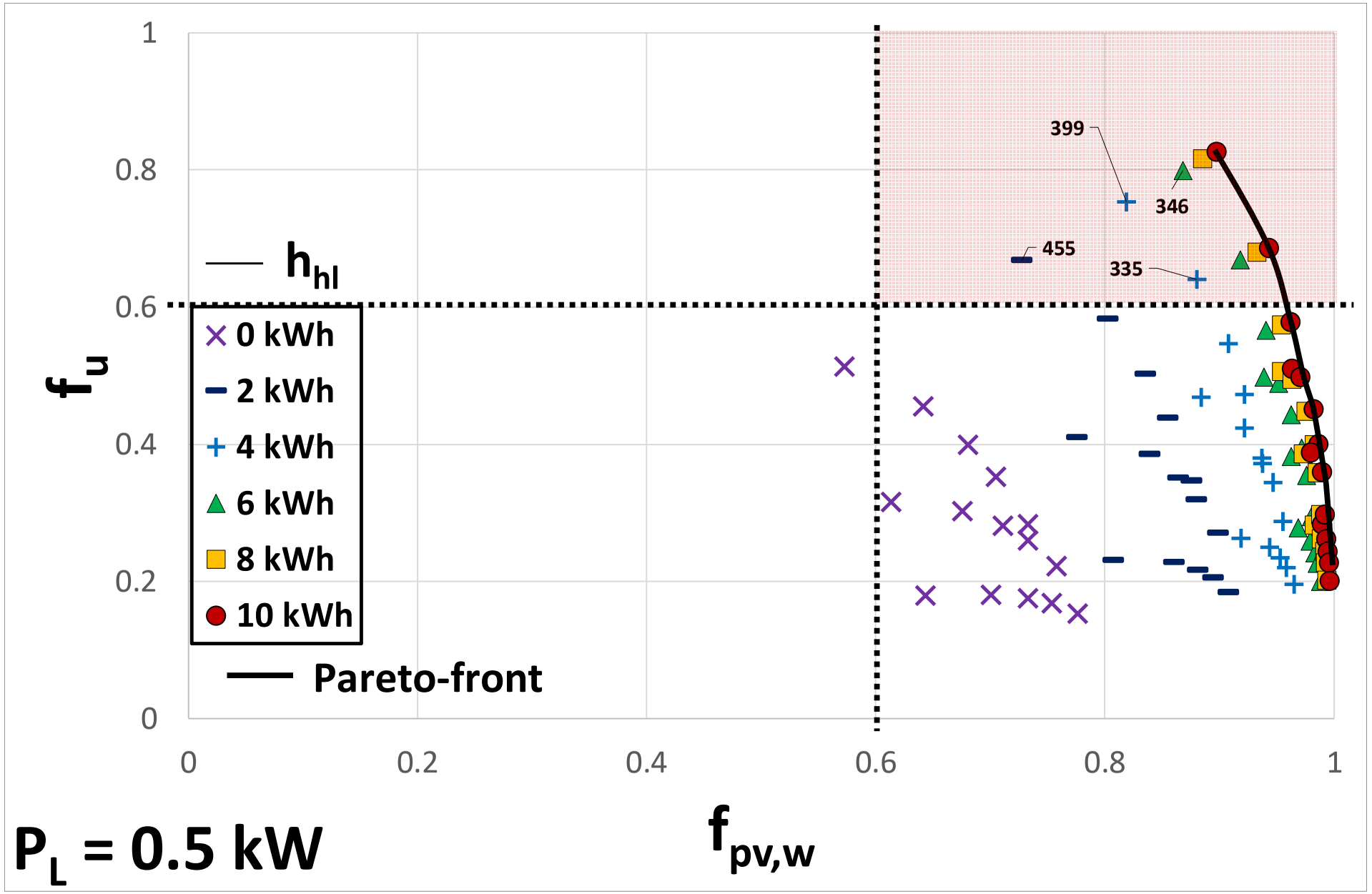
1
0.8
0.6
0.4
0.2
0
0
0.2
0.4
0.6
0.8
1
f_u
$f_{pv,w}$
h_{hl}
0 kWh
2 kWh
4 kWh
6 kWh
8 kWh
10 kWh
Pareto-front
399
346
455
335
P_L = 0.5 kW

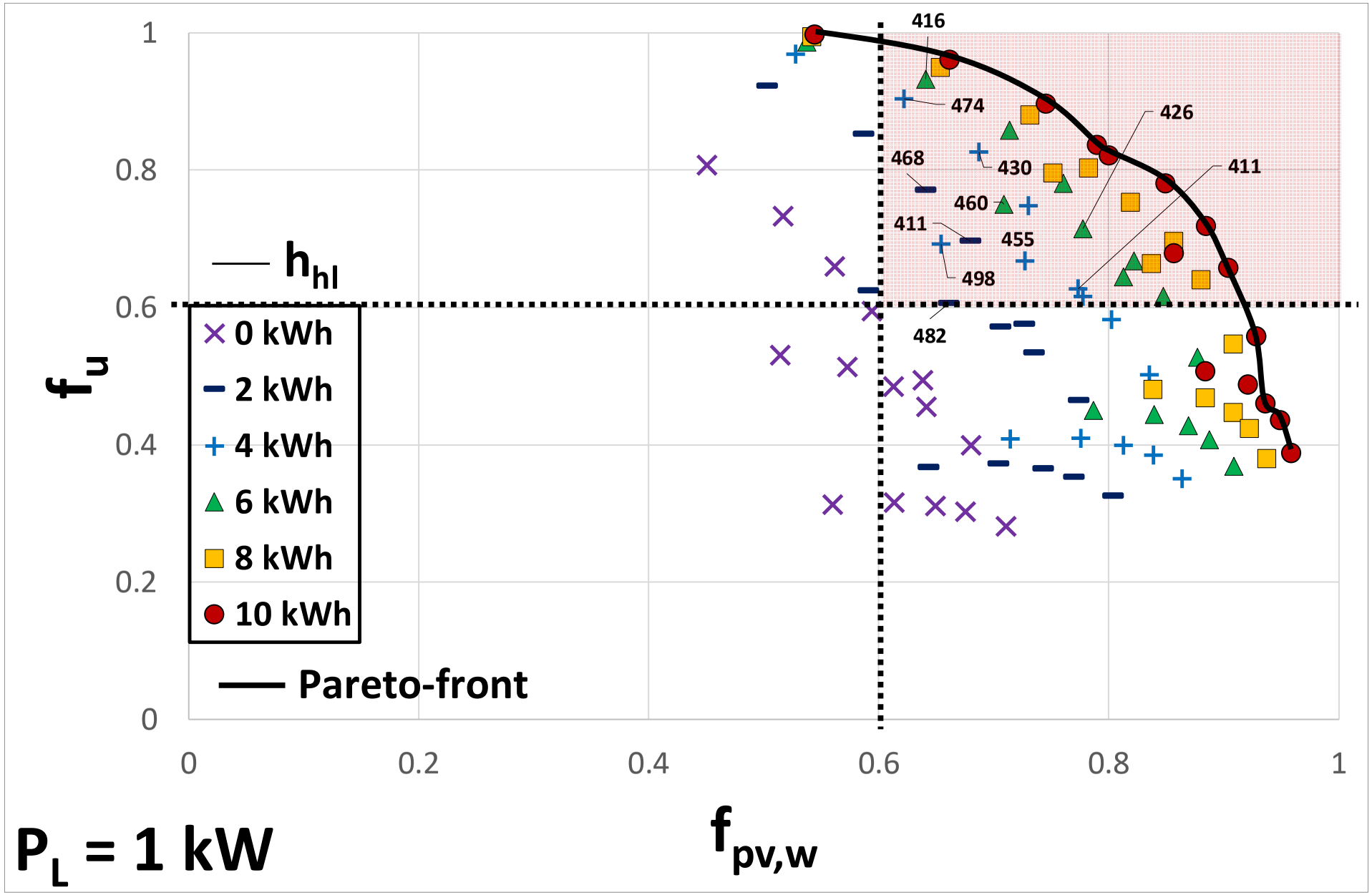
1
0.8
0.6
0.4
0.2
0
0
0.2
0.4
0.6
0.8
1
f_u
$f_{pv,w}$
h_{hl}
0 kWh
2 kWh
4 kWh
6 kWh
8 kWh
10 kWh
Pareto-front
416
474
426
468
430
411
460
411
455
498
482
P_L = 1 kW

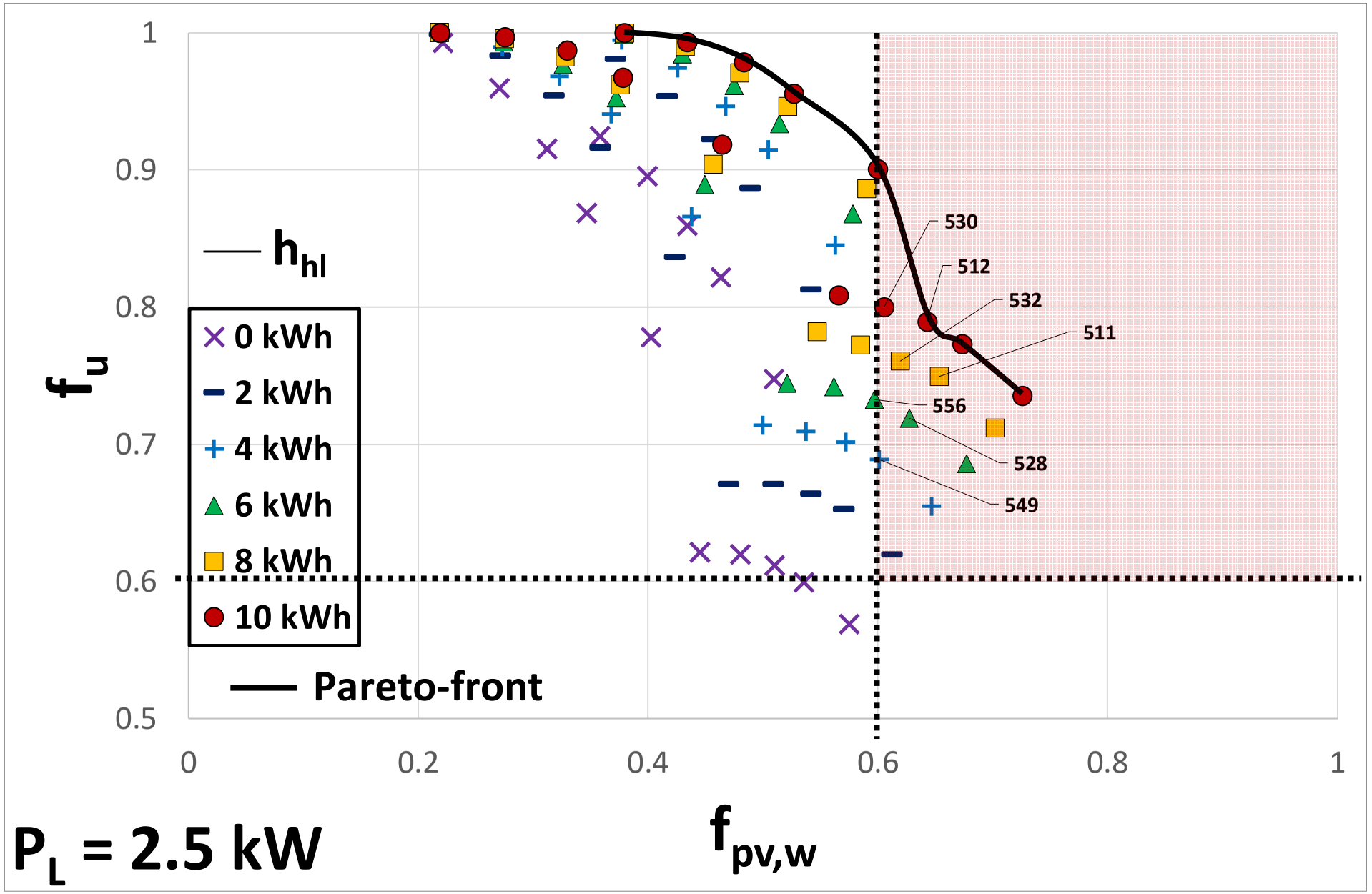
1
0.9
0.8
0.7
0.6
0.5
0
0.2
0.4
0.6
0.8
1
f_u
$f_{pv,w}$
h_{hl}
0 kWh
2 kWh
4 kWh
6 kWh
8 kWh
10 kWh
Pareto-front
530
512
532
511
556
528
549
P_L = 2.5 kW

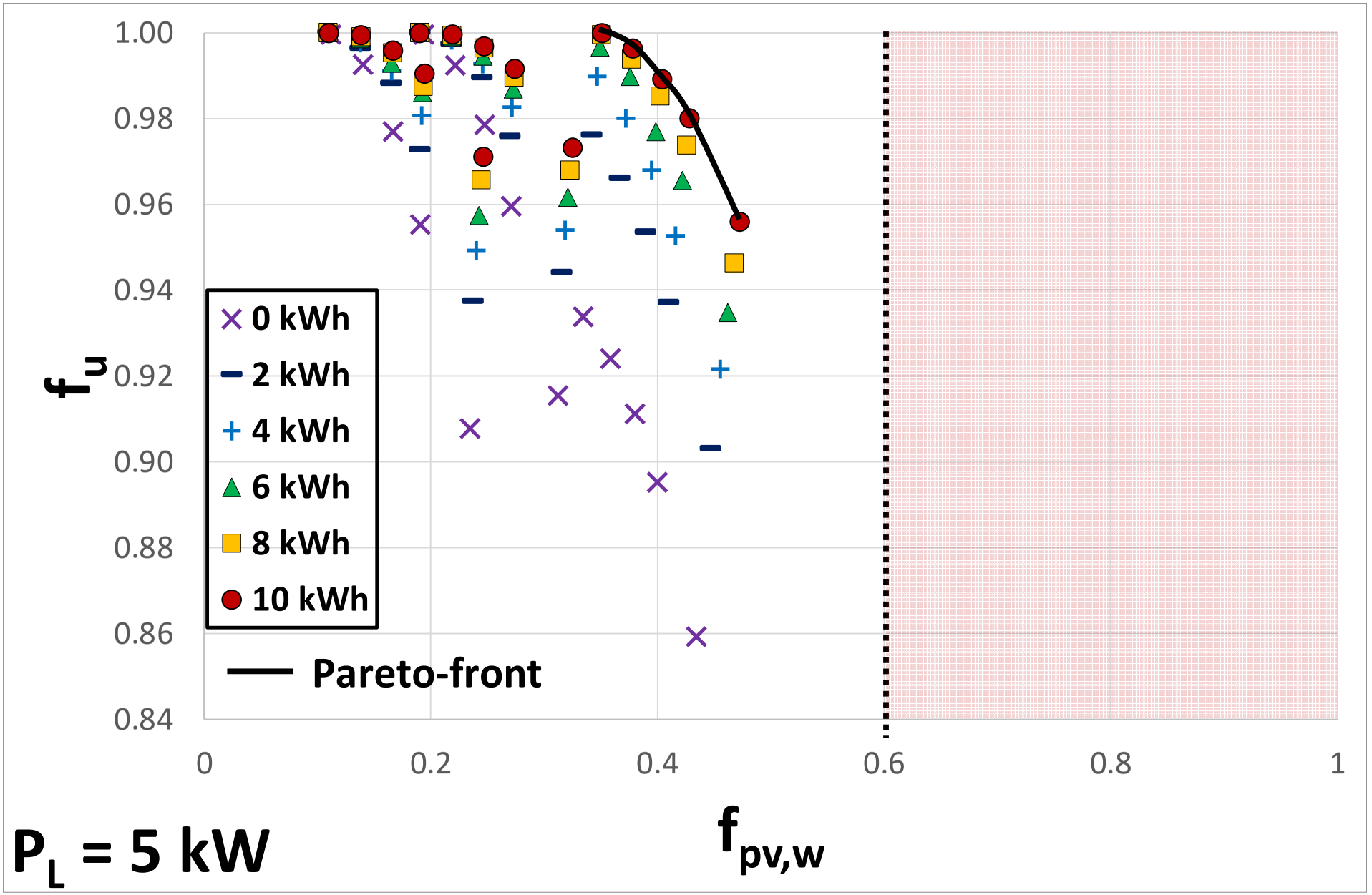
1.00
0.98
0.96
0.94
0.92
0.90
0.88
0.86
0.84
f_u
0
0.2
0.4
0.6
0.8
1
$f_{pv,w}$
0 kWh
2 kWh
4 kWh
6 kWh
8 kWh
10 kWh
Pareto-front
P_L = 5 kW

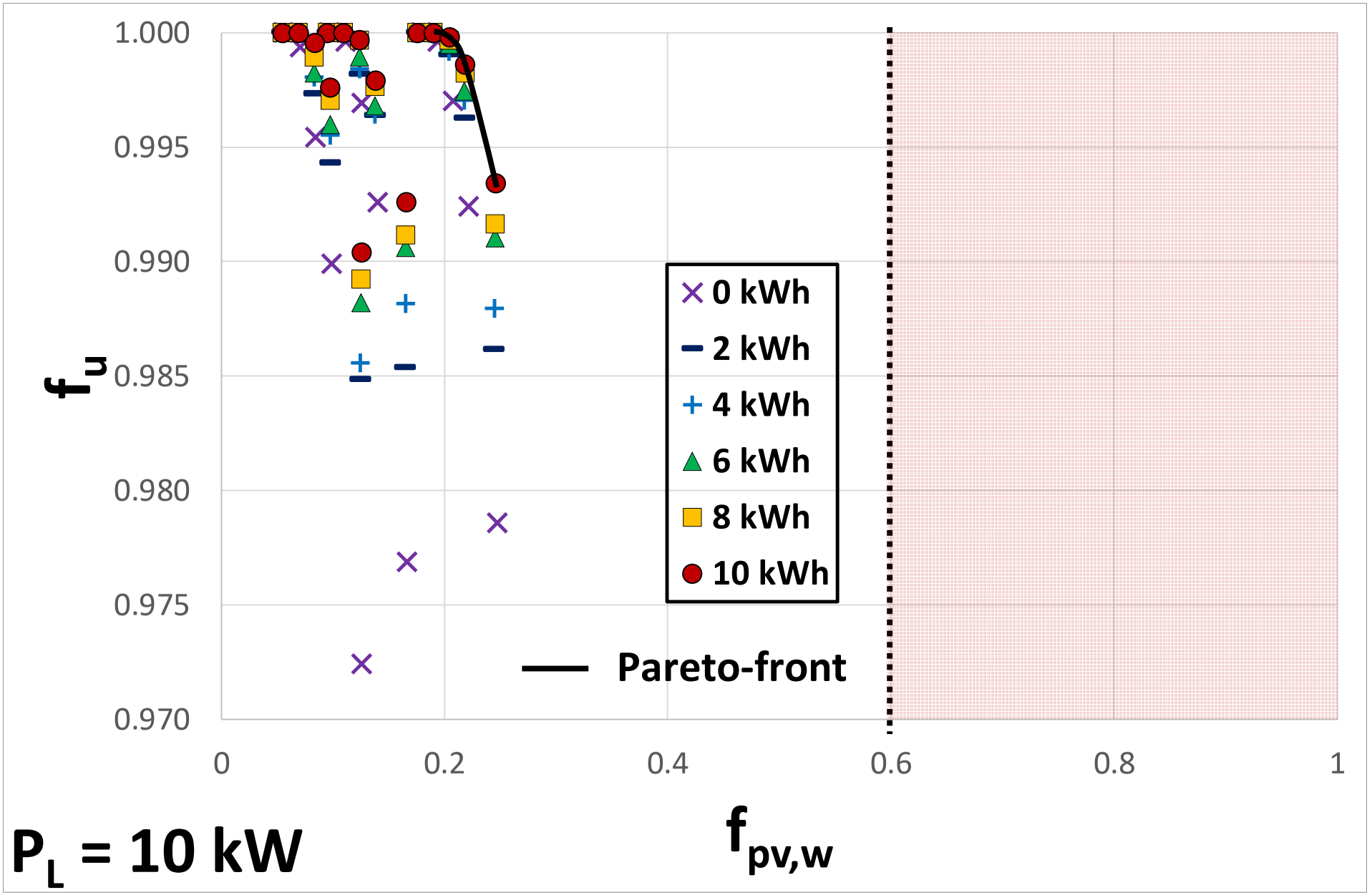
1.000
0.995
0.990
0.985
0.980
0.975
0.970
f_u
0
0.2
0.4
0.6
0.8
1
$f_{pv,w}$
0 kWh
2 kWh
4 kWh
6 kWh
8 kWh
10 kWh
Pareto-front
P_L = 10 kW

List of tables

Nomenclature

G hourly solar radiation
$G_{b,h}$ direct components of solar radiation
$G_{d,h}$ diffused components of solar radiation
R_b mean-hours inclination factor of the direct radiation R_d inclination factors of diffused radiation
R_r inclination factors of reflected radiation
I current (A)
V voltage (V)
I_L light current (A)
I_o diode reverse saturation current (A)
R_s series resistance (Ω)
R_{sh} shunt resistance (Ω)
a modified ideality factor
N_s number of cells in series
n_I usual ideality factor
k Boltzmann's constant
q electron charge
Tc cell temperature (°C)
P_{pv} electric power from the photovoltaic generator (W)
I_{mp} current at the point of the maximum power (A)
V_{mp} voltage at the point of the maximum power (V)
v_h wind speed at the quote of the effective turbine operation (m/s)
v_{an} wind speed at the quote of the anemometric measurement (m/s)
z_h quote of the effective turbine operation (m)
z_{an} quote of the anemometric measurement (m)
α shear exponent
P_o turbine power at the effective working quote (W)
P_ρ turbine correct power
$v_{nom,\rho}$ correct nominal speed
$v_{nom,\rho o}$
P_w wind power (W)
$P_{\rho,net}$ net power (W)
l miscellaneous losses
SOC charge state
P power (W)
P_{tb} power send to the battery (<0) (W)
P_{fb} power from the battery (>0) (W)
C_{bat} battery capacity
$P_{pv,eff}$ power produced by the photovoltaic generator (W)
$P_{w,eff}$ power produced by the wind generator (W)
$P_{inv,out}$ inverter output power(W)
$P_{inv,inp}$ inverter input power(W)
P_g overall power generated (W)
P_L power required by the load (W)
P_{tg} power sent to the grid (W)
P_{fg} power drawn from the grid (W)
η_{reg} regulator efficiency
P_{tl} power required by the HPWBS (W)
E_L energy required by the load (Wh)
E_{tl} energy required by the HPWBS (Wh)
E_{fg} energy from the power grid (Wh)
E_g overall annual energy produced by the generators PV/Wind (Wyear)
E_{dtl} energy sent directly to the load (Wh)
E_{tb} energy stored in the battery (Wh)
E_{tg} energy sent to the grid (Wh)
e_g fractions of annual energy
e_{dtl} fractions of energy sent directly to the load
e_{tb} fractions of energy sent to the battery
e_{tg} fractions of energy sent to the grid
p_w fraction of wind power compared to overall power
p_b fraction of battery power compared to overall power
p_l fraction of load power compared to overall power
$f_{pw,w}$ ratio between the energy supplied from the HPWBS to the load and the energy required by load
f_u ratio between the energy supplied by the plant to the load and the generated energy
h_{tl} ratio between the energy provided by the HPWBS plant to the load and the total nominal power of the plant (Wh/W)
p_{hbl} total load fraction

Greek letters

ρ air density (kg/ m^3)
ρ_0
η_{bat} battery efficiency
$\eta_{AC/AC}$ DC/DC converter efficiency
$\eta_{AC/DC}$ AC/DC rectifier efficiency
η_{inv} inverter efficiency

Subscripts

b direct components of solar radiation
d diffused components of solar radiation
r reflected radiation
s series
sh shunt
h effective quote
an anemometric quote
ρ
nom,ρ
nom,ρ_o
ρ,net
pv photovoltaic generator
mp maximum power
w wind generator
tb to battery
fb from battery
tg to grid
fg from grid
reg regulator
tl HPWBS
g overall annual
dtl directly to load
hbl

Table 1. Characteristics at reference conditions of the components and parameters set in TRNSYS

Photovoltaic module		**Wind generator**		**Inverter**	
Sharp - ND-Serie A5		Angel Wind Energy - ProvenEnergy		ABB Group- PVI-6000-TL-OUTD	
Power at maximum power point P_{mp} (W)	250	Rated power of the turbine $P_{n,w}$ (kW)	2.5	Inverter efficiency η_{inv} (-)	0.97
Open-circuit voltage V_{sc} (V)	37.6	Rated wind speed V_n (m/s)	12	**Regulator**	
Short-circuit current I_{sc} (A)	8.68	Hub height H (m)	14.5	Steca - Steca Solarix MPPT	
Voltage at maximum power point V_{mp} (V)	30.9	Turbine power loss l (%)	6	Regulator efficiency η_{reg} (-)	0.98
Current at maximum power point I_{mp} (A)	8.10	Rotor Diameter D (m)	3.5	High limit on f_{SOC} (-)	0.97
Module conversion efficiency η_{pv} (%)	15.2	Air density ρ (kg/m^3)	1.225	Low limit on f_{SOC} (-)	0.10
NOCT (°C)	47.5	Data collection height h (m)	10	**Battery storage**	
Cell area A_c (cm^2)	156.5	Site shear exponent m (-)	0.14	Lg chem - BAT-2.0-A-SE-10	
Module area A_m (m^2)	1.65	Barometric pressure p (kPa)	101.3	Energy capacity C_B (kWh)	2
Number of cells wired in series n_c (-)	60	Site elevation alt (m)	220	Charging efficiency η_{bat} (-)	0.98
Temperature coefficient of I_{sc} μ_{Isc} (-)	0.038	**AC/DC Rectifier**			
Temperature coefficient of V_{oc} μ_{Voc} (-)	-0.329	3D Company -EOREG700V54			
Array slope β (degree)	33	Efficiency $\eta_{AC/DC}$ (-)	0.90		
DC/DC Converter					
EpSolar - 20A Serie A					
Efficiency $\eta_{DC/DC}$ (-)	0.94				

Table 2. Parametric analysis: nominal power of the PV generator and of the wind generator, and the storage capacity of electrical battery

P_{PV} (kW)	**P_W (kW)**	**C_B (kWh)**
2.5	2.5	0
5	5	2
10	7.5	4
	10	6
	15	8
		10

Table 3. Pareto front HPWBS configurations

P_L (Kw)		P_B (Kw)	P_{PV} (Kw)	P_W (Kw)	P_n (Kw)	$f_{pv,w}$ (-)	f_u (-)
0.5 kW	1	10	2.5	2.5	15	0.90	0.83
	2	10	2.5	5	17.5	0.94	0.69
	3	10	2.5	7.5	20	0.96	0.58
	4	10	2.5	10	22.5	0.97	0.50
	5	10	5	5	20	0.98	0.45
	6	8	5	5	18	0.98	0.45
	7	10	5	7.5	22.5	0.99	0.40
	8	10	10	10	30	1.00	0.23
1 kW	1	10	2.5	2.5	15	0.54	1.00
	2	10	2.5	5	17.5	0.66	0.96
	3	10	2.5	7.5	20	0.75	0.90
	4	10	5	2.5	17.5	0.79	0.84
	5	10	2.5	10	22.5	0.80	0.82
	6	10	5	5	20	0.85	0.78
	7	10	5	7.5	22.5	0.88	0.72
	8	10	5	10	25	0.90	0.66
	9	10	5	15	30	0.93	0.56
	10	10	10	7.5	27.5	0.94	0.46
	11	10	10	10	30	0.95	0.44
	12	10	10	15	35	0.96	0.39
2.5 kW	1	10	5	2.5	17.5	0.38	1.00
	2	8	5	2.5	15.5	0.38	1.00
	3	6	5	2.5	13.5	0.38	1.00
	4	10	5	5	20	0.43	0.99
	5	8	5	5	18	0.43	0.99
	6	10	5	7.5	22.5	0.48	0.98
	7	10	5	10	25	0.53	0.96
	8	10	5	15	30	0.60	0.90
	9	10	10	5	25	0.61	0.80
	10	10	10	7.5	27.5	0.64	0.79
	11	10	10	10	30	0.67	0.77
	12	10	10	15	35	0.73	0.74
5 kW	1	10	2.5	2.5	18.50	0.35	1.00
	2	10	10	5	25	0.38	1.00
	3	10	10	7.5	27.5	0.40	0.99
	4	10	10	10	30	0.43	0.98
	5	10	10	15	35	0.47	0.96
10 kW	1	8	10	10	28	0.22	1.00
	2	6	10	10	26	0.22	1.00
	3	4	10	10	24	0.22	1.00
	4	2	10	10	22	0.22	1.00
	5	10	10	15	35	0.25	0.99
	6	8	10	15	33	0.25	0.99

	7	6	10	15	31	0.25	0.99

Table 4. Optimal HPWBS configurations

P_L (kW)	P_B (kW)	P_{PV} (kW)	P_W kW	P_n (kW)	p_w (-)	p_b (-)	p_l (-)	p_{hbl} (-)	e_{dtl} (-)	e_{fb} (-)	e_{fg} (-)	e_g (-)	e_{lb} (-)	e_{tb} (-)	e_{tg} (-)	e_{dtl}/e_g (-)	e_{tb}/e_g (-)	e_{tg}/e_g (-)	$f_{pv,w}$ (-)	f_u (-)	h_{hl} (h)
0.5	6	2.5	2.5	11	0.50	0.55	0.10	0.05	0.57	0.30	0.13	1.09	0.01	0.30	0.22	0.52	0.28	0.20	0.87	0.80	345.6
0.5	4	2.5	2.5	9	0.50	0.44	0.10	0.06	0.57	0.25	0.18	1.09	0.01	0.26	0.27	0.52	0.23	0.25	0.82	0.75	398.6
0.5	2	2.5	2.5	7	0.50	0.29	0.10	0.07	0.57	0.16	0.27	1.09	0.00	0.16	0.36	0.52	0.15	0.33	0.73	0.67	455.0
0.5	4	2.5	5	11.5	0.67	0.35	0.07	0.04	0.64	0.24	0.12	1.38	0.01	0.25	0.50	0.46	0.18	0.36	0.88	0.64	335.3
1	6	2.5	5	13.5	0.67	0.44	0.13	0.07	0.51	0.13	0.36	0.69	0.00	0.13	0.05	0.74	0.19	0.07	0.64	0.93	416.0
1	4	2.5	5	11.5	0.67	0.35	0.13	0.09	0.51	0.11	0.38	0.69	0.00	0.12	0.07	0.74	0.17	0.10	0.62	0.90	473.8
1	4	2.5	7.5	14	0.75	0.29	0.10	0.07	0.55	0.13	0.31	0.84	0.00	0.14	0.15	0.66	0.16	0.17	0.69	0.83	429.9
1	8	5	2.5	15.5	0.33	0.52	0.13	0.06	0.51	0.24	0.25	0.95	0.01	0.25	0.19	0.54	0.26	0.20	0.75	0.80	424.7
1	2	2.5	7.5	12	0.75	0.17	0.10	0.08	0.55	0.09	0.36	0.84	0.00	0.10	0.19	0.66	0.11	0.23	0.64	0.77	468.0
1	6	5	2.5	13.5	0.33	0.44	0.13	0.07	0.51	0.20	0.29	0.95	0.00	0.20	0.24	0.54	0.21	0.25	0.71	0.75	460.0
1	6	5	5	16	0.50	0.38	0.10	0.06	0.57	0.21	0.22	1.09	0.00	0.21	0.31	0.52	0.19	0.29	0.78	0.71	425.8
1	4	5	2.5	11.5	0.33	0.35	0.13	0.09	0.51	0.15	0.35	0.95	0.00	0.15	0.29	0.54	0.16	0.31	0.65	0.69	498.2
1	4	5	5	14	0.50	0.29	0.10	0.07	0.57	0.16	0.27	1.09	0.00	0.16	0.36	0.52	0.15	0.33	0.73	0.67	455.0
1	4	5	7.5	16.5	0.60	0.24	0.08	0.06	0.61	0.17	0.23	1.24	0.00	0.17	0.46	0.49	0.14	0.37	0.77	0.63	410.6
1	2	5	5	12	0.50	0.17	0.10	0.08	0.56	0.10	0.34	1.09	0.00	0.10	0.43	0.51	0.09	0.39	0.66	0.61	482.3
2.5	10	10	5	25	0.33	0.40	0.17	0.10	0.48	0.13	0.39	0.76	0.00	0.13	0.15	0.63	0.17	0.20	0.61	0.80	530.4
2.5	10	10	7.5	27.5	0.43	0.36	0.14	0.09	0.50	0.14	0.36	0.82	0.00	0.14	0.17	0.62	0.17	0.21	0.64	0.79	511.9
2.5	8	10	7.5	25.5	0.43	0.31	0.14	0.10	0.50	0.12	0.38	0.82	0.00	0.12	0.20	0.62	0.15	0.24	0.62	0.76	532.2
2.5	8	10	10	28	0.50	0.29	0.13	0.09	0.53	0.13	0.35	0.88	0.00	0.13	0.22	0.60	0.15	0.25	0.65	0.75	511.0
2.5	6	10	7.5	23.5	0.43	0.26	0.14	0.11	0.50	0.09	0.40	0.82	0.00	0.10	0.22	0.61	0.12	0.27	0.60	0.73	556.4
2.5	6	10	10	26	0.50	0.23	0.13	0.10	0.53	0.10	0.37	0.88	0.00	0.10	0.25	0.60	0.12	0.28	0.63	0.72	528.4
2.5	4	10	10	24	0.50	0.17	0.13	0.10	0.52	0.08	0.40	0.88	0.00	0.08	0.27	0.60	0.09	0.31	0.60	0.69	548.7